Zoological Journal of the Linnean Society, 2023, **199**, 771–831
https://doi.org/10.1093/zoolinnean/zlad057
Advance access publication 25 July 2023
Original Article

OXFORD

Original Article

Limb anatomy of the Triassic turtles: appendicular osteology of *Proterochersis* (Testudinata, Proterochersidae)

Tomasz Szczygielski[1,*] and Rafał Piechowski[2]

[1]Institute of Paleobiology, Polish Academy of Sciences, Warsaw, Poland
[2]Institute of Evolutionary Biology, Faculty of Biology, Biological and Chemical Research Centre, University of Warsaw, Warsaw, Poland

[*]Corresponding author. Institute of Paleobiology, Polish Academy of Sciences, Twarda 51/55, 00-818 Warsaw, Poland. E-mail: t.szczygielski@twarda.pan.pl

ABSTRACT

The turtle locomotor system is heavily modified owing to the severe impact of development of the shell on the body plan of these reptiles. Although limb and girdle osteology of the earliest, Triassic turtles is relatively well understood in general, the exact impacts of variability, ontogeny and preservation (e.g. deformation) on the observed morphologies have rarely been considered in detail. Here, we describe in detail and document the osteology and intraspecific variability of the limbs and girdles of *Proterochersis* spp., the basalmost true turtles (Testudinata). We also provide a synthesis of currently available data and detailed comparisons with other Triassic stem turtles to gain a better understanding of the diagnostic value of the early turtle appendicular skeleton and to pave the way for future biomechanical and functional studies. Our data suggest that *Proterochersis* spp. could be at least partly aquatic and could change their preferred habitat during ontogeny, with larger (and, presumably, older) specimens presenting more characters suggestive of a more terrestrial environment.

Keywords: anatomy; Cholonia; forelimb; limb bones; osteology; morphology; postcranium; scapulocoracoid; Triassic

INTRODUCTION

The research on Triassic turtles has a long history, spanning ≥ 160 years (e.g. Meyer 1863, 1865, Baur 1887, Fraas 1913, Jaekel 1914, 1918). However, until the very last decade of the 20th century (Gaffney 1990), much of the circulating information was based on fragmentary, often misidentified and distorted specimens, and the available data concerning limb morphology and function were extremally sparse. At the turn of the 21st century, the record and understanding of non-turtle pantestudinates (representatives of the turtle lineage but lacking the complete shell) and Triassic turtles improved substantially, but still most of the attention was given to the development of the shell, mainly its axial component. Limbs of the earliest turtles and their closest relatives were rarely, if at all, treated as taxonomically diagnostic and compared extensively between the species. The impact of ontogeny and preservation (e.g. deformation) on the observed morphologies is currently ambiguous, and intra- and interspecific variability is poorly understood. Given the recent increase in available material, the aim of this work is to organize the available information and present the variability within the earliest stem turtle limbs, to gain a better understanding of the evolution of the appendicular skeleton and to pave the way for future studies of their function and locomotion.

Despite a number of recent and historical works (e.g. Seeley 1892, Watson 1914, Cox 1969, Keyser and Price 1981, Gow 1997, Gow and Klerk 1997, Lyson *et al.* 2010, 2013a, 2014, 2016, Bever *et al.* 2015), information on the girdles and, particularly, limbs of the Permian *Eunotosaurus africanus* Seeley, 1892, commonly considered as a stem turtle, is very limited. This is because most of the specimens have bones that are damaged, lack articular ends, are encased in matrix or were not sufficiently figured and described. *Pappochelys rosinae* Schoch & Sues, 2015, from the Ladinian of Germany, received a more comprehensive treatment (Schoch and Sues 2015, 2017) and, despite its miniscule size, disarticulation and mostly two-dimensional preservation, its appendicular skeleton is almost completely known. The specimens of *Eorhynchochelys sinensis* Li *et al.*, 2018 and *Odontochelys semitestacea* Li *et al.*, 2008, from the Carnian of China, also include virtually complete and wonderfully preserved, mostly articulated limbs and gridles but, unfortunately, their descriptions are very succinct, and many details are obscured by the matrix or surrounding bones. Some additional data and figures of the appendicular skeleton of *O. semitestacea* were

Received 1 December 2022; revised 18 April 2023; accepted 2 May 2023

provided by Nagashima *et al.* (2013), Rothschild and Naples (2015), Lyson *et al.* (2016), Schoch and Sues (2017) and Sterli *et al.* (2021), but both taxa remain less understood than could be expected based on their completeness and state of preservation.

Proganochelys quenstedtii Baur, 1887, from the Norian of Germany and Switzerland, remains the most complete and best-described Triassic (or even fossil in general) turtle. The German material of that species includes complete (although, in some cases, distorted and lacking surface detail) limbs and girdles belonging to individuals of various sizes, in part described by Jaekel (1914, 1918; with the drawings of the scapulocoracoid subsequently copied by numerous authors), and later revised, elaborated upon and supplemented by Gaffney (1985, 1990). Additional photographs of the scapulocoracoid were published by Sterli *et al.* (2021). Huene (1926) described and figured another left humerus from the *Proganochelys quenstedtii*-yielding locality of Trossingen. Although this specimen was not mentioned by Gaffney (1990) and is now apparently lost, Joyce (2017) attributed it to *Proganochelys quenstedtii*; this assessment seems correct, given not only the locality from which it was recovered, but also its congruent morphology. Another specimen belonging to that species, found recently in Switzerland and exhibited in the Sauriermuseum Frick, incorporates flattened appendicular elements (Scheyer *et al.* 2022). Aff. *Proganochelys ruchae* de Broin, 1984, from the Norian of Thailand, preserves only damaged epiplastra and a splinter of the entoplastron (de Broin 1984). Relatively well-represented, but also fragmentary and distorted material with mediocre preservation, of a new Norian/Rhaetian taxon, from the Ørsted Dal Member of the Fleming Fjord Formation in Greenland, was described in an unpublished thesis by Marzola (2019). A second taxon from the same formation ('cf. *Proganochelys*') is represented by some poorly preserved limb and girdle elements but was not figured in detail or described aside from short notes (Jenkins *et al.* 1994, Marzola *et al.* 2018, Marzola 2019). Marzola *et al.* (2018) also mentioned the pelvis of a third taxon from there, but this was never figured. *Chinlechelys tenertesta* Joyce *et al.*, 2009, from the Norian of the USA, is represented by a proximal left femur and two acetabular parts of the pelvis (Lichtig and Lucas 2021).

Limbs and girdles are present in the material of both known Triassic species of Australochelyidae. *Palaeochersis talampayensis* Rougier *et al.*, 1995, from the Norian of Argentina, preserves mostly complete limbs and girdles described by Sterli *et al.* (2007) and with additional photographs of the scapulocoracoid provided by Sterli *et al.* (2021), but its preservation is markedly poorer than that of most European specimens. The material of the younger (Norian/Rhaetian) Argentinian *Waluchelys cavitesta* Sterli *et al.*, 2020 includes nearly complete girdles (Martínez *et al.* 2015, Sterli *et al.* 2021).

Among the Proterochersidae, *Keuperotesta limendorsa* Szczygielski & Sulej, 2016 preserves both almost complete scapulocoracoids (the left one distorted) and pelvis figured and described (as *Proterochersis robusta* Fraas, 1913) by Joyce *et al.* (2013) and later (as the new taxon) by Szczygielski and Sulej (2016), while Sterli *et al.* (2021) provided additional views of the scapulocoracoid. *Proterochersis robusta* material preserves no limb bones and only limited insight into the girdles, most notably in the form of several good pelves (only one of which was partly described and figured by Fraas 1913; the drawing was subsequently copied by numerous authors, many apparently unaware that the specimen was only partly prepared and concluding that the epipubis was absent) and an entoplastron with sutural edges (de Broin 1984). Some additional information about the attachment of the pelvis to the carapace and sacrum in *Proterochersis robusta* can be observed on the specimens described historically as '*Chelytherium obscurum*' Meyer, 1863 (Meyer 1863, 1865, Lydekker 1889, Szczygielski 2020). Given that most of the material of *Proterochersis robusta* was never described and that it agrees very closely with the morphologies observed in *Proterochersis porebensis* Szczygielski & Sulej, 2016, both species will be presented here together for supplementation. The remains of *Proterochersis porebensis* include numerous specimens of varied sizes, allowing insight into the development and intraspecific variability much better than is possible in the case of any other Triassic stem turtle. Furthermore, many of them are much better preserved, apparently undistorted and free from loss of surface definition owing to cracking, which plagues the specimens from Argentina (Rougier *et al.* 1995, Sterli *et al.* 2007, 2021, Martínez *et al.* 2015), Germany (Jaekel 1914, 1918, Gaffney 1985, 1990, Joyce *et al.* 2013, Szczygielski and Sulej 2016, 2019, Szczygielski *et al.* 2018) and Greenland (Jenkins *et al.* 1994, Marzola 2019). Finally, the Proterochersidae are among the most ancient and basal true turtles (Testudinata) and present a number of plesiomorphic characters, including the morphology of the girdles, such as the size and shape of the coracoids and posterior process of the entoplastron (interclavicle), small obturator foramina in the pelvis, and the general morphology of the pubis (Joyce *et al.* 2013, Szczygielski and Sulej 2016, 2019, Szczygielski 2017, Sterli *et al.* 2021). Therefore, they are a fitting example of the locomotory adaptations of the earliest turtles. Thus far, only Sulej *et al.* (2012) figured, but did not describe, an incomplete humerus and femur of *Proterochersis porebensis*, and Szczygielski and Sulej (2016, 2019) and Szczygielski *et al.* (2018) described the scapulocoracoid, pelvis, femur, epiplastra and entoplastron. These descriptions will be supplemented here with addition of new specimens. Fragments of proterochersid pubis and femur recently discovered in Poland, possibly belonging to the same species, were figured and described by Czepiński *et al.* (2020).

Institutional abbreviations: CSMM, Carl-Schweizer-Museum, Murrhardt, Germany; IVPP, Institute of Vertebrate Paleontology and Paleoanthropology, Chinese Academy of Sciences, Beijing, China; MB, Museum für Naturkunde, Berlin, Germany; NHMD, Natural History Museum of Denmark, Copenhagen, Denmark; NHMUK, Natural History Museum, London, UK; NMMNH, New Mexico Museum of Natural History and Science, Albuquerque, NM, USA; PULR, Universidad Nacional de La Rioja, La Rioja, Argentina; PVSJ, Paleontología de Vertebrados, Museo de Ciencias Naturales de San Juan, San Juan, Argentina; SMF, Sauriermuseum Frick, Frick, Switzerland; SMMP, Sanya Museum of Marine Paleontology, Sanya, China; SMNS, Staatliches Museum für Naturkunde Stuttgart, Stuttgart, Germany; ZPAL, Institute of Paleobiology, Polish Academy of Sciences, Warsaw, Poland.

MATERIALS AND METHODS

The limb and girdle material of *Proterochersis porebensis* was collected in the locality of Poręba (Poland), from the Norian sediments of the Patoka Member of the Grabowa Formation (for more information about the locality, its geological setting and the fossil assemblage, including the turtle remains found there, see Sulej *et al.* 2012, Niedźwiedzki *et al.* 2014, Szulc and Racki 2015, Szulc *et al.* 2015, Zatoń *et al.* 2015, Szczygielski and Sulej 2016, 2019, Szczygielski 2017, Szczygielski *et al.* 2018, Bajdek *et al.* 2019). *Proterochersis porebensis* is the only turtle species found there thus far, hence the limb bones are attributed to that taxon. The relevant specimens are as follows: ZPAL V. 39/13, ZPAL V. 39/17, ZPAL V. 39/22, ZPAL V. 39/25, ZPAL V. 39/26, *ZPAL V. 39/34*, *ZPAL V. 39/48*–ZPAL V. 39/50, ZPAL V. 39/52, ZPAL V. 39/53, ZPAL V. 39/57, ZPAL V. 39/58, ZPAL V. 39/63, ZPAL V. 39/69, *ZPAL V. 39/72*, ZPAL V. 39/156, ZPAL V. 39/157, ZPAL V. 39/161, ZPAL V. 39/162, ZPAL V. 39/164–ZPAL V. 39/166, ZPAL V. 39/177, ZPAL V. 39/193, ZPAL V. 39/216–ZPAL V. 39/220, ZPAL V. 39/223, ZPAL V. 39/225, ZPAL V. 39/276, ZPAL V. 39/279, ZPAL V. 39/280, ZPAL V. 39/318, *ZPAL V. 39/370*, ZPAL V. 39/379, ZPAL V. 39/385, ZPAL V. 39/387, ZPAL V. 39/390, ZPAL V. 39/391, ZPAL V. 39/402, ZPAL V. 39/404, ZPAL V. 39/420–ZPAL V. 39/461, ZPAL V. 39/463, ZPAL V. 39/464, ZPAL V. 39/467, ZPAL V. 39/468, ZPAL V. 39/471, ZPAL V. 39/475, ZPAL V. 39/481, ZPAL V. 39/482–ZPAL V. 39/485, ZPAL V. 39/486–ZPAL V. 39/488, ZPAL V. 39/491, ZPAL V. 39/498–ZPAL V. 39/500 and ZPAL V. 39/502. See the Supporting Information, Material for more information on the specimens. In addition, specimens ZPAL V. 66/12 (base of the proximal end of the left femur, large) and ZPAL V.66/20 (left pubis missing the epipubic process and dorsal branch) of *Proterochersis* cf. *porebensis* from Kocury (for more information about the locality and description of the specimens, see Czepiński *et al.* 2020) were studied. Finally, osteological specimens of extant Cryptodira and Pleurodira from the collections of the University of Warsaw (Warsaw, Poland) and the Institute of Systematics and Evolution of Animals, Polish Academy of Sciences (Cracow, Poland) were examined for comparative purposes.

The locality of Poręba yielded numerous turtle specimens of various sizes, from isolated bones of supposed hatchlings to fragments of massive old individuals reaching up to ~70 cm of estimated carapace length (see discussion and descriptions by Szczygielski and Sulej 2016, 2019, Szczygielski *et al.* 2018). Given that no specimen preserves articulated limbs, the exact proportions between the bones cannot be determined. Nonetheless, the presence of the pelvis, scapulocoracoid and femur within the nearly complete shell of the holotype (*ZPAL V. 39/48*, carapace ~42.5 cm long, identified as a subadult), comparisons with other Triassic pantestudinates and the varied degree of ossification of gathered remains allow general assumptions about the relative size of any given individual. The categories used are as follows: small (significantly smaller than in *ZPAL V. 39/48*, with anatomical details poorly expressed and articular ends poorly ossified, supposedly juvenile), middle-sized (about the size of *ZPAL V. 39/48*, with all or most anatomical details well defined but articular ends still not entirely ossified, supposedly subadult or early adult) and large (significantly larger than *ZPAL V. 39/49*, with massive, well-ossified bones, supposedly adult). These categories are only provisional and aimed at providing a general idea about the size and stage of ossification of the specimens. As in modern turtles, the possibility of differences in size and development between coeval individuals attributable to factors such as individual variation, extrinsic factors and/or potential sexual dimorphism must be kept in mind (Szczygielski *et al.* 2018), and some discrepancies between the relative size and ossification stage are apparent in the analysed material (see Results).

Material of limbs, girdles and associated shell structures of *K. limendorsa* (*SMNS 17757*; see Joyce *et al.* 2013, Szczygielski and Sulej 2016, Szczygielski 2017), *O. semitestacea* (*IVPP V 13240*, *IVPP V 15639* and IVPP V 15653; see Li *et al.* 2008), *Palaeochersis talampayensis* (*PULR 068* and PULR 069; see Rougier *et al.* 1995, Sterli *et al.* 2007), *Pappochelys rosinae* (*SMNS 91360*, SMNS 91606, SMNS 91895, SMNS 92085 and SMNS 96938; see Schoch and Sues 2015, 2017), *Proganochelys quenstedtii* (MB.1910.42.2, MB.1910.45.3, SMNS 15759, SMNS 16980, SMNS 17203, SMNS 17204 and SMNS 51600; see Gaffney 1990; and SMF 09-F2; see Scheyer *et al.* 2022), *Proterochersis robusta* (all specimens except SMNS 50918; the most relevant are NHMUK 38650, NHMUK 38653, *SMNS 12777*, SMNS 16442, SMNS 16603, SMNS 17930, SMNS 50917 and SMNS 56606; see Meyer 1863, 1865, Lydekker 1889, Fraas 1913, Szczygielski and Sulej 2016, 2019, Szczygielski *et al.* 2018, Szczygielski 2020; and the Supporting Information, Material for short characterization) and the Triassic turtle material (including cf. *Proganochelys* sp.) from Greenland (most importantly: NHMD 163389, NHMD 163390, NHMD 163393–NHMD 163396, NHMD 163398, NHMD 163406, NHMD 163408, NHMD 163450 and NHMD 190349; see Jenkins *et al.* 1994, Marzola *et al.* 2018, Marzola 2019) was studied personally by T. Szczygielski in their respective collections. Some additional photographs of *W. cavitesta* (PVSJ 903 and PVSJ 904; see Sterli *et al.* 2021) were shared by Dawid Dróżdż (ZPAL). Photographs of the femur and acetabulum of *Chinlechelys tenertesta* (*NMMNH P-16697*, NMMNH P-16621 and NMMNH P-4315; see Lucas *et al.* 2000, Joyce *et al.* 2009, Lichtig and Lucas 2021) were shared by Tomasz Sulej (ZPAL).

The directional and anatomical terminology generally follows Walker (1973) and Gaffney (1990). In cases when multiple names for a given structure are used in the literature, these variants are given in parentheses.

Given that the Proterochersidae represent the oldest and most basal group of turtles, soon after the co-option of the dermal parts of the pectoral girdle (Szczygielski and Sulej 2016, 2019, Sterli *et al.* 2021), we consider here also the homologues of those elements incorporated into the shell: the nuchal bone, epiplastra and entoplastron, i.e. the homologues of the cleithra, clavicles and interclavicle, respectively (e.g. Oken 1823, Parker 1868, Gilbert *et al.* 2007, Lyson *et al.* 2013b), regardless of their functional role in locomotion. Given that limits of individual shell bones are usually not traceable in proterochersids and other Triassic turtles (Szczygielski and Słowiak 2022 and references therein), we also consider the internal (visceral) surface of the carapace (mostly the nuchal region and area around the pelvis; Figs 1–5) and plastron (Figs 6–12).

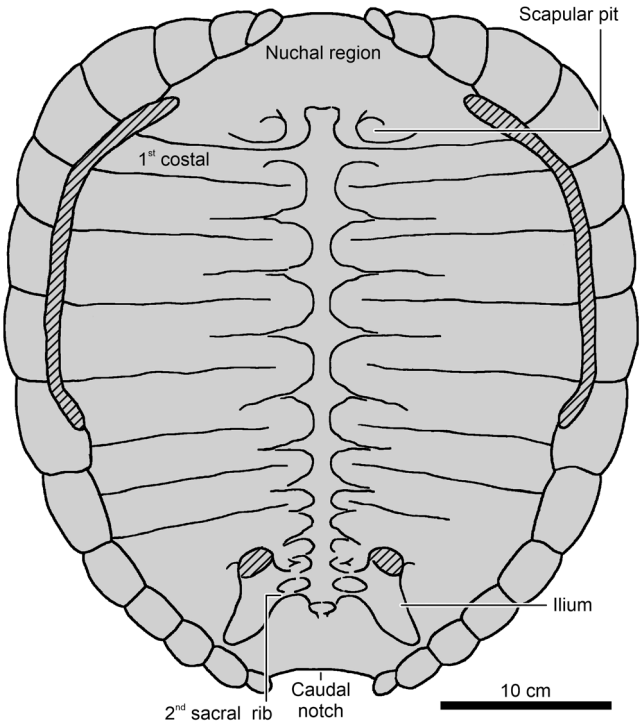

Figure 1. *Proterochersis porebensis*, restoration of the inner surface of the carapace.

Three-dimensional (3D) surface scans were created using the Shining 3D EinScan Pro 2X 3D scanner fixed on a tripod with EinScan Pro 2X Color Pack (texture scans), Ein-Turntable (alignment based on features) and EXScan Pro 3.2.0.2–3.7.0.3 software. The number of turntable steps was varied, chosen depending on the specimen. The models were meshed using the Watertight Model and High Detail presets. For figures, snapshots of the 3D models were captured in MeshLab v.2021.10 (Cignoni *et al.* 2008) in orthographic view with Radiance Scaling (Lit Sphere) shader (Vergne *et al.* 2010) enabled to enhance the surface detail and lighting. Larger, more complex specimens were digitized photogrammetrically, using a Canon EOS M6 mark II camera, LED lighting (LED rings mounted on the lens and/or on tripods) and Agisoft Metashape Pro 1.5.0–2.0.1.

DESCRIPTION

Nuchal bone (cleithrum)

The nuchal bone (which is likely to be homologous to the cleithrum; Lyson *et al.* 2013b) of *Proterochersis porebensis* is best represented by the specimen ZPAL V. 39/22 exhibiting sutural edges of the left nuchal (Szczygielski and Sulej 2019; Fig. 2F, H–M). A new specimen, ZPAL V. 39/482 (Szczygielski and Słowiak 2022), preserves only the ventrolateral part of the right nuchal bone, but also shows sutures. Although there is no overlap between these two specimens and they come from animals roughly the same size, the differences in layout of their sulci (the first marginal having broader contact with the first vertebral scute in ZPAL V. 39/482 than in ZPAL V. 39/22), geometry (subtle differences in prominence of particular scute areas) and colour suggest that they represent two separate individuals. Both specimens, in addition to the typical components building the anterior region of the turtle carapace (i.e. the nuchal, peripherals, neurals and costals), indicate the presence of a mosaic of additional dermal bones, absent in more derived species (Szczygielski and Sulej 2019, Szczygielski and Słowiak 2022). This region is also preserved in a number of other *Proterochersis porebensis* specimens, either completely (*ZPAL V. 39/34*, Fig. 2A; *ZPAL V. 39/48*, Figs 2C, 3A; *ZPAL V. 39/49*, Figs 2G, 3B) or in part (ZPAL V. 39/57; *ZPAL V. 39/72*, Fig. 2D; ZPAL V. 39/161, Fig. 2E; ZPAL V. 39/390, Fig. 2B), but no sutures are traceable in them. Likewise, the nuchal region with a co-ossified nuchal bone is preserved in three specimens of *Proterochersis robusta*: CSMM uncat., SMNS 17561 and SMNS 17930 (Karl and Tichy 2000, Szczygielski and Sulej 2016, Szczygielski *et al.* 2018). Out of these, only SMNS 17930 (Fig. 4A, B) provides useful information on the nuchal region anatomy. CSMM uncat. lacks the anterior edge of its cervical scute area and the rest is not exposed viscerally, while in SMNS 17561 only the anterior part of that area is exposed, and it appears to be partly restored. SMNS 16442 preserves the general nuchal region exposed both externally and viscerally (Fig. 4C–E), but the nuchal bone itself seems to be missing (a poorly preserved imprint is present on the associated steinkern, i.e. a natural mould of the interior of the shell, Fig. 4D, E), and much of the surface is severely damaged (Szczygielski *et al.* 2018, Szczygielski and Sulej 2019). This is supplemented by other steinkerns, at least three of which (*SMNS 12777*, Fig. 4H; SMNS 16603; SMNS 17930, Fig. 4B) preserve the imprints of the visceral surface, albeit the anteriormost region, including the nuchal bone, is poorly represented or completely absent. The mould of the fourth steinkern with that part preserved, SMNS 51441 (Fig. 4G; found at Hüttenbachklinge near Strümpfelbach, Remstal; original housed in the Steinzeitmuseum Kleinheppach; covering the anterior part of the shell up to the fifth costal), agrees in all discernible details with *Proterochersis robusta* but, owing to a complete lack of bone and posterior part of the trunk and the pelvis, which could provide diagnostic features, its taxonomic identification is tentative.

Unlike crown-group turtles, the nuchal bone in at least some individuals of *Proterochersis porebensis* is paired and very short (for a detailed description and photographs, see Szczygielski and Sulej 2019). It is a geometrically complex element supporting almost half of the cervical scute, with the lateralmost part being supported by at least one additional dermal ossification (element of the carapacial mosaic; see Szczygielski and Sulej 2019). It has nearly straight posterior and dorsolateral edges. Posteriorly, it contacts another element, which (based on SMNS 16442) is identified as a preneural (Szczygielski and Sulej 2019). The posterodorsal suture mostly coincides with the sulcus separating the cervical and the first vertebral scute. In ZPAL V. 39/22, this sulcus enters the area of the nuchal in the medial part. The nuchal is generally ovoid in longitudinal cross-section, with the anterior edge thinner than the posterior, convex ventral surface and most of the dorsal surface, and (at least in ZPAL V. 39/22, Fig. 2F, H–M) the posterodorsal convexity disturbed by the cervicovertebral sulcus. In the anteroposterior aspect, its dorsal surface is gently bowed (convex dorsolaterally), and its ventral surface is gently sinuous (concave ventromedially in the medial part and convex ventromedially in the lateral part, such that two nuchals formed a smooth arch above the neck). In ventral view,

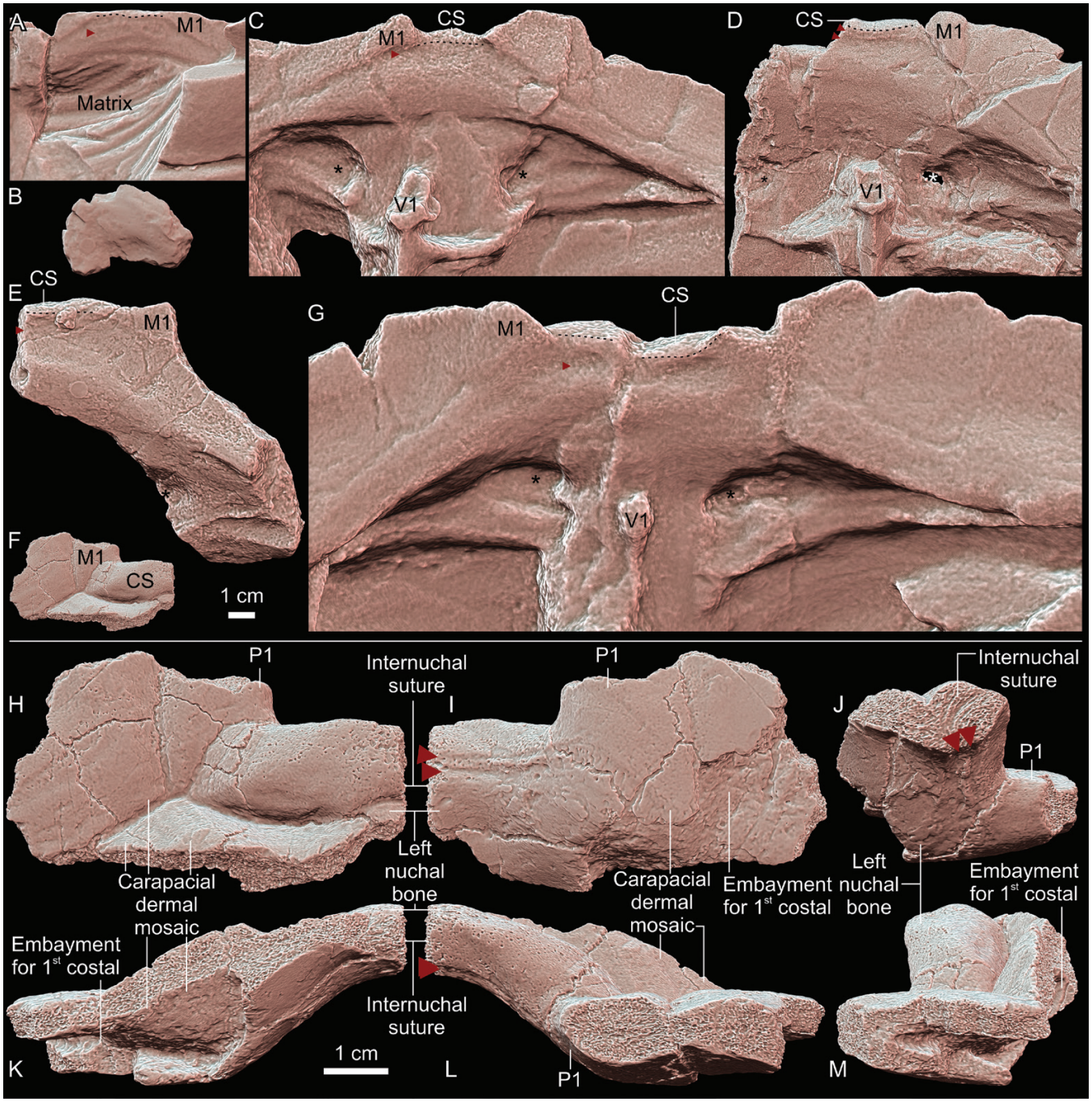

Figure 2. *Proterochersis porebensis*, nuchal region of the carapace in ventral (A–E, G, I), dorsal (F, H), medial (J), posterior (K), anterior (L) and lateral (M) view. A, *ZPAL V. 39/34*. B, ZPAL V. 39/390, left part of the nuchal region. C, *ZPAL V. 39/48*. D, *ZPAL V. 39/72*. E, ZPAL V. 39/161, left part of the nuchal region. F, H–M, ZPAL V. 39/22, left part of the nuchal region with preserved sutures. G, *ZPAL V. 39/49*. Specimens are presented as three-dimensional models in orthographic projection with Radiance Scaling enabled, sorted roughly by size. Asterisks indicate scapular pits; dashed line indicates inferred attachment of the body wall; red arrowheads indicate transverse grooves. Abbreviations: CS, cervical scute; M1, first marginal scute; P1, first peripheral bone; V1, first dorsal vertebra.

the posterior edge is wider than dorsally owing to the presence of a ventrolateral projection contacting the anteromedial corner of the first costal. The lateral edge is directed posterolaterally in the anterior two-thirds of its length, then turns posteromedially; these portions are set at an oblique angle. The anterior third of the ventral surface presents rough sculpture resulting from a mix of numerous nutrient vascular openings piercing the cortex and an imprinted network of vascular grooves, indicative of keratinous covering closely associated with the bone (e.g. Scheyer and Sander 2007, Szczygielski and Słowiak 2022), followed by a transverse groove, a rounded ridge with numerous vascular openings and another groove, parallel to the first, but widening laterally. The anterior groove apparently coincides with the attachment of the body wall, and an associated band of increased vasculature continues laterally and slightly anteriorly past the anterolateral suture of the nuchal onto the neighbouring

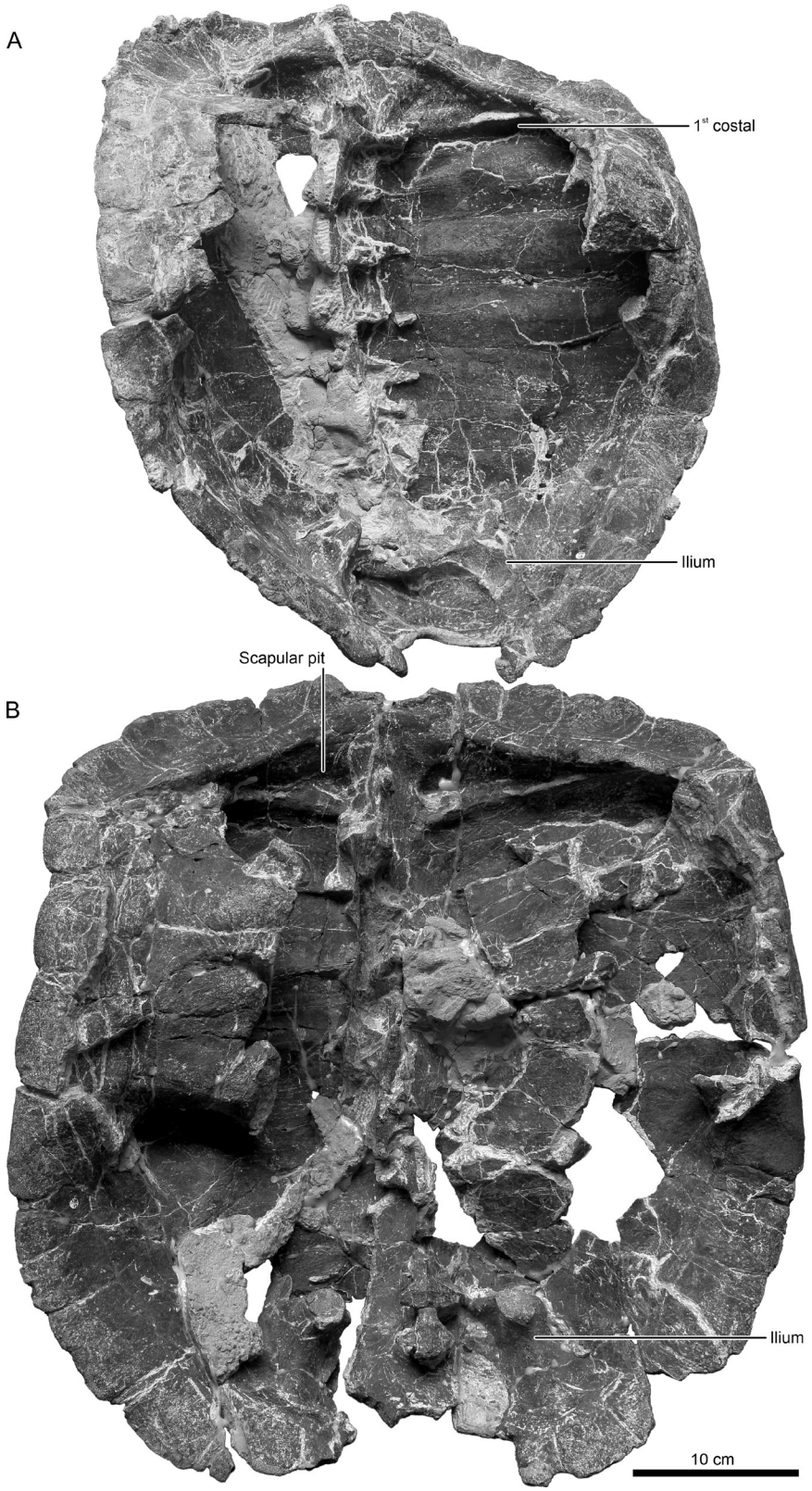

Figure 3. *Proterochersis porebensis*, photographs of the inner surface of the carapace. A, *ZPAL V. 39/48*. B, *ZPAL V. 39/49*.

dermal ossification (carapacial mosaic; see Szczygielski and Sulej 2019), then turns posterolaterally, subparallel to the anterolateral suture of the nuchal. The transverse ridge and the posterior transverse groove end around the level of the medial edge of the first marginal. The visceral surface in the posterior half of the bone is mostly smooth with some isolated vascular openings, particularly along the sutures.

In *ZPAL V. 39/34* (Fig. 2A) this region is very flat; the body wall appears to have been attached closer to the anterior edge of the carapace, leaving a very narrow anterior margin. There is a

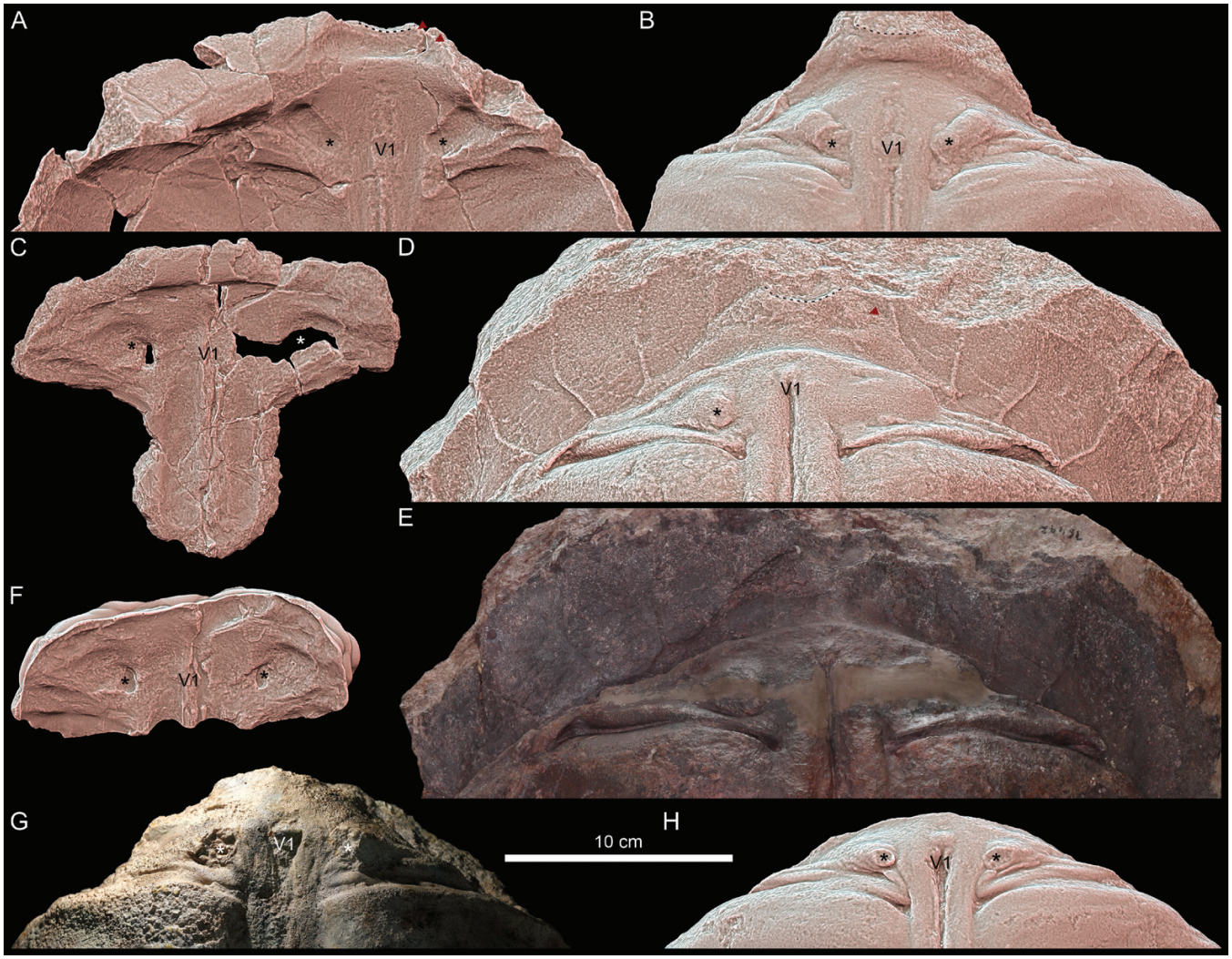

Figure 4. *Proterochersis robusta*, nuchal region of the carapace. A, B, SMNS 17930, nuchal region of the carapace in ventral view (A) and natural cast of the visceral surface of the carapace in dorsal view (B). C–F, SMNS 16442, preserved part of the carapace in ventral (visceral) view (C), natural cast of the interior of the carapace in dorsal view as a three-dimensional model (D) and photograph (E) showing the anterior extent of the nuchal (note that part of the mould crossing the scapular pits is restored), and plaster cast of the visceral surface showing the morphology of the scapular pits before damage (F). G, SMNS 51441 (cf. *Proterochersis robusta*), nuchal region of a cast of a steinkern in dorsal view. H, *SMSN 12777*, nuchal region of a steinkern in dorsal view. Specimens in A–D, F, H are presented as three-dimensional models in orthographic projection with Radiance Scaling enabled. Asterisks indicate dorsal processes of epiplastra; dashed line indicates inferred attachment of the body wall; red arrowheads indicate transverse grooves; V1 indicates the location of the first dorsal vertebra.

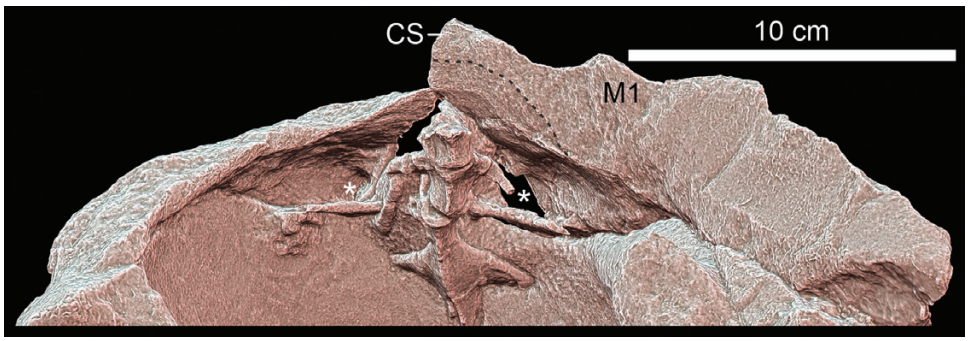

Figure 5. *Keuperotesta limendorsa, SMNS 17757*, nuchal region of the carapace in ventral view. Asterisks indicate scapular pits; dashed line indicates inferred attachment of the body wall. Abbreviations: CS, cervical scute; M1, first marginal. The specimen is presented as a three-dimensional model in orthographic projection with Radiance Scaling enabled.

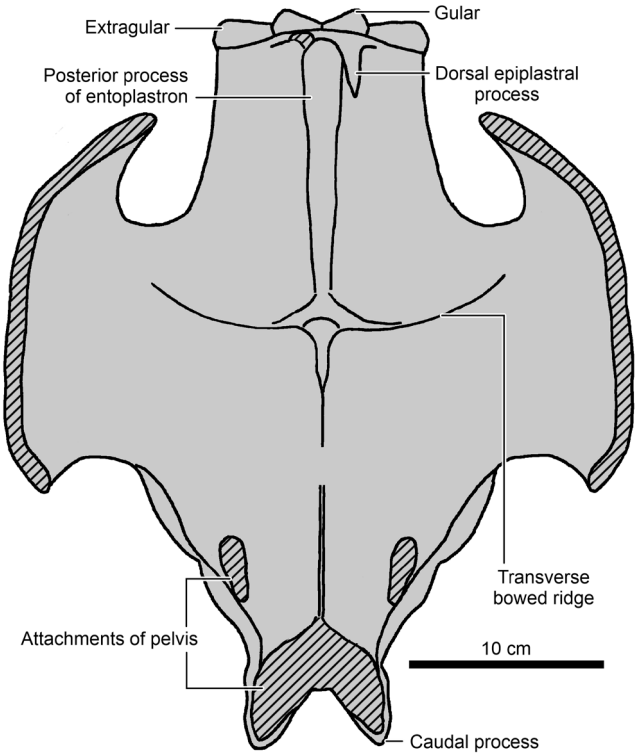

Figure 6. *Proterochersis porebensis*, restoration of the inner surface of the plastron.

very subtle transverse groove located ~1 cm from the anterior edge, but other than that the specimen presents no detectable features. A similar featureless visceral surface is also present in another small specimen, ZPAL V. 39/390 (Fig. 2B). *ZPAL V. 39/48* (Figs 2C, 3A) has the body wall boundary also very close to the anterior edge, followed by a more marked, wide groove, laterally widening, deepening and continuing into the marginal scute sulci. Despite some damage, *ZPAL V. 39/72* (Fig. 2D) presents morphology mostly resembling ZPAL V. 39/22, with two narrow transverse grooves separated by a ridge. ZPAL V. 39/161 (Fig. 2E) and *ZPAL V. 39/49* (Fig. 2G, 3B) are more similar to *ZPAL V. 39/34* and *ZPAL V. 39/48*, with a single, laterally broadening and deepening transverse groove, more pronounced than in the latter two, and the body wall very close to the anterior edge of the nuchal (i.e. with little to no ventral exposition of the cervical scute). They differ, however, from the remaining specimens in having a much thicker anterior edge, as if the anterior, scute-covered anteroventral third of the nuchal of ZPAL V. 39/22 and *ZPAL V. 39/72* turned completely anteriorly (vertically, perpendicularly to the long axes of the anterior marginals).

Proterochersis robusta SMNS 17930 (Fig. 4A, B) is the only specimen of that species with preserved and viscerally exposed nuchal bone, and fortunately, the preservation is very good, showing a combination of the morphologies observed in the specimens of *Proterochersis porebensis*. The body wall boundary is separated from the anterior edge of the carapace by a rough band followed by a narrow transverse groove and ridge, as in ZPAL V. 39/22 and *ZPAL V. 39/72*. Behind that, there is a wide, laterally broadening and deepening groove. The anterior part of that groove is rugose. The area around the first dorsal vertebra and scapular pits in SMNS 16442 (Fig. 4C–E) is damaged in the actual carapace fragment (Fig. 4C) but documented in a slightly better, more complete state as a plaster cast (Fig. 4F). However, the area of the nuchal is only imprinted on the associated steinkern (Fig. 4D, E); the preservation is poor, but the morphology appears to be roughly similar to that in SMNS 17930. SMNS 17561 shows only that the body wall boundary was separated from the anterior edge of the carapace, but most of the visceral surface of that region is embedded in matrix. Although ankylosed and thus devoid of sutures, based on a comparison of topological features (grooves, cervical and marginal scute sulci, etc.), these more complete specimens show that the nuchal is well separated from the attachment of the first dorsal vertebra and pits for the scapulae, and that the body wall projected far anteriorly above the neck, compared with the areas immeditately lateral to it (Szczygielski 2017).

Scapular pits, in both *Proterochersis porebensis* and *Proterochersis robusta*, are well marked (Figs 1–4). They are elongated anterolaterally and exhibit some variability in shape, from drop-shaped (e.g. *Proterochersis porebensis ZPAL V. 39/48*, Figs 2C, 3A; *Proterochersis robusta SMNS 12777*, Fig. 4H; SMNS 16442, Fig. 4C–F) to elongated oval (e.g. *Proterochersis porebensis ZPAL V. 39/72*, Fig. 2D; *Proterochersis robusta* SMNS 17930, Fig. 4A, B). This variability does not correspond in a clear way to the size and deformation of the specimens.

The carapace reaches its maximum medial thickness between the scapular pits and the nuchal. It is, therefore, possible that many of the soft tissue structures attaching to the nuchal in recent turtles were located behind that bone in *Proterochersis* spp.

The cleithrum in *Eunotosaurus africanus* is small, splint-like, and articulated along the anterior edge of the scapula, dorsal to the clavicle (Cox 1969, Lyson *et al.* 2013a). No data are available on the cleithrum/nuchal in *Pappochelys rosinae*, *Eorhynchochelys sinensis* and *O. semitestacea*. Unfortunately, owing to ankylosis (eradication of sutures; Pritchard 2008, Szczygielski and Słowiak 2022) commonly occurring in most Late Triassic turtles (especially carapaces, and particularly problematic in the case of the nuchal, pygal and suprapygals, which typically lack features that allow easy tracing of their limits), virtually no data are available on the exact boundaries of the nuchal bone in these taxa. Therefore, all observations and available morphological descriptions concern the cervical scute and associated areas rather than the nuchal per se. In *Proganochelys quenstedtii*, this region is rather featureless, but Gaffney (1990) noted that the body wall was attached very close to the anterior edge of the carapace, and the nuchal did not form any overhang. This is different from some specimens of *Proterochersis* spp., albeit not by much. Moreover, in *Proganochelys quenstedtii*, the scapular pits are more rounded, smaller, and separated further away from the midline than in the proterochersids (Fraas 1899, Jaekel 1918, Gaffney 1990). *K. limendorsa* appears to have a substantially larger overhang (Fig. 5; Joyce *et al.* 2013, Szczygielski and Sulej 2016, Szczygielski 2017), but this area is preserved only in part in that turtle, and the state of preservation of the bone surface commands caution. This region is too damaged in *Palaeochersis talampayensis* and *W. cavitesta* to provide any useful information (Sterli *et al.* 2007, 2021; T. Szczygielski, personal observation).

In recent turtles, the nuchal is single (unpaired) and proportionally much larger than in *Proterochersis porebensis*, although at least in some extant species it arises from small, paired anlagen

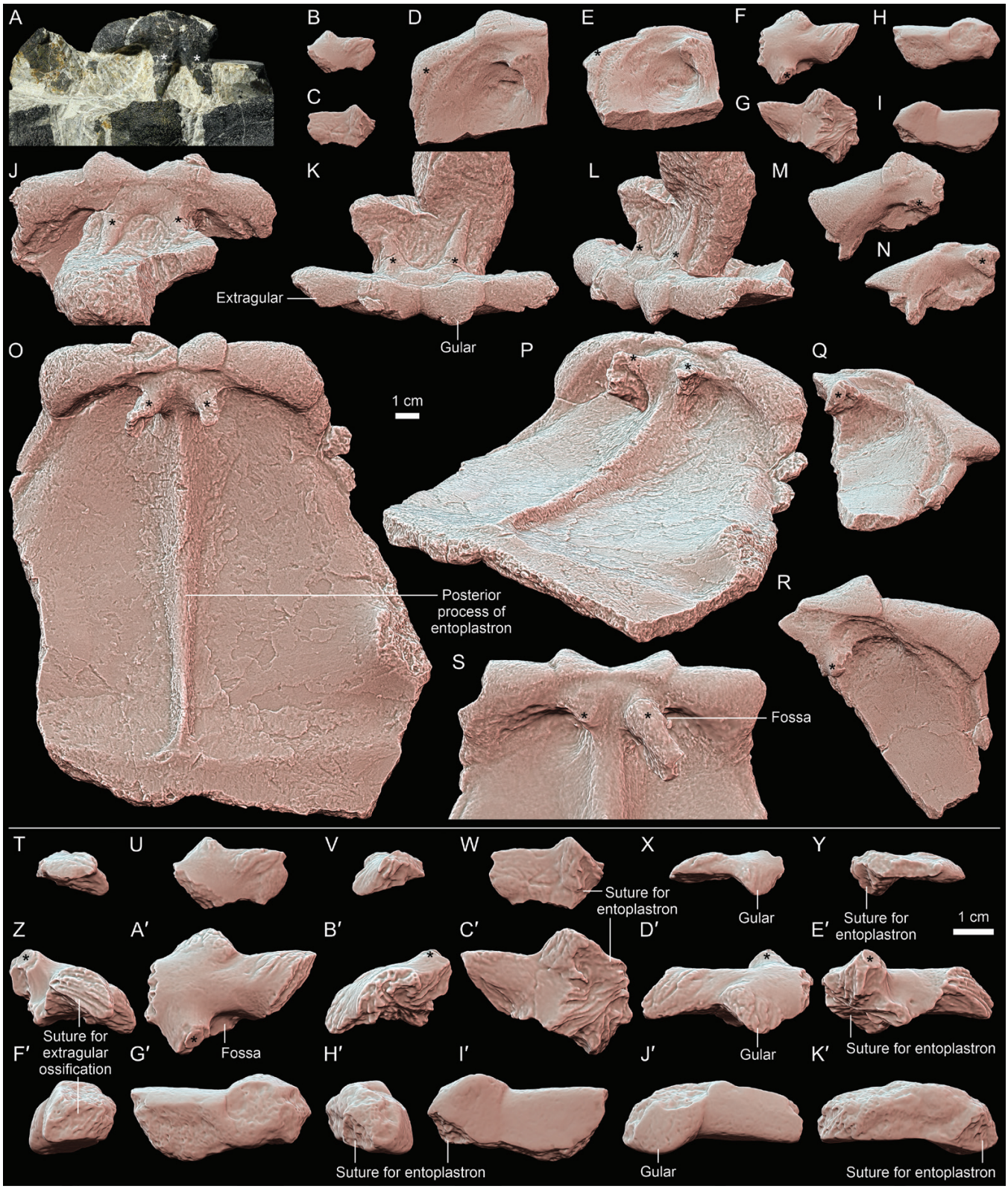

Figure 7. *Proterochersis porebensis*, gular region of the plastron. A, *ZPAL V. 39/34*, gular region in dorsal view. B, C, T–Y, ZPAL V. 39/501, isolated right epiplastron in dorsal (B, U), ventral (C, W), lateral (T), medial (V), anterior (X) and posterior (Y) view. D, E, ZPAL V. 39/387, left half of the gular region in dorsal (D) and posterodorsal (E) view. F, G, Z–E', ZPAL V. 39/404, isolated right epiplastron in dorsal (F, A'), ventral (G, C'), lateral (Z), medial (B'), anterior (D') and posterior (E') view. H, I, F'–K', ZPAL V. 39/503, isolated left epiplastron in dorsal (H, G'), ventral (I, I'), lateral (F'), medial (H'), anterior (J') and posterior (K') view. J–L, *ZPAL V. 39/48*, gular region in dorsal (J), anterior (K) and left anterolaterodorsal (L) view. M, N, ZPAL V. 39/420, left half of the gular region in dorsal (M) and posterolaterodorsal (N) view. O, P, ZPAL V. 39/385, anterior plastral lobe in dorsal (O) and right posterolaterodorsal (P) view. Q, R, ZPAL V. 39/379, right half of the gular region in posterolaterodorsal (Q) and dorsal (R) view. S, *ZPAL V. 39/49*, gular region in dorsal view. Specimens are sorted roughly by size, in B–K' presented as three-dimensional models in orthographic projection with Radiance Scaling enabled. Asterisks indicate dorsal processes of epiplastra.

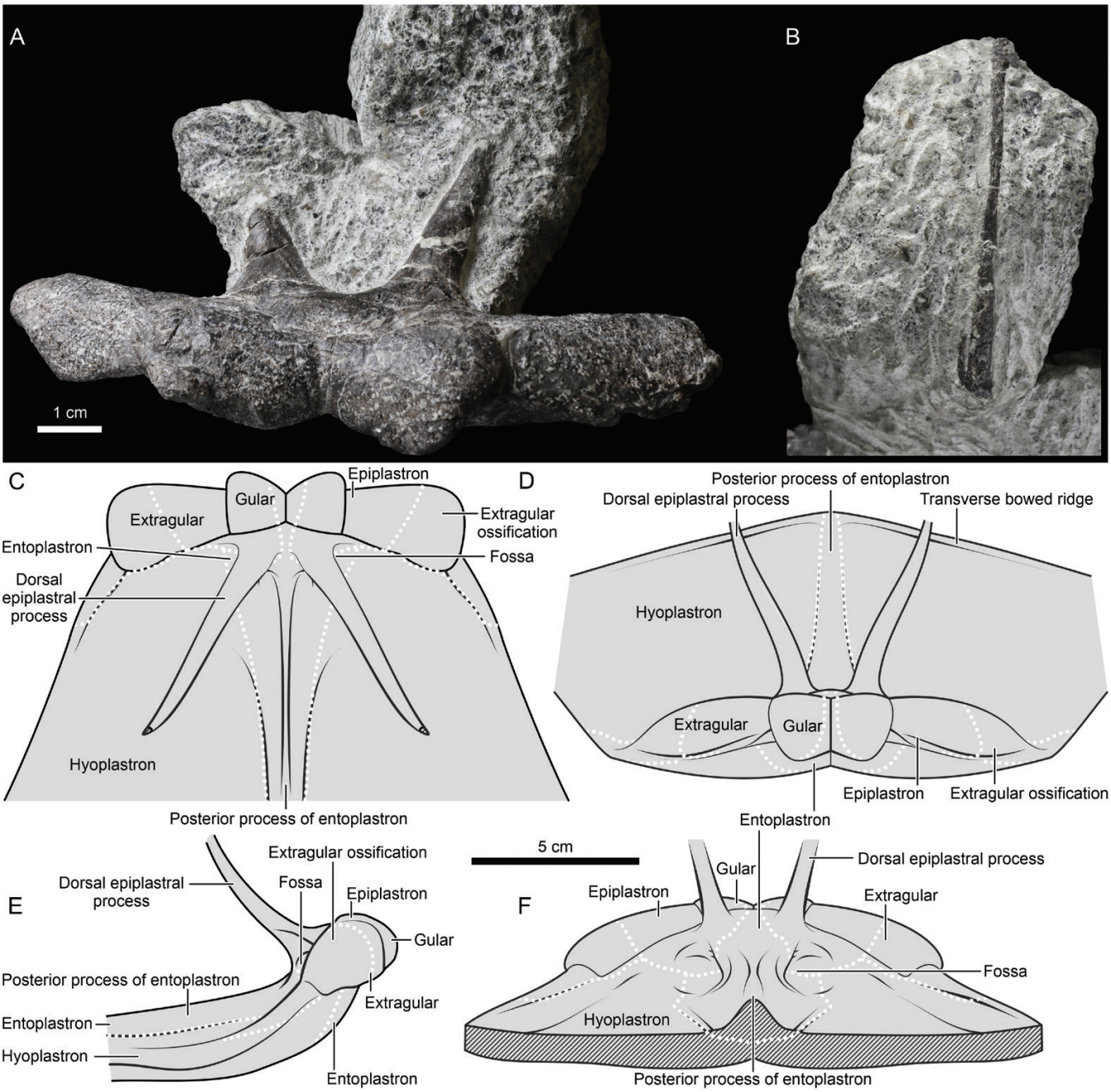

Figure 8. *Proterochersis porebensis*, gular region of the plastron. A, B, *ZPAL V. 39/48*, dorsal processes of the epiplastra: bases in anterodorsal view (A) and probable broken off dorsal fragment in probable posterior view (B). C–F, restoration of the gular region of the plastron in dorsal (C), anterodorsal (D), lateral right (E) and posterior (F) view. Sutures are indicated by white dotted lines. Note that the inclination of the dorsal processes of the epiplastra is only approximate.

(e.g. Vallén 1942, Cherepanov 1995, Sánchez-Villagra *et al.* 2009, Lyson *et al.* 2013b). In the Australochelyids and *Proganochelys quenstedtii*, dorsal attachments of the dorsal (ascending) epiplastral processes were present in this area, shielding the scapular pits anteriorly (Jaekel 1914, 1918, Gaffney 1985, 1990, Sterli *et al.* 2007, 2021).

Epiplastron (clavicle)

The epiplastra of *Proterochersis porebensis* are represented both in isolation (right: ZPAL V. 39/404, Fig. 7F, G, Z–E', see Szczygielski and Sulej 2019; and ZPAL V. 39/501, Fig. 7B, C, T–Y; left: ZPAL V. 39/503, Fig. 7H, I, F'–K') and as parts of more complete plastra (numerous specimens, with the most informative being *ZPAL V. 39/34*, Fig. 7A; *ZPAL V. 39/48*, Figs 7J–L, 8A, B, 9A; *ZPAL V. 39/49*, Figs 7S, 9B; ZPAL V. 39/379, Fig. 7Q, R; ZPAL V. 39/385, Fig. 7O, P; ZPAL V. 39/387, Fig. 7D, E; and ZPAL V. 39/420, Fig. 7M, N; for a more complete list, see Szczygielski *et al.* 2018). *Proterochersis robusta* preserves the epiplastra as parts of largely complete shells, CSMM uncat. (partial right) and SMNS 17561 (left and right) without visceral exposure (Karl and Tichy 2000, Szczygielski and Sulej

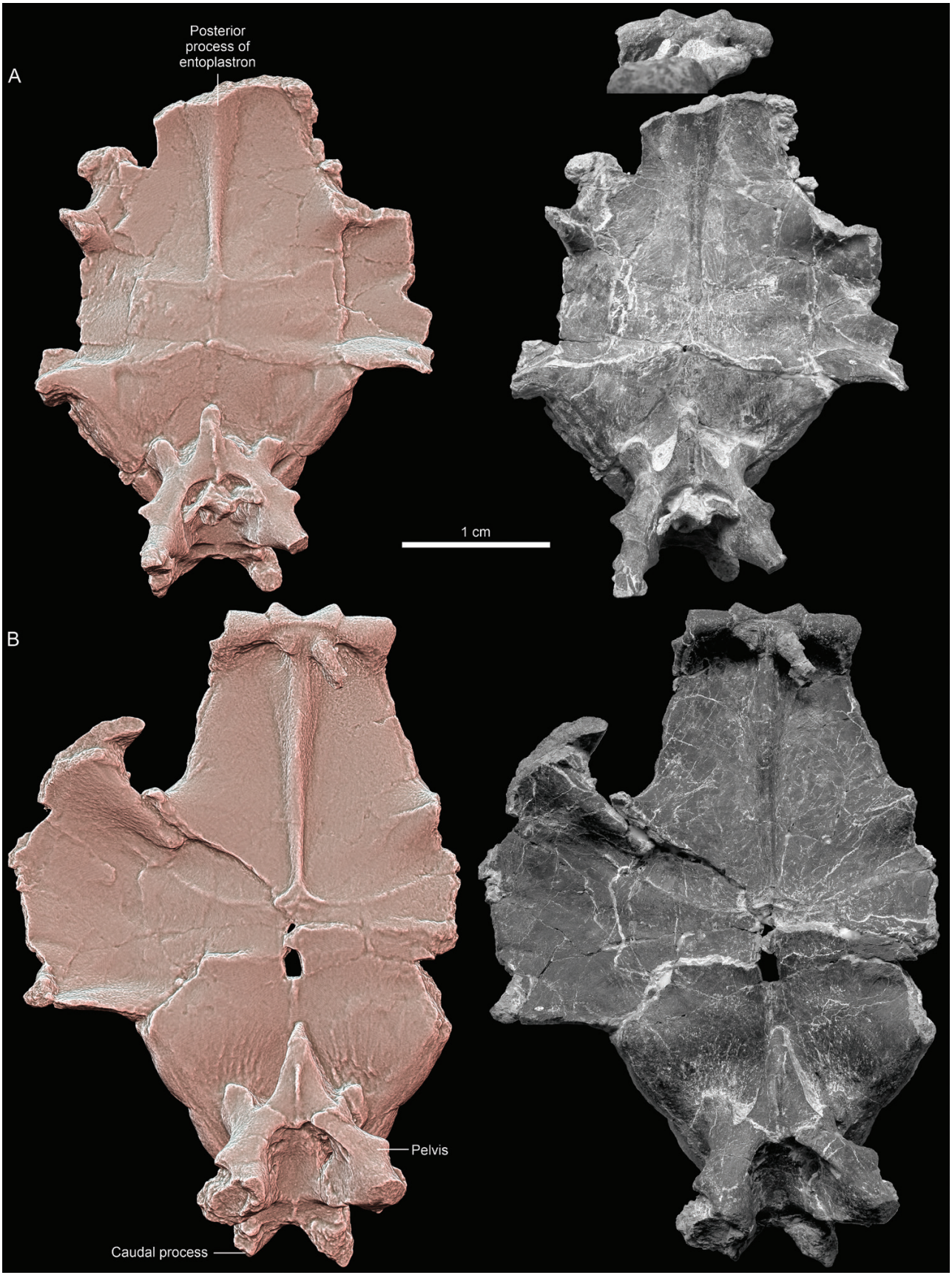

Figure 9. *Proterochersis porebensis*, plastra with attached pelves in dorsal view. A, *ZPAL V. 39/48*; B, *ZPAL V. 39/49*. Specimens are presented as three-dimensional models in orthographic projection with Radiance Scaling enabled (left) and photographs (right).

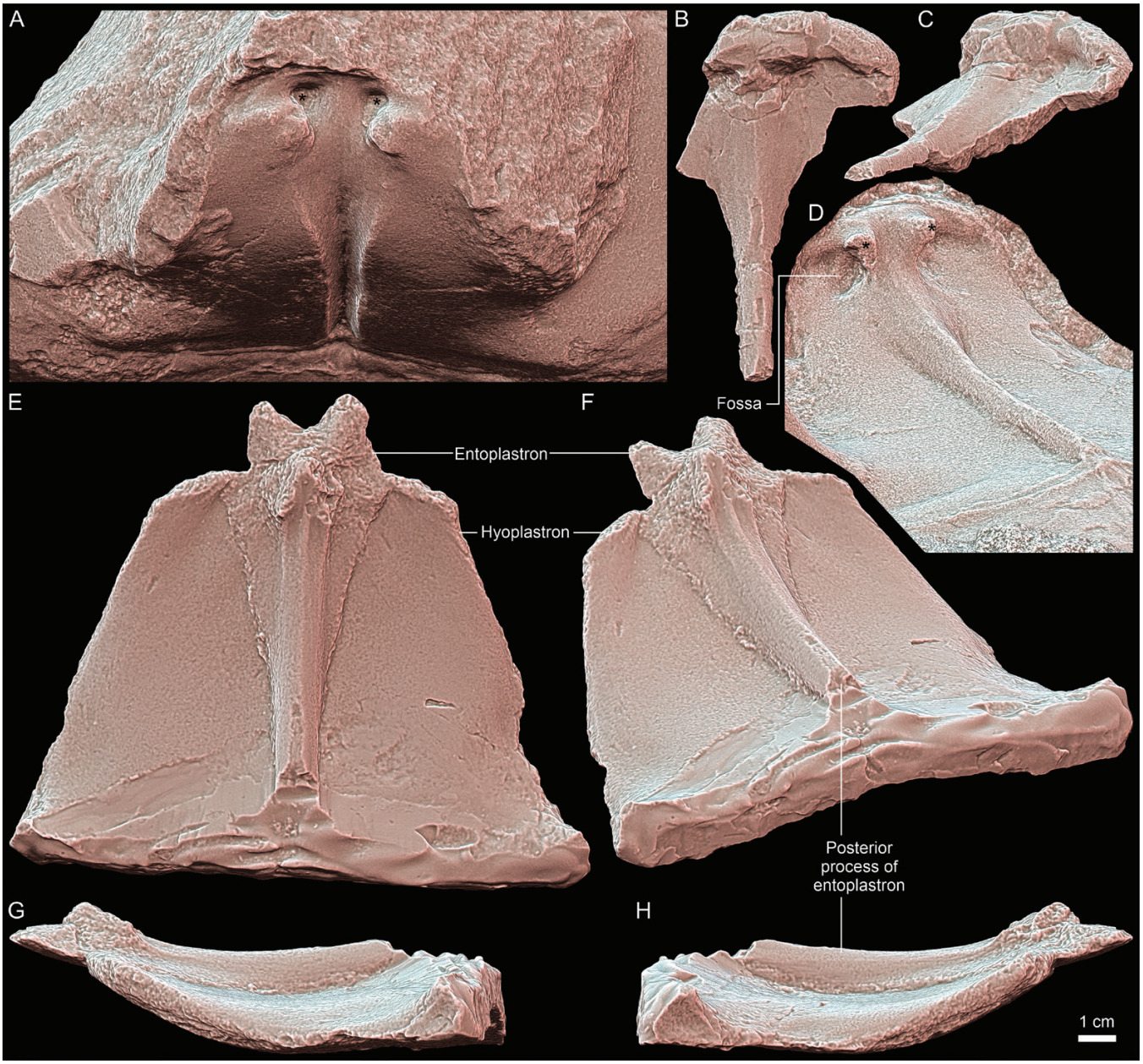

Figure 10. *Proterochersis robusta*, gular region of the plastron. A–D, SMNS 16603, natural cast of the visceral surface of the plastron in anterior view (A), preserved part of the plastron in dorsal (B) and right posterolaterodorsal (C) view, and digitally inverted cast (the same as in A) in left posterolaterodorsal view, showing morphology in a less damaged state. E–H, SMNS 16442, anterior plastral lobe missing epiplastra in dorsal (E), left posterolaterodorsal (F), left lateral (G) and right lateral (H) view. Specimens are presented as three-dimensional models in orthographic projection with Radiance Scaling enabled. Asterisks indicate dorsal processes of epiplastra.

2016, Szczygielski *et al.* 2018) and, viscerally exposed but damaged, in the juvenile SMNS 16603 (Fig. 10A–D; de Broin 1984, Szczygielski and Sulej 2016, 2019, Szczygielski *et al.* 2018).

The epiplastron of *Proterochersis porebensis* (and, inferred based on the comparison of SMNS 16603 with other specimens, also in *Proterochersis robusta*) is not particularly plate-like compared with other turtles, Late Triassic species included (de Broin 1984, Gaffney 1985, 1990, Jenkins *et al.* 1994, Rougier *et al.* 1995, Sterli *et al.* 2007, 2021, Marzola 2019). In the mediolateral aspect, it has a markedly convex dorsal surface and concave ventral surface. Its anteromedial and anterolateral edges project anteroventrally curved processes supporting the lateral parts of the gular scutes and medial parts of the extragular scutes (absent in juveniles). It articulates with the anterodorsolateral surface of the entoplastron via a large ventromedial suture. The anterior extent of this suture varies between the specimens: it extends significantly further anteriorly relative to the length of the gular projection in ZPAL V. 39/404 and ZPAL V. 39/501 than in ZPAL V. 39/503, and the suture is more (but not completely) vertical in the latter specimen than in the former two, although the available sample makes it uncertain whether that difference results from differences in the ontogenetic age of the respective individuals or whether it represents intraspecific variability. The contralateral epiplastra probably do not meet

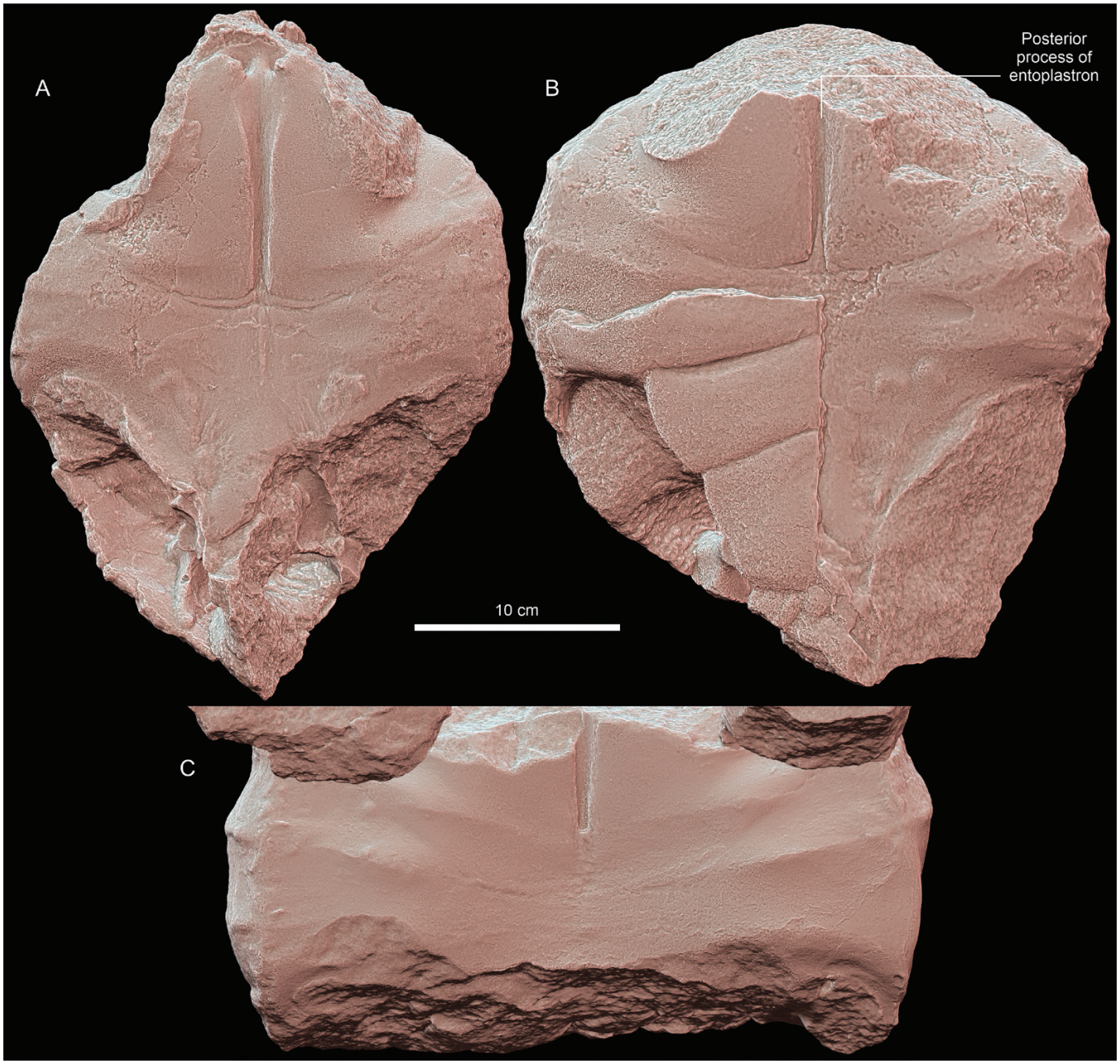

Figure 11. *Proterochersis robusta*, visceral surface of the plastra as represented by steinkerns in ventral view. A, SMNS 16603, showing an impression of the dorsal (visceral) surface of the plastron. B, *SMNS 12777*, showing partly preserved plastron (posterior right quarter) and an impression of the dorsal (visceral) surface of the rest, except for the missing anterior lobe. C, SMNS 16442, showing partial impression of the dorsal (visceral) surface of the plastron, missing the anterior and posterior lobes (but see Figs 10E–H, 27U). Specimens are presented as three-dimensional models in orthographic projection with Radiance Scaling enabled.

mesially (Fig. 8C–F; *contra* de Broin 1984), as suggested by SMNS 16442 (Fig. 10E–H) and the anterolateral direction and position relative to the dorsal process of the medial suture of ZPAL V. 39/404 (Fig. 7F, G, Z–E'). Laterally, along an elongated, anterolaterally aligned suture, the epiplastron contacts the supernumerary (extragular) plastral ossification, which supports the remainder of the extragular scute, separating it from the anterolateral corner of the anterior plastral lobe (Fig. 8C–F; Szczygielski and Sulej 2019). Depending on the specimen, only about the lateral half of the ventral surface of the epiplastron can be exposed on the external (ventral) surface of the plastron (Fig. 7G, W, C', I'; note that ZPAL V. 39/501 and ZPAL V. 39/503 are missing large parts of their posteromedial portions, meaning that the amount of ventrally exposed area is exaggerated in those specimens).

Posterodorsally, each epiplastron projects a splinter-like dorsal (ascending) process (Figs 6, 7–9, 10A–D). Usually, only the very bases of these processes are preserved, with the exception of *ZPAL V. 39/34* (Fig. 7A), *ZPAL V. 39/48* (the largest part preserved; Figs 7J–L, 8A, B, 9A) and *ZPAL V. 39/49* (unprepared; Figs 7S, 9B). The presence of large dorsal processes of the epiplastra is a plesiomorphic character, present in the

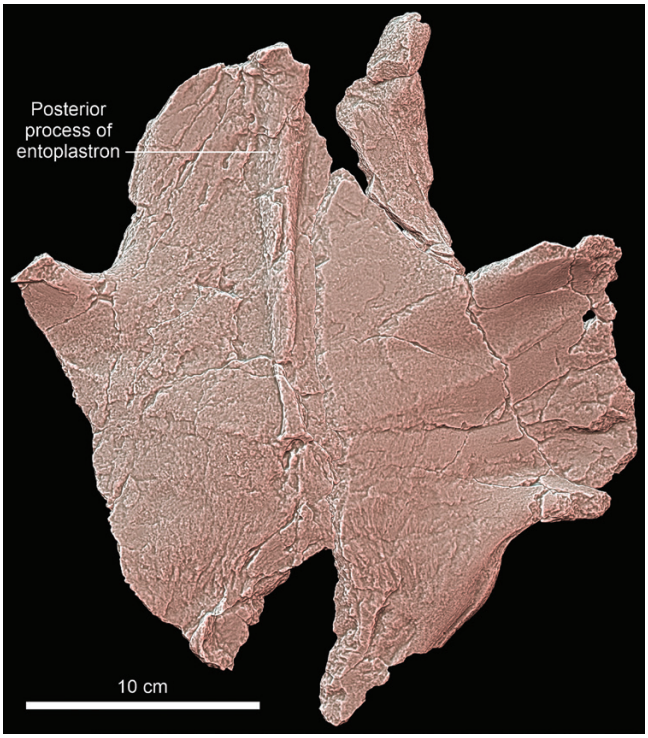

Figure 12. *Keuperotesta limendorsa*, *SMNS 17757*, plastron in dorsal (visceral) view. The specimen is presented as a three-dimensional model in orthographic projection with Radiance Scaling enabled.

Triassic in *O. semitestacea* (see Li *et al.* 2008), Proterochersidae (Szczygielski and Sulej 2016, 2019, Szczygielski *et al.* 2018), *Proganochelys quenstedtii* (see Gaffney 1990), aff. *Proganochelys ruchae* (see de Broin 1984), 'cf. *Proganochelys*' from Greenland (Jenkins *et al.* 1994, Marzola 2019), *Palaeochersis talampayensis* (see Rougier *et al.* 1995, Sterli *et al.* 2007) and *W. cavitesta* (see Sterli *et al.* 2021). In a reduced form, the dorsal epiplastral processes are present in a number of stem turtles (e.g. Gaffney 1996, Joyce *et al.* 2006, Sukhanov 2006, Anquetin 2010; for the most recent discussion of the historically proposed homology of those elements with cleithra, see Lyson *et al.* 2013b; and for an extensive list of historical literature on the topic, see Szczygielski and Sulej 2019).

The dorsal processes of the epiplastra in *Proterochersis porebensis* and *Proterochersis robusta* are small in comparison to other Triassic turtles and occupy only a restricted area in the median region of the anterior edge of the plastron, approximately defined by the lateral extent of the gular scutes. In *Proganochelys quenstedtii*, aff. *Proganochelys ruchae*, *Palaeochersis talampayensis* and *W. cavitesta* they are larger, more widely separated, and stem from a very pronounced elevation stretching across the whole anterior edge of the plastron, or only barely narrower (de Broin 1984, Gaffney 1985, 1990, Sterli *et al.* 2007, 2021). This is particularly visible in *Palaeochersis talampayensis* and *W. cavitesta*, in which the bases of the dorsal epiplastral processes together with the elevation they are set upon are nearly pyramidal, anteroposteriorly flattened, and project well-defined anterolateral ridges to the lateralmost corners of the anterior plastral lobe (Sterli *et al.* 2007, 2021). The difference in the lateral extent of the processes is probably caused by the presence of an additional ossification lateral to each epiplastron in *Proterochersis porebensis* (and, probably, *Proterochersis robusta*), which is absent in more derived forms (Szczygielski and Sulej 2019). The bases of the dorsal epiplastra processes in *Proterochersis* spp., *Proganochelys quenstedtii* and aff. *Proganochelys ruchae* are located immediately behind the sulci of the anterior plastral scutes (extragulars and/or gulars), which coincide with the attachment of the body wall and the nuchal ligament (Bojanus 1819; Figs 6–9, 10A–D), and thus were covered by only a thin layer of soft tissues. The morphology in the australochelyids had to be the same, but the shape of the anterior part of the plastron in these turtles makes it uncertain how close the scutes approached the processes, and the preservation prohibits identification of the boundary based on the sculpture (Sterli *et al.* 2007, 2021; T. Szczygielski, personal observation). The cross-section of the base of each dorsal epiplastral process is kidney-shaped (concave posterolaterally) to subtriangular in *Proterochersis porebensis*, subcircular in *Proganochelys quenstedtii*, aff. *Proganochelys ruchae* (see de Broin 1984, Gaffney 1990) and 'cf. *Proganochelys*' from Greenland (Jenkins *et al.* 1994, Marzola 2019), and oval in *Palaeochersis talampayensis* (see Sterli *et al.* 2007). In comparison to the dorsally or dorsolaterally projecting dorsal epiplastral processes of the remaining Triassic turtles (Jaekel 1918, Gaffney 1985, 1990, Sterli *et al.* 2007, 2021), the processes in *Proterochersis porebensis* appear to be directed more posteriorly. This, however, might be caused by post-mortem deformation of these delicate structures.

Posteroventrolaterally to the dorsal process of the epiplastron is a distinct fossa (Figs 7–10), in ZPAL V. 39/404 containing a vascular foramen in its lateral part (Fig. 7E'). This fossa is medially walled and mostly floored by the entoplastron. It is very prominent, underlying a significant part of the dorsal process of the epiplastron and having a subvertical anterior wall. Laterally, it is shielded, in part, by the elevation of the anterolateral corner of the plastron, meaning that it opens mostly posteroventrolaterally. A very similar morphology is also present in the juvenile *Proterochersis robusta* individual SMNS 16603, although, as preserved on the plastron of that specimen, the fossae appear inconspicuous owing to damage (de Broin 1984), the natural mould on the ventral surface of the associated steinkern shows relatively deep fossae. Nonetheless, it is relatively shallow (roofed only by a low, dorsolaterally directed ridge on the gently concave posterior surface of the elevation for the dorsal process) and completely open laterally in *Palaeochersis talampayensis* (T. Szczygielski, personal observation). Paradoxically, in *Palaeochersis talampayensis*, although the dorsal processes themselves are more widely separated than in *Proterochersis* spp., the fossae in that region approach the midline and are separated by only a narrow mesial ridge, probably formed by the entoplastron (Sterli *et al.* 2007). In *Proganochelys quenstedtii*, aff. *Proganochelys ruchae* and 'cf. *Proganochelys*' from Greenland, owing to the rounder profile of the bases of the dorsal epiplastral processes, their elevation and the anterior part of the entoplastron, there are basically no pouch-like fossae in that region (de Broin 1984, Gaffney 1985, 1990, Jenkins *et al.* 1994, Marzola 2019).

The dorsal process of the epiplastron in *Proterochersis porebensis* does not form any strong connection to the visceral surface of the carapace, unlike *Proganochelys quenstedtii*, *Palaeochersis talampayensis* and *W. cavitesta*, in which it broadens dorsally and creates a wide suture posteroventrally to the anterior marginals and anteriorly to the pit for the scapula (Jaekel

1918, Gaffney 1985, 1990, Sterli *et al.* 2007, 2021). Instead, it remains splint-like along at least most of its length, as evidenced by *ZPAL V. 39/48* (Fig. 8B). If any connection was formed, it would have to be so minor that it is indistinguishable in the preserved material (Figs 2, 3). The same is true for *Proterochersis robusta* (Fig. 4), in which the lack of connection is also supported by the steinkerns.

The main plate of the epiplastron in *Proganochelys quenstedtii*, aff. *Proganochelys ruchae* and *Palaeochersis talampayensis* (ambiguously, owing to preservation) has a conspicuous posterolateral projection supporting the anterolateral part of the humeral scute (Gaffney 1985, 1990, Rougier *et al.* 1995, Sterli *et al.* 2007). This projection is absent in *Proterochersis porebensis*, and the epiplastron ends laterally in a posteromedial suture before reaching the lateral edge of the extragular scute (ZPAL V. 39/404, Fig. 7F, G, Z–E'; ZPAL V. 39/503, Fig. 7H, I, F'–K'). The anterolateral edge of the hyoplastron of SMNS 16442 is rounded (Fig. 10E–H), suggesting that it was indeed supplemented by another bone. This was most probably done by the extragular ossification (Fig. 8C–F; Szczygielski and Sulej 2019; ZPAL V. 39/186, an isolated specimen of that ossification, does not have this posterolateral projection preserved but has a broken surface in that part, suggesting that some, probably smaller, projection was indeed there). ZPAL V. 39/501 (Fig. 7B, C, T–Y), an epiplastron of a probable juvenile, lacks the slanted posterolateral suture, and its extragular process is relatively narrow mediolaterally and rugose; given that this is a small specimen, it seems plausible that the separate extragular ossification was either not yet present at this stage of development (its presence is not verifiable in *ZPAL V. 39/34*, but that specimen also lacks any distinct extragular projection; Fig. 7A; Szczygielski and Sulej 2016, Szczygielski *et al.* 2018) or did not yet form a sutural connection with the epiplastron.

Given that *Eunotosaurus africanus*, *Pappochelys rosinae* and *Eorhynchochelys sinensis* have no plastra, their clavicles are free but, at least in the latter two, their general form is close to that in *O. semitestacea* and *Proterochersis* spp., being slender and subvertical in their dorsal part, and flattened and subhorizontal in their ventral part (Watson 1914, Cox 1969, Lyson *et al.* 2013a, Schoch and Sues 2015, 2017, Li *et al.* 2018). In *Pappochelys rosinae* and *Eorhynchochelys sinensis*, ventral parts of the clavicles are expanded (Schoch and Sues 2015, 2017, Li *et al.* 2018). In *O. semitestacea*, the morphology is intermediate between *Pappochelys rosinae* and *Proterochersis* spp.: the clavicles are gently curved, rod-shaped elements with expanded ventral parts, which articulated with the interclavicle via a complex, ventromedial suture (Li *et al.* 2008, Nagashima *et al.* 2013). The extent of their ventral exposure in that animal is ambiguous, and various interpretations have been proposed (Li *et al.* 2008, Nagashima *et al.* 2013, Lyson *et al.* 2014). Based on personal examination of the described specimens (particularly, IVPP V 15653), the version of Nagashima *et al.* (2013) is preferred here, with little to no ventral exposure of the clavicles and with the extragular projection probably formed by a separate element (T. Szczygielski, personal observation). The clavicles in non-testudinate pantestudinates differ from the epiplastra of true testudinates in the lateral position of their dorsal projections, whereas in turtles the dorsal processes, if present, arise close to the medial edges of the epiplastra (de Broin 1984, Gaffney 1985, 1990, 1996, Joyce *et al.* 2006, Sukhanov 2006, Sterli *et al.* 2007, Szczygielski and Sulej 2019). In more derived turtles, the epiplastra lack the dorsal processes, although mesenchymatic primordia of the clavicles arising dorsally (deep) to the epiplastra and subsequently descending to enter the plastral dermis are detectable at early developmental stages of extant turtles (Vallén 1942, Walker 1947, Cherepanov 1989).

Entoplastron (interclavicle)

The entoplastron of *Proterochersis porebensis* is known only as a part of plastra, with no identifiable sutural edges. The shape of that bone can be inferred, in part, from the sutures around the isolated epiplastra ZPAL V. 39/404 (Fig. 7F, G, Z–E'), ZPAL V. 39/501 (Fig. 7B, C, T–Y) and ZPAL V. 39/503 (Fig. 7H, I, F'–K'), and from the specimen SMNS 16442 of *Proterochersis robusta* (Fig. 10E–H), which reveals the sutural edges around most of its entoplastron (Szczygielski and Sulej 2019). Other than that, the visceral morphology of the entoplastron is best presented by *ZPAL V. 39/48* (Fig. 9A), *ZPAL V. 39/49* (Figs 7S, 9B) and ZPAL V. 39/385 (Fig. 7O, P) for *Proterochersis porebensis* and by SMNS 16603 (anterior part, Fig. 10A–D) and SMNS 16442 (Fig. 10E–H) for *Proterochersis robusta* (Szczygielski and Sulej 2016, 2019, Szczygielski *et al.* 2018). Aside from that, a number of fragmentary anterior plastral lobes of *Proterochersis porebensis* have some fragments of the entoplastron or its posterior process, usually not providing much morphological information. *Proterochersis robusta* steinkerns *SMNS 12777* (Fig. 11B), SMNS 16603 (Fig. 11A), SMNS 16442 (Fig. 11C) and SMNS 51441 preserve imprints of the posterior process of the entoplastron. The entoplastron is also present as a part of the more complete shells of the latter species, but not prepared from the visceral side, in CSMM uncat. and SMNS 17651.

Based on the available material, it can be inferred that the entoplastron of *Proterochersis porebensis* reaches the anterior edge of the plastron, contacts the ventromedial facets of the epiplastra, and supports the medial parts of the gular scutes and anteromedial parts of the humeral scutes. In *Proterochersis robusta* (SMNS 16442, Fig. 10E–H), externally (ventrally) it has a small, V-shaped exposure (Szczygielski and Sulej 2019), much smaller than in *Palaeochersis talampayensis* (see Sterli *et al.* 2007). It is exposed viscerally as a narrow band between the dorsal processes of the epiplastra, where it reaches its maximum thickness and ventral width. Its visceral exposure widens and thickness decreases anteriorly (towards the anterior edge of the plastron, underlying the intergular sulcus and adjacent areas) and posteriorly from that point, to start gradually to taper again posteriorly to the epiplastra. Unlike *Proganochelys quenstedtii* and *Palaeochersis talampayensis*, the entoplastron in *Proterochersis robusta* is widely separated from the lateral edges of the anterior plastral lobe and does not form posterolateral projections (Gaffney 1985, 1990, Sterli *et al.* 2007).

The anterior part of the entoplastron in *Proterochersis* spp. forms viscerally a relatively wide, rounded mesial elevation (Figs 6, 7D, E, O, P, S, 8–11), in contrast to a very narrow mesial ridge present in *Palaeochersis talampayensis* (see Sterli *et al.* 2007). In *Proterochersis robusta* SMNS 16442, the dorsal surface of that elevation bears three longitudinal ridges, with the middle one continuing onto the posterior process and the lateral ones

disappearing earlier (Fig. 10E–H), which are absent from the remaining specimens.

As in the remaining Late Triassic turtles (Jaekel 1914, 1918, Gaffney 1985, 1990, Jenkins *et al.* 1994, Rougier *et al.* 1995, Sterli *et al.* 2007, 2021, Szczygielski and Sulej 2016, 2019, Marzola 2019), the entoplastron in *Proterochersis porebensis* continues posteriorly as the viscerally exposed, very long posterior process (stem; Figs 6, 7O, P, S, 8–11). It takes the form of a prominent ridge, which gradually decreases in width and height posteriorly. In *Proterochersis porebensis*, it terminates in a triangular structure (rounded dorsally in *ZPAL V. 39/48*, Fig. 9A, and ZPAL V. 39/385, Fig. 7O, P, and convex in the middle part and rugose in *ZPAL V. 39/49*, Fig. 9B) at the level of about the middle of the bridge region, where it meets a transverse bowed (concave anteriorly) ridge (Figs 6, 7O, P, 8, 9). Roughly the same morphology is observed also in *Proterochersis robusta*, particularly in *SMNS 12777* (Fig. 11B) and SMNS 16603 (Fig. 11A). The posterior process of the entoplastron is preserved only in part in SMNS 16442 (Fig. 10E–H), and the associated steinkern suggests that it ended bluntly (Fig. 11C). However, the blunt end is followed by a mesial rugosity ending in a faint but otherwise normal-looking transverse bowed ridge (Fig. 11C). Given the mode of preservation of that region as a steinkern, it is uncertain whether this captures a genuine morphology or whether it is a result of damage to the visceral surface of the plastron. In *K. limendorsa*, the posterior process of the entoplastron also appears to end bluntly (although this might be influenced by damage), but it is gently widened and reaches the transverse bowed ridge (Fig. 12). Overall, in the Proterochersidae there seems to be some variability regarding the anteroposterior position of this ridge (and thus, the relative length of the posterior process of the entoplastron), but owing to the small sample of specimens presenting this area and the incompleteness of some of them, this variability is difficult to quantify, and its nature (e.g. ontogenetic, taxonomic, intraspecific) is difficult to establish. A similar transverse ridge, but rounder, wider and located closer to the inguinal notch, is also present in *Palaeochersis talampayensis* (see Sterli *et al.* 2007), but apparently not in *Proganochelys quenstedtii* (Jaekel 1914, 1918, Gaffney 1985, 1990; T. Szczygielski, personal observation). The triangular area at the end of the posterior process of the entoplastron corresponds to the attachment point of the pericardium (Bojanus 1819). In *Palaeochersis talampayensis* and *W. cavitesta*, the posterior process of the entoplastron retains roughly uniform, with a relatively small width along its whole length, but is longer in proportion to the length of the plastron, reaching the level of the inguinal notch (Sterli *et al.* 2007, 2021).

In *Eunotosaurus africanus*, the interclavicle takes the plesiomorphic form of a slender, flattened rod with an expanded, roughly pentagonal anterior end articulating with the dorsomedial surfaces of the clavicles, gradually increasing in width posteriorly along most of its length and not much longer than the scapulocoracoids (Watson 1914, Cox 1969, Gow 1997, Lyson *et al.* 2013a, 2014, 2016).

In *Pappochelys rosinae* (and, apparently, *Eorhynchochelys sinensis*, although in that animal it is largely obscured by other bones), the interclavicle is more cruciform, with a well-developed anterior process and thin, tapering lateral processes (Schoch and Sues 2015, 2017, Li *et al.* 2018).

In *O. semitestacea*, the interclavicle (best visible as an articulated element in IVPP V 15653) participates in the plastron as the entoplastron (Li *et al.* 2008). It is a polygonal plate with short, posterolaterally directed lateral processes, viscerally bearing sharp, pronounced ridges running along the anterolateral edges of the main plate, a low and wide mesial ridge, and geometrically complex, anterodorsolaterally facing sutures/articulation surfaces for the clavicles (Nagashima *et al.* 2013, Schoch and Sues 2017; T. Szczygielski, personal observation). The length of the posterior process of the entoplastron is unknown in that animal.

Scapulocoracoid

The scapulocoracoid of *Proterochersis porebensis* (Figs 13–16) is known as a nearly complete bone of the holotype, *ZPAL V. 39/48* (descibed in detail by Szczygielski and Sulej 2016; Figs 14A–F, 15, 16), in addition to 18 fragmentary specimens of various sizes, ranging from probable juveniles (ZPAL V. 39/431, Fig. 13M–Q; ZPAL V. 39/475, Fig. 13G–L; ZPAL V. 39/502, Fig. 13A–F) to adults (ZPAL V. 39/17, Fig. 14I'–N'; ZPAL V. 39/162, Fig. 14C'–H'). Eighteen of these represent scapulae (ZPAL V. 39/162, Fig. 14C'–H'; ZPAL V. 39/318, Fig. 14X–B'; ZPAL V. 39/391, Fig. 14R–W; ZPAL V. 39/421, Fig. 14M–Q; ZPAL V. 39/422, Fig. 13C'–H'; ZPAL V. 39/423; ZPAL V. 39/424, Fig. 13W–B'; ZPAL V. 39/425; ZPAL V. 39/426; ZPAL V. 39/427; ZPAL V. 39/428, Fig. 13R–V; ZPAL V. 39/429; ZPAL V. 39/430; ZPAL V. 39/431, Fig. 13M–Q; ZPAL V. 39/475, Fig. 13G–L; ZPAL V. 39/483, Fig. 13I'–M'; ZPAL V. 39/484, Fig. 14G–L; ZPAL V. 39/502, Fig. 13A–F). ZPAL V. 39/17 (Fig. 14I'–N') preserves the glenoid area and point of contact between the scapula and coracoid; and a nearly complete coracoid (missing a seemingly narrow posteromedial margin, as a result of either damage or incomplete ossification) is preserved only in *ZPAL V. 39/48* (Figs 14A–F, 15, 16).

As is typical for the Late Triassic turtles, the scapulocoracoid has a long dorsal process, nearly as long, plate-like coracoid and shorter acromion (Fig. 16). In *ZPAL V. 39/48*, the dorsal process of the scapula and acromion are set at an angle of ~105°, and the acromion and coracoid are set at an angle of ~120°. The latter angle is much smaller than in *K. limendorsa* (Fig. 17), *Palaeochersis talampayensis*, *Proganochelys quenstedtii* or *W. cavitesta* (see Szczygielski and Sulej 2016, Sterli *et al.* 2021), but this lower value is consistent with the fragmentary scapulae ZPAL V. 39/17 (Fig. 14I'–N'), ZPAL V. 39/162 (Fig. 14C'–H') and ZPAL V. 39/422 (Fig. 13C'–H'). When put on a flat surface, that scapulocoracoid rests on three support points: the tips of the acromion and coracoid, and the posteroventral edge of the glenoid (Figs 14A–F, 15, 16). Most of the ventral surface is therefore slightly raised. In that position, the dorsal process of the scapula is almost completely vertical, with its dorsal tip directed very slightly (~3°) anteriorly. This is significantly different from the known material of *Proganochelys quenstedtii*, in which the dorsal process is clearly turned anterodorsally (Jaekel 1914, 1918, Gaffney 1990), but more in line with *Keuperostesta limendorsa*, *O. semitestacea*, *Palaeochersis talampayensis*, *Pappochelys rosinae*, *W. cavitesta* and the new taxon from Greenland, which have a more vertical alignment of the scapula (Sterli *et al.* 2007, 2021, Li *et al.* 2008, Joyce *et al.* 2013, Schoch and Sues 2015, 2017, Szczygielski and Sulej 2016,

Figure 13. *Proterochersis porebensis*, scapulocoracoids in anterior (A, G, M, R, W, C', I'), medial (B, H, N, S, X, D', J'), posterior (C, I, O, T, Y, E', K'), lateral (D, J, P, U, Z, F', L'), dorsal (E, K, Q, V, A', G', M') and ventral (F, L, B', H') view. A–F, ZPAL V. 39/502, left acromion. G–L, ZPAL V. 39/475, right scapula. M–Q, ZPAL V. 39/431, dorsal process of the probable right scapula. R–V, ZPAL V. 39/428, dorsal process of the left scapula. W–B', ZPAL V. 39/424, ventral part of the left scapula. C'–H', ZPAL V. 39/422, right scapula. I'–M', ZPAL V. 39/483, dorsal process of the left scapula. Specimens are presented as three-dimensional models in orthographic projection with Radiance Scaling enabled, sorted roughly by size. Asterisks indicate coracoid foramina.

Marzola 2019). Although it is possible that the unusual orientation of the scapula in *Proganochelys quenstedtii* might be a result of post-mortem deformation (Joyce *et al.* 2013), this seems unlikely given that a similar inclination of the dorsal scapular process is shared between all *Proganochelys quenstedtii* specimens, and if the angle between the dorsal process of the scapula and the coracoid were to be reduced, the scapulacoracoid would be too short to articulate with the scapular pits on the visceral surface of the carapace (Gaffney 1990; T. Szczygielski, personal observation). The acromion is connected with the dorsal process of the scapula, glenoid and coracoid by web-like bone laminae, giving it a subtriangular cross-section. The web of bone stretching between the acromion and coracoid (horizontal ridge *sensu* Gaffney 1990 and Sterli *et al.* 2007) is herein called the acromiocoracoidal lamina (Fig. 16). Smaller webs of bone stretch between the acromion and the dorsal scapular process (acromioscapular lamina, resulting in a tear-shaped/subtriangular cross-section of the base of that process; anterodorsal ridge *sensu* Gaffney 1990 and Sterli *et al.* 2007) and between the acromion and the glenoid (acromioglenoidal lamina; ventral ridge *sensu* Gaffney 1990 and Sterli *et al.* 2007; Fig. 16). The acromioglenoidal lamina in *Proterochersis porebensis* is directed anteroventrally, rather than ventrally as in *Proganochelys quenstedtii* (Jaekel 1918, Gaffney 1990). This difference probably results from the (possibly artificial) more anterior direction of the dorsal scapular process in the specimens of the latter species.

The dorsal process of the scapula (scapular prong *sensu* Walker 1973) is nearly straight. In its elongation and slenderness, it is more similar to *K. limendorsa* (see Joyce *et al.* 2013), *Palaeochersis talampayensis* (see Sterli *et al.* 2007), *W. cavitesta* (see Sterli *et al.* 2021) or the new taxon from Greenland (Marzola 2019) than to *Eunotosaurus africanus* (Cox 1969, Gow 1997), *Pappochelys*

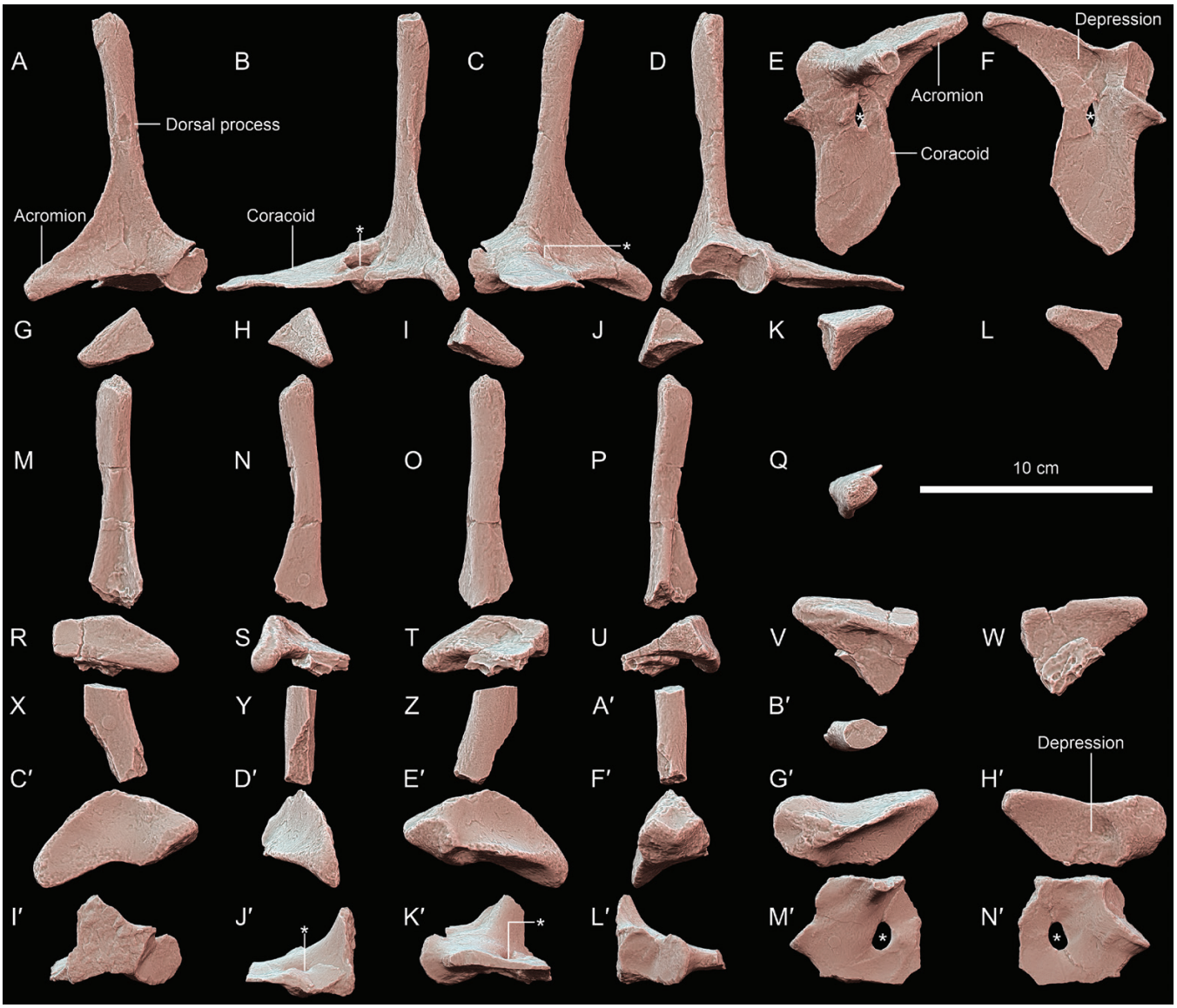

Figure 14. *Proterochersis porebensis*, scapulocoracoids in anterior (A, G, M, R, X, C', I'), medial (B, H, N, S, Y, D', J'), posterior (C, I, O, T, Z, E', K'), lateral (D, J, P, U, A', F', L'), dorsal (E, K, Q, V, B', G', M') and ventral (F, L, W, H', N') view. A–F, *ZPAL V. 39/48*, left scapulocoracoid. G–L, ZPAL V. 39/484, left acromion. M–Q, ZPAL V. 39/421, dorsal process of the left scapula. R–W, ZPAL V. 39/391, right acromion. X–B', ZPAL V. 39/318, dorsal process of the left scapula. C'–H', ZPAL V. 39/162, ventral part of the left scapula. I'–N', ZPAL V. 39/17, partial left scapulocoracoid. Specimens are presented as three-dimensional models in orthographic projection with Radiance Scaling enabled, sorted roughly by size. Asterisks indicate coracoid foramina.

rosinae (see Schoch and Sues 2015, 2017), *Eorhynchochelys sinensis* (see Li *et al.* 2018), *O. semitestacea* (see Li *et al.* 2008) or *Proganochelys quenstedtii* (see Jaekel 1914, 1918, Gaffney 1990). Anteromedially, it bears a longitudinal groove (Fig. 16A, B). This groove starts as a wide, triangular depression, limited by the edges of the acromioscapular and acromioglenoidal laminae and the broader, anterolateral edge of the dorsal process, which connects to the dorsal part of the glenoid area (Fig. 16A, B). This gives the base of the dorsal scapular process a subtriangular or teardrop-shaped cross-section. Dorsally, the groove decreases in width and continues past the dorsal limit of the acromioscapular lamina, in total extending along the ventral two-thirds of the dorsal process. The dorsal part of the groove is particularly pronounced in ZPAL V. 39/422 (Fig. 13C'–H'), which probably belonged to an individual slightly smaller than *ZPAL V. 39/48*. In that specimen, it bears longitudinal ridges (Fig. 13C', D'), which are absent from the remaining specimens. A similar, in some cases less pronounced, groove or depression is present in a corresponding area on the scapulae of *Pappochelys rosinae* (in an incipient form; see Schoch and Sues 2015, 2017), *O. semitestacea* (T. Szczygielski, personal observation; Li *et al.* 2008), *K. limendorsa* (see Joyce *et al.* 2013; T. Szczygielski, personal observation), *Proganochelys quenstedtii* (see Jaekel 1914, 1918, Gaffney 1990; T. Szczygielski, personal observation) and *W. cavitesta* (Sterli *et al.* 2021). Most of the dorsal two-thirds of the dorsal scapular process length shows a lanceolate, flat anterolateral surface, separated from the anteromedial groove by a low ridge, meaning that the process is never completely cylindrical. This flattened area is well visible in

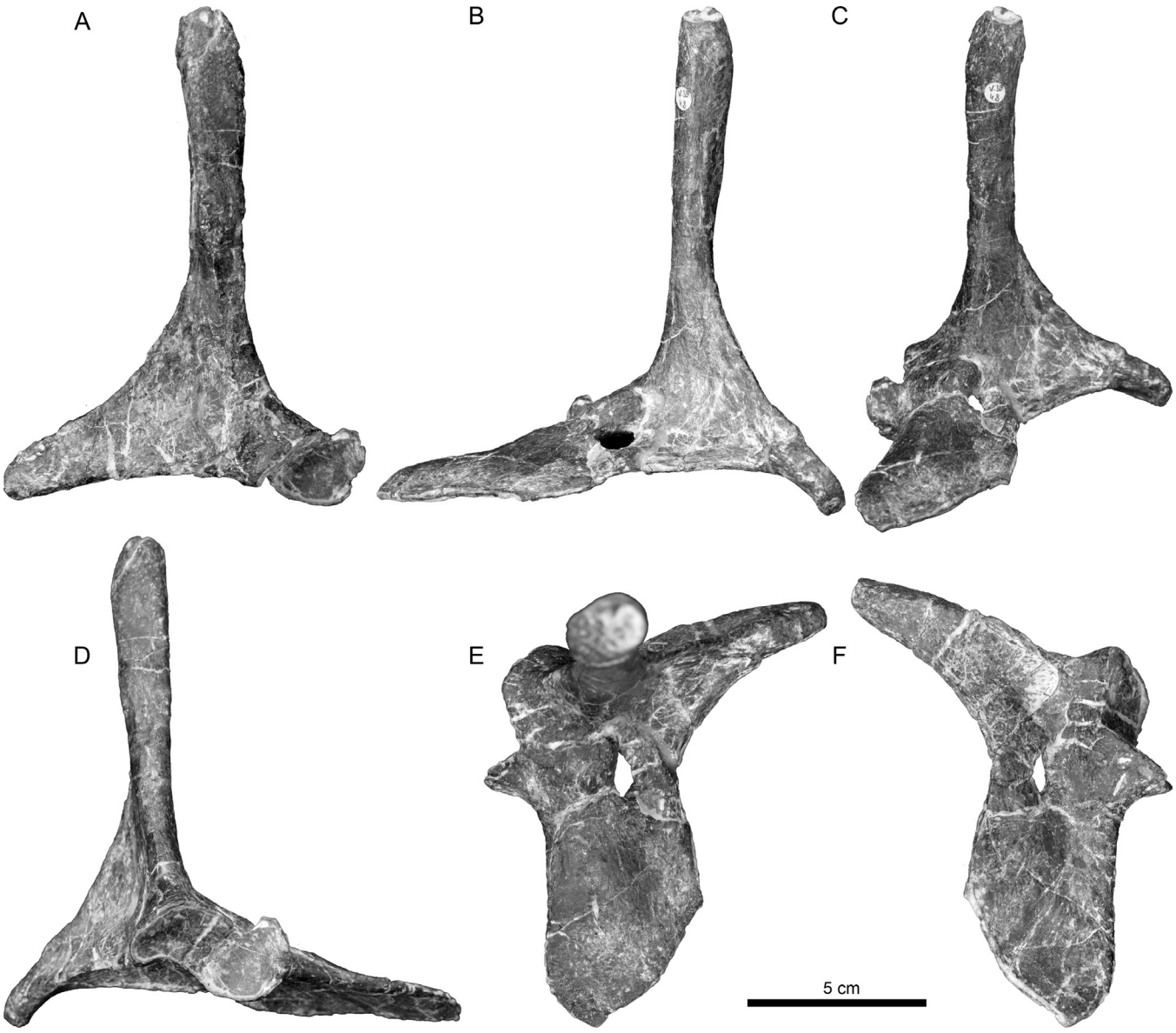

Figure 15. *Proterochersis porebensis*, *ZPAL V. 39/48*, photographs of the left scapulocoracoid in anterior (A), medial (B), posterior (C), lateral (D), dorsal (E) and ventral (F) view.

ZPAL V. 39/48 (Figs 14A, D, 15A, D), the similar-sized ZPAL V. 39/421 (Fig. 14M, P) and ZPAL V. 39/422 (Fig. 14C', F'), and is also present in *Pappochelys rosinae* (see Schoch and Sues 2015, 2017), *O. semitestacea* (T. Szczygielski, personal observation; Li *et al.* 2008), *K. limendorsa* (see Joyce *et al.* 2013; T. Szczygielski, personal observation), *Proganochelys quenstedtii* (see Jaekel 1914, 1918, Gaffney 1990; T. Szczygielski, personal observation), *W. cavitesta* (see Sterli *et al.* 2021) and the new taxon from Greenland (Marzola 2019). The scapulae of *Palaeochersis talampayensis* are insufficiently preserved to allow detection of these characters (T. Szczygielski, personal observation). The posteromedial surface of the process is rounded along its entire length. In *ZPAL V. 39/48*, in the dorsal end of the dorsal process of the scapula is a circular pit (Fig. 14E), which is likely to be a remnant of a suprascapular cartilage, pointing towards a subadult age of the individual (Szczygielski and Sulej 2016). This pit has sharp edges, and chemical preparation revealed that its surface is rugose and densely perforated by minute vascular openings, but no spongiosa is exposed, proving that the morphology is not a result of breakage or deformation. A shallower pit is present in the similar-sized specimen ZPAL V. 39/483 (Fig. 13M'), although this specimen shows some wear. It is apparent that the dorsal tip of the dorsal scapular process, ZPAL V. 39/421 (Fig. 14Q), was originally better ossified but is damaged. Dorsal parts of the scapulae of *K. limendorsa* (Fig. 17) and the new taxon from Greenland show longitudinal striation (Joyce *et al.* 2013, Marzola 2019), which is absent in *Proterochersis porebensis*, although in ZPAL V. 39/422 a smaller-scale striation is visible on the whole surface of the scapula (Fig. 13C'–F').

The acromion (Fig. 16) is gently curved away from the glenoid and lightly twisted, such that towards the apex its ventral surface becomes turned posteroventrally, slightly towards the coracoid. The apex of the acromion was capped by cartilage, as evidenced by its porous, unfinished surface in all specimens. The extent of

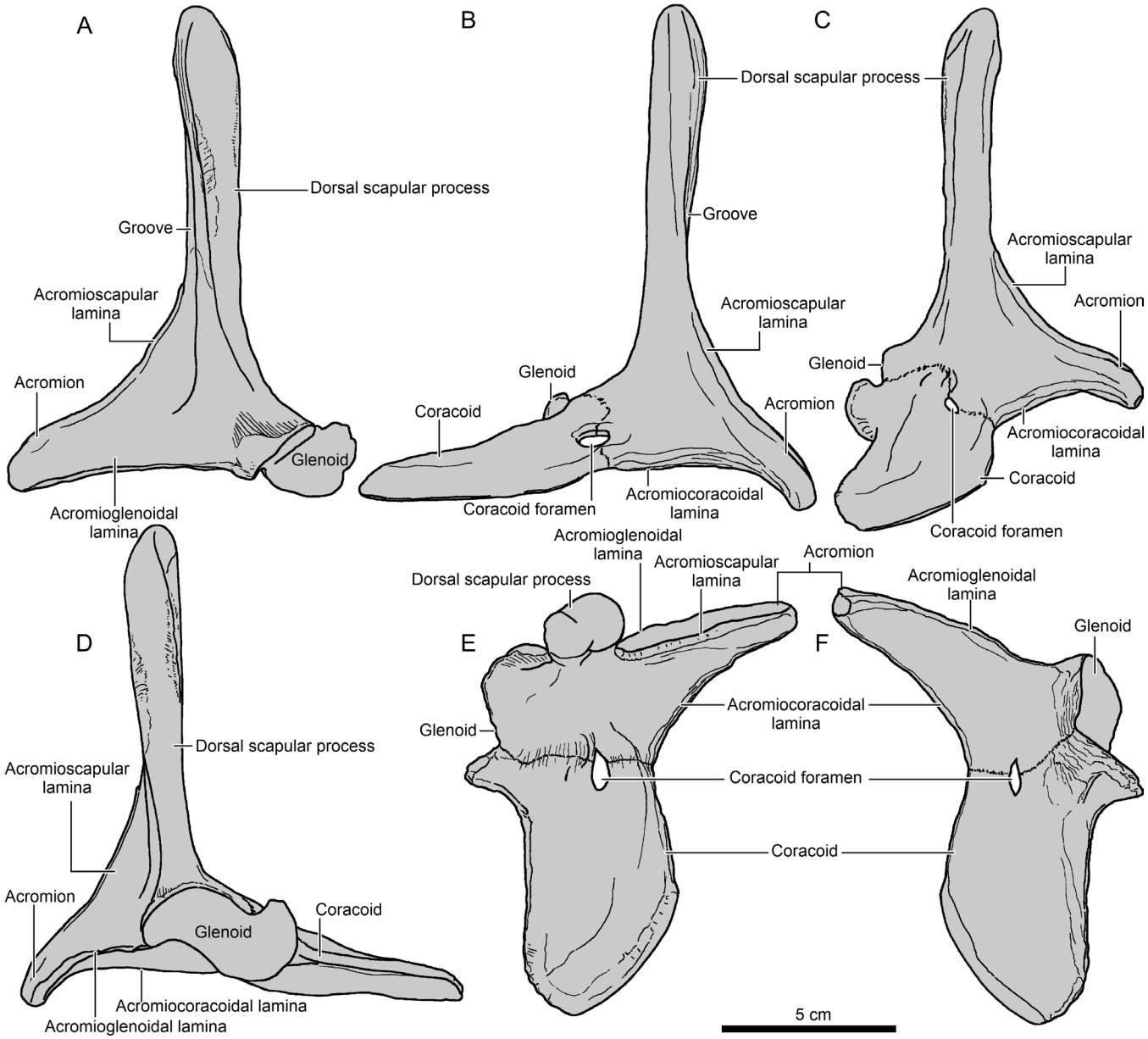

Figure 16. *Proterochersis porebensis*, restoration of the left scapulocoracoid in anterior (A), medial (B), posterior (C), lateral (D), dorsal (E) and ventral (F) view.

the cartilage was apparently variable; therefore, the proportional length of the acromion, the distance between the tip of the bony acromion and the origin of the acromioscapular lamina, and thus, its perceived robustness, varies independently from the general size of the specimen. The acromion is particularly slender and elongate in *ZPAL V. 39/48* (Figs 14A–F, 15, 16) and the larger ZPAL V. 39/391 (Fig. 14R–W), resembling the proportions of the unbroken left acromion of *K. limendorsa SMNS 17757* (Fig. 17A–F; Joyce *et al.* 2013: fig. S1; T. Szczygielski, personal observation), but proportionally shorter and stouter in the relatively small ZPAL V. 39/422 (Fig. 13C'–H') and the significantly larger ZPAL V. 39/162 (Fig. 14C'–H'), in which it approaches proportions similar to those in *Proganochelys quenstedtii* (see Jaekel 1914, 1918, Gaffney 1990). The small acromion ZPAL V. 39/502 at first glance appears relatively slender in the dorsoventral aspect (Fig. 13E, F), but this might be an artefact of damage to the acromiocoracoid lamina and still proceeding ossification of the acromioglenoidal lamina (in that specimen, it is remarkably thin, and its edge is more concave than in other specimens); in contrast, the acromioscapular lamina is relatively very tall, giving the specimen a comparatively truncated profile in other views (Fig. 13A–D). In general, the acromion of *Proterochersis porebensis* is, nonetheless, longer and more pronounced that in the less derived *Eunotosaurus africanus* (see Lyson *et al.* 2016), *Pappochelys rosinae* (see Schoch and Sues 2015, 2017), *Eorhynchochelys sinensis* (see Li *et al.* 2018) and *O. semitestacea* (see Li *et al.* 2008). The base of the acromion is concave, and in the presumed subadult (*ZPAL V. 39/48*, Figs 14F, 15F) and larger, probably adult specimen (ZPAL V. 39/162, Fig. 14H') it bears a smaller, more pronounced, rounded depression. In smaller, probably juvenile

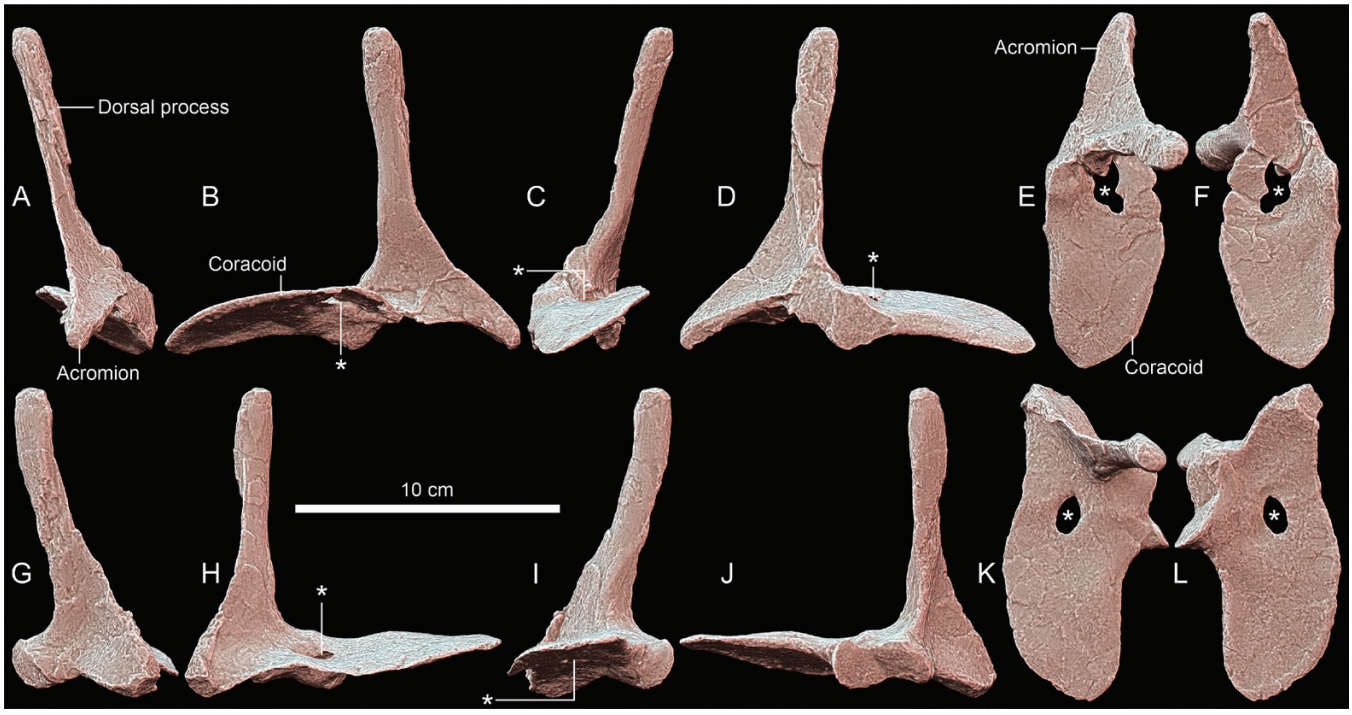

Figure 17. *Keuperotesta limendorsa*, *SMNS 17757*, left (A–F) and right (G–L) scapulocoracoid in anterior (A, G), medial (B, H), posterior (C, I), lateral (D, J), dorsal (E, K) and ventral (F, L) view. Specimens are presented as three-dimensional models in orthographic projection with Radiance Scaling enabled. Asterisks indicate coracoid foramina.

specimens (ZPAL V. 39/422, Fig. 13H'; ZPAL V. 39/424, Fig. 13W–B'; ZPAL V. 39/475, Fig. 13L; ZPAL V. 39/502, Fig. 13F), the ventral surface of the acromion is concave but lacks the depression. A very faint depression is present in the same area in the right scapulocoracoid of *K. limendorsa* (Fig. 17F, L). There is no trace of such a separate depression in the known specimens of other Triassic turtles; in *Proganochelys quenstedtii* the whole ventral surface of the acromion is uniformly concave, and in *Palaeochersis talampayensis* the preservation does not allow reliable determination of this feature (Gaffney 1990, Sterli *et al.* 2007, 2021; T. Szczygielski, personal observation).

The glenoid is peanut- or roughly N-shaped and composed of two facets set at an angle of ~120° to each other (Figs 13–16). The scapular facet is directed ventrolaterally and has its dorsal edge convex and ventral edge concave, resulting in formation of an anteroventral process at the point of contact with the acromioglenoidal lamina. The coracoidal facet is directed predominantly anteroventrally and has its dorsal edge concave and ventral edge convex, resulting in formation of a freely protruding dorsal process. The glenoid is not completely horizontal but rotated slightly anterodorsally, such that the dorsal edge of the scapular part of the facet is slightly higher than the dorsal process of the coracoidal part, and the ventral edge of the coracoidal part of the facet reaches slightly lower than the anteroventral process of the scapular part. Some variability is observable in proportions (relative width to height) of the glenoid facets (Figs 13, 14). Generally, the middle part of the glenoid, close to the scapulocoracoidal suture, is dorsoventrally (or, taking into account the anterodorsal direction of the glenoid, posterodorso-anteroventrally) constricted. This shape seems to be shared with all the Triassic testudinates (Jaekel 1914, 1918, Gaffney 1990, Sterli *et al.* 2007, 2021, Joyce *et al.* 2013, Marzola 2019), but not *Eunotosaurus africanus*, in which the middle part of the glenoid is dorsoventrally expanded and the glenoid is horizontal (Cox 1969). In the fossil material of *Pappochelys rosinae*, *Eorhynchochelys sinensis* and *O. semitestacea*, relevant details of the glenoid are not visible (Li *et al.* 2008, 2018, Schoch and Sues 2015, 2017; T. Szczygielski, personal observation). The glenoidal area of ZPAL V. 39/17 (Fig. 14I'–N') is significantly more massive and lateromedially wider than in *ZPAL V. 39/48* (Figs 14A–F, 15, 16; 4.2 vs. 2.8 cm in the narrowest part, respectively), and the glenoid is higher (2.1 vs. 1.6 cm in the middle part, respectively). Both are nearly identical in length (as preserved, 3.8 cm); ZPAL V. 39/17 has its edges broken and is missing its anterior end, but ≤ 1 cm seems to be missing.

The suture between the scapula and coracoid runs approximately at the level of the contact between the two glenoid facets. In the specimen ZPAL V. 39/424, a partial disarticulated scapula of a juvenile individual, this area is covered by a relatively smooth layer of compact bone, devoid of rugosities (Fig. 13Y). This indicates that at this stage the formation of the suture was still incipient, and the connection was fully cartilaginous. A clear rugose sutural surface between these bones is visible on the disarticulated scapula of a slightly larger individual, ZPAL V. 39/422 (Fig. 13E'). In the supposed subadult *ZPAL V. 39/48* (Figs 14E, F, 15E, F, 16E, F) and the even larger ZPAL V. 39/17 (Fig. 14M', N'), a remnant of the suture is visible as a rough thickening, but the suture itself appears to be completely fused. As in the remaining Late Triassic species, with the probable exceptions of *W. cavitesta* (see Martínez *et al.* 2015, Sterli *et al.* 2021) and the new taxon from Greenland (Marzola 2019), the coracoid foramen is oval and enclosed by the acromiocoracoidal lamina (Fig.

16). The foramen is located right between the scapula and the coracoid, and both bones appear to contribute equally to formation of its edges. This position of the coracoid foramen is shared at least by *Eunotosaurus africanus* (see Cox 1969), *Pappochelys rosinae* (likely; Schoch and Sues 2017), *O. semitestacea* (see Li *et al.* 2008), *Proganochelys quenstedtii* (see Jaekel 1914, 1918, Gaffney 1990) and *W. cavitesta* (see Sterli *et al.* 2021). The condition in *Eorhynchochelys sinensis* is unknown (Li *et al.* 2018). At early developmental stages the coracoid foramen is enclosed in recent turtles by condensed mesenchyme of the scapulocoracoid primordium, but opens soon after (Walker 1947).

The coracoid is plate-like, being slightly thicker anterolaterally (towards the glenoid) than posteromedially. As described by Szczygielski and Sulej (2016), its shape resembles the shape of a bee wing, with a nearly straight lateral edge, rounded posterior edge and bowed medial edge (Fig. 16E, F). This shape is most reminiscent of *O. semitestacea*, *K. limendorsa* (Fig. 17E, F, K, L), non-adult *Proganochelys quenstedtii* specimens and, probably, *W. cavitesta* (Gaffney 1990, Li *et al.* 2008, Joyce *et al.* 2013, Szczygielski and Sulej 2016, Sterli *et al.* 2021). In adult *Proganochelys quenstedtii*, the coracoid is more rectangular (Jaekel 1918, Gaffney 1990, Szczygielski and Sulej 2016). The coracoid of *Palaeochersis talampayensis*, as preserved, is subrectangular (Sterli *et al.* 2007, 2021), but the state of preservation makes it difficult to confirm whether this accurately represents the original shape of the bone or whether it is a result of damage (T. Szczygielski, personal observation). There is a rough, posteromedially directed tubercle below the coracoidal part of the glenoid, which is more pronounced in ZPAL V. 39/17 (Fig. 14N') than in *ZPAL V. 39/48* (Fig. 14F). This tubercle is also present in the paratype (*IVPP V 13240*) of *O. semitestacea*, *Palaeochersis talampayensis* and *Proganochelys quenstedtii* (Sterli *et al.* 2007; T. Szczygielski, personal observation). The dorsal surface *ZPAL V. 39/48* is wavy owing to two low ridges running along the posteromedial edge of that bone (Figs 14E, 15E). A subtle waviness is also visible on the dorsal surface of the right coracoid *PULR 068* of *Palaeochersis talampayensis* (T. Szczygielski, personal observation), but it is unclear whether this might be a preservation artefact. Unlike *Eunotosaurus africanus*, there is no well-developed process for the triceps muscle (Cox 1969, Lyson *et al.* 2016). The ventral surface of the coracoid is gently concave.

Owing to the incompleteness of the available specimens, aside from the relative length of the acromion and shape of the glenoid, the insight into the ontogenetic and intraspecific variability of the scapulocoracoid in *Proterochersis porebensis* is limited.

Humerus

The humerus of *Proterochersis porebensis* (Figs 18–20) is represented by 14 specimens, including three nearly complete bones (right: ZPAL V. 39/50, Figs 18K''–P'', 19G–J, 20; ZPAL V. 39/156, Figs 18U'–Z', 19C–F; and left: ZPAL V. 39/446, Figs 18Z–E', 19A, B), five proximal ends (right: ZPAL V. 39/443, Fig. 18P–T; ZPAL V. 39/445, Fig. 18Q''–U''; and left: ZPAL V. 39/25, Fig. 18F–J; ZPAL V. 39/164, Fig. 18F''–J''; ZPAL V. 39/165, Fig. 18U–Y) and six distal ends (right: ZPAL V. 39/433, Fig. 18A''–C''; ZPAL V. 39/439, Fig. 18K–O; ZPAL V. 39/442, Fig. 18P'–T'; ZPAL V. 39/444, Fig. 18F'–J'; and left: ZPAL V. 39/440, Fig. 18A–E; ZPAL V. 39/441, Fig. 18K'–O') of various sizes. The humeri of Triassic turtles are asymmetric, allowing easy determination of the side (left vs. right) they come from; in particular, the distinct lateral process, shoulder and ectepicondylar groove/foramen reliably indicate the lateral (anterior) edge. The degree of ossification, revealed by the completeness and detailing of the articular heads, is mostly consistent with size, although there are some exceptions. Particularly ZPAL V. 39/25 (Fig. 18F–J), the smallest of the proximal ends, and ZPAL V. 39/444 (Fig. 18F'–J'), a middle-sized distal end, appear to be relatively well ossified. On the contrary, the similar-sized ZPAL V. 39/446 (Figs 18Z–E', 19A, B) seems to be comparatively poorly ossified and has relatively featureless articular ends. These differences, nonetheless, seem to stem from varied tempos of ossification owing to individual variation or extrinsic factors (developmental plasticity), or perhaps size differences owing to sexual dimorphism rather than constituting meaningful taxonomic differences. The best-ossified specimen, hence providing the most morphological details, is ZPAL V. 39/50 (Figs 18K''–P'', 19G–J, 20), one of the largest specimens. Unfortunately, it shows some damage to the proximal end and lacks the lateral process. Likewise, the largest preserved proximal end (and, at the same time, part of the largest recovered humerus of *Proterochersis porebensis*), ZPAL V. 39/445 (Fig. 18Q''–U''), is badly damaged and shows very little morphological detail.

The proximal end of the humerus is expanded anteroposteriorly, constituting the widest part of the humerus, and fan-shaped in the dorsoventral aspect (Fig. 20). The expansion of the proximal part of the bone is more abrupt than that of the distal.

The humeral head (Fig. 20) is located roughly on the same axis as the shaft and is clearly marked in all well-preserved specimens, although in most of them it has a rounded, featureless appearance and a rough surface, probably attributable to its significant cartilaginous cap *in vivo*. This incomplete ossification is probably also the reason for its variable distal extent; in smaller specimens (ZPAL V. 39/156, Figs 18U'–W', 19C–E; ZPAL V. 39/165, Fig. 18U–W; ZPAL V. 39/446, Figs 18Z–B', 19A), the distal limit of the articular surface is rounded, and the base of the head is directed dorsoproximally to subvertical. In large specimens (ZPAL V. 39/50, Figs 18K''–M'', 19G–I; ZPAL V. 39/164, Fig. 18F''–H''), the distal edge of the articular surface forms a slight, hook-like overhang, such that the base of the head becomes C-shaped. ZPAL V. 39/50 (Figs 18K''–M'', 19G–I) is the only specimen with clear, ridge-like edges around the articular surface, indicative of its adult age, agreeing with its large size. Even in that specimen, however, the head is relatively smaller and less distally expanded than in *Palaeochersis talampayensis* (see Sterli *et al.* 2007). The curvature of the articular surface of the head (measured in posterior view) is ~50° in ZPAL V. 39/165 (Fig. 18W), 100° in ZPAL V. 39/156 (Fig. 18W') and 110° in ZPAL V. 39/50 (Fig. 18M''). The surface is not completely hemispherical, but slightly flattened, similar to *O. semitestacea* (see Li *et al.* 2008) and *Proganochelys quenstedtii* (see Huene 1926, Gaffney 1990, Scheyer *et al.* 2022). Overall, the articular surface is sub-ovoid in dorsal view, with its long axis directed anterodistally, differing from the more spherical

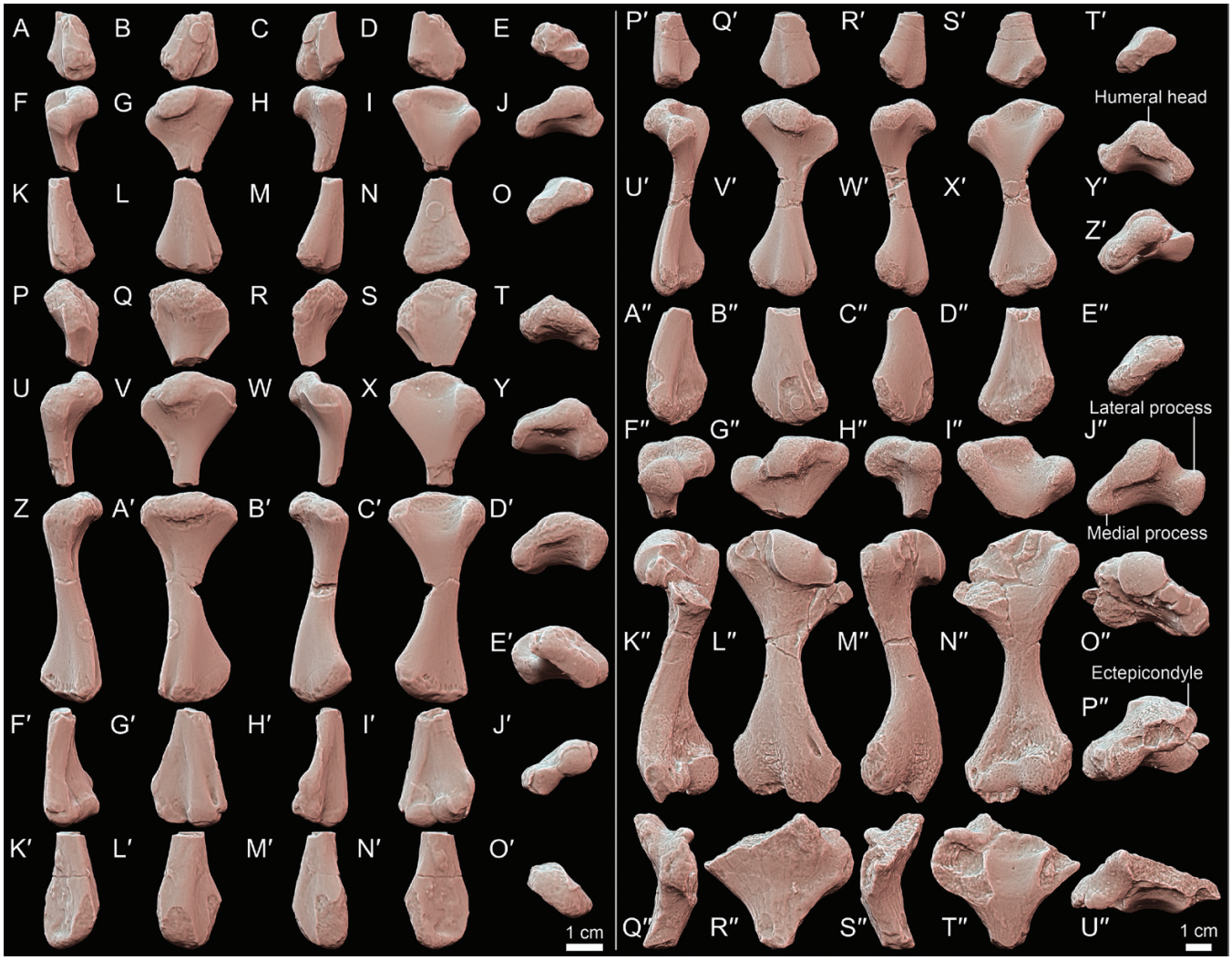

Figure 18. *Proterochersis porebensis*, humeri in anterior (A, F, K, P, U, Z, F', K', P', U', A", F", K", Q"), dorsal (B, G, L, Q, V, A', G', L', Q', V', B", G", L", R"), posterior (C, H, M, R, W, B', H', M', R', W', C", H", M", S"), ventral (D, I, N, S, X, C', I', N', S', X', D", I", N", T"'), proximal (J, T, Y, D', Y', J", O", U") and distal (E, O, E', J', O', T', Z', E", P") view. A–E, ZPAL V. 39/440, distal part of the left humerus. F–J, ZPAL V. 39/25, proximal part of the left humerus. K–O, ZPAL V. 39/439, distal part of the right humerus. P–T, ZPAL V. 39/443, proximal part of the right humerus. U–Y, ZPAL V. 39/165, proximal part of the left humerus. Z–E', ZPAL V. 39/446, left humerus. F'–J', ZPAL V. 39/444, distal part of the right humerus. K'–O', ZPAL V. 39/441, distal part of the left humerus. P'–T', ZPAL V. 39/442, distal part of the right humerus. U'–Z', ZPAL V. 39/156, right humerus. A"–C", ZPAL V. 39/433, distal part of the right humerus. F"–J", ZPAL V. 39/164, proximal part of the left humerus. K"–P", ZPAL V. 39/50, right humerus. Q"–U", ZPAL V. 39/445, proximal part of the right humerus. Specimens are presented as three-dimensional models in orthographic projection with Radiance Scaling enabled, sorted roughly by size.

articular surface of *Proganochelys quenstedtii* (see Gaffney 1990, Scheyer *et al.* 2022). In *Proterochersis porebensis*, the articular surface is predominantly directed dorsally and proximally, with slight (although larger than in *Proganochelys quenstedtii* and *Palaeochersis talampayensis*; see Gaffney 1990, Sterli *et al.* 2007, Scheyer *et al.* 2022) anterior inclination. In the large specimens ZPAL V. 39/50 (Figs 18K", L", O", 19G, H) and ZPAL V. 39/164 (Fig. 18F", G", J"), with progressing ossification, the initially convex, subhemispherical articular surface of the humeral head differentiates into the convex main surface posteriorly and the saddle-shaped shoulder anteriorly (Fig. 20A–C). The latter is also present in *Proganochelys quenstedtii* (although proportionally smaller anteroposteriorly and less excavated proximally in that species) and many Cryptodira, but absent in Pleurodira (Gaffney 1990, Scheyer *et al.* 2022). The shoulder is absent in the holotype and seems to be absent in the paratype of *O. semitestacea* (*IVPP V 13240*); owing to preservation it cannot be be observed reliably in *Palaeochersis talampayensis*, although it seems also to be absent or poorly developed (Sterli *et al.* 2007, Li *et al.* 2008).

The lateral process (homologous to the deltopectoral crest of other tetrapods; Walker 1973) and medial process of the humerus (Fig. 20) are subequal in size, the medial process being only slightly larger than the lateral, and significantly less prominent than in *Palaeochersis talampayensis* (see Sterli *et al.* 2007). In large specimens (ZPAL V. 39/50, Figs 18K", N", O", 19G, I; ZPAL V. 39/164, Fig. 18F", G", I", J"; ZPAL V. 39/445, Fig. 18Q", R", T", U"), as in *O. semitestacea* (see Li *et al.* 2008, Rothschild and Naples 2015), *Palaeochersis talampayensis* (see Sterli *et al.* 2007) and *Proganochelys quenstedtii* (see Huene 1926, Gaffney

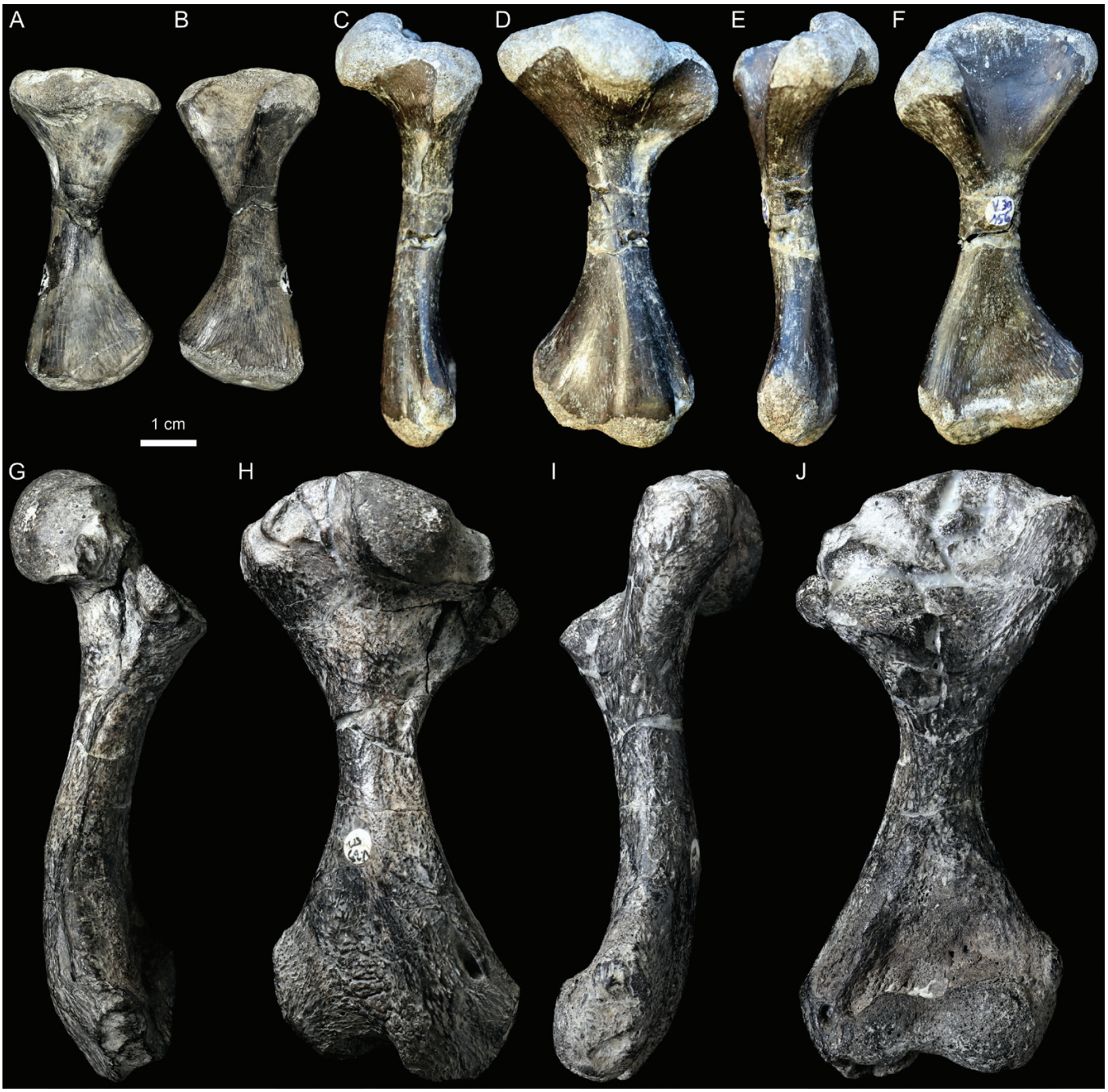

Figure 19. *Proterochersis porebensis*, humeri in dorsal (A, D, H), anterior (C, G), posterior (E, I) and ventral (B, F, J) view. A, B, ZPAL V. 39/446, left humerus. C–F, ZPAL V. 39/156, right humerus. G–J, ZPAL V. 39/50, right humerus.

1990, Scheyer *et al.* 2022), the lateral process is separated from the head by a rounded, smooth notch. This notch is much less prominent and rough surfaced in the less ossified, smaller specimens (ZPAL V. 39/25, Fig. 18F, G, I, J; ZPAL V. 39/156, Figs 18U', V', X', Y', 19C, D, F; ZPAL V. 39/165, Fig. 18U, V, X, Y; ZPAL V. 39/446, Figs 18Z, A', C', D', 19A, B). Particularly in ZPAL V. 39/446, the lateral process is level with the humeral head (Figs 18A', C', 19A, B).

Although slightly shorter than the medial process, the lateral process is much thicker (Fig. 20). It projects laterally and ventrally, which gives it a subtriangular outline in proximal view. As in the remaining Late Triassic pantestudinates and more derived turtles (Huene 1926, Gaffney 1990, Sterli *et al.* 2007, Li *et al.* 2008, Rothschild and Naples 2015), it is rounded and relatively robust, thicker than the prong-like deltopectoral process of *Eunotosaurus africanus* (see Cox 1969, Lyson *et al.* 2016) and larger than the subtle process of *Pappochelys rosinae* (Schoch and Sues 2017).

The medial process is continuous with the humeral head, and so was the cartilaginous covering of these structures, as evidenced by their rough proximal surface. The connection between the humeral head and the medial process is gently constricted. The posterior part of the medial process projects slightly ventrally, but not as strongly as the lateral process.

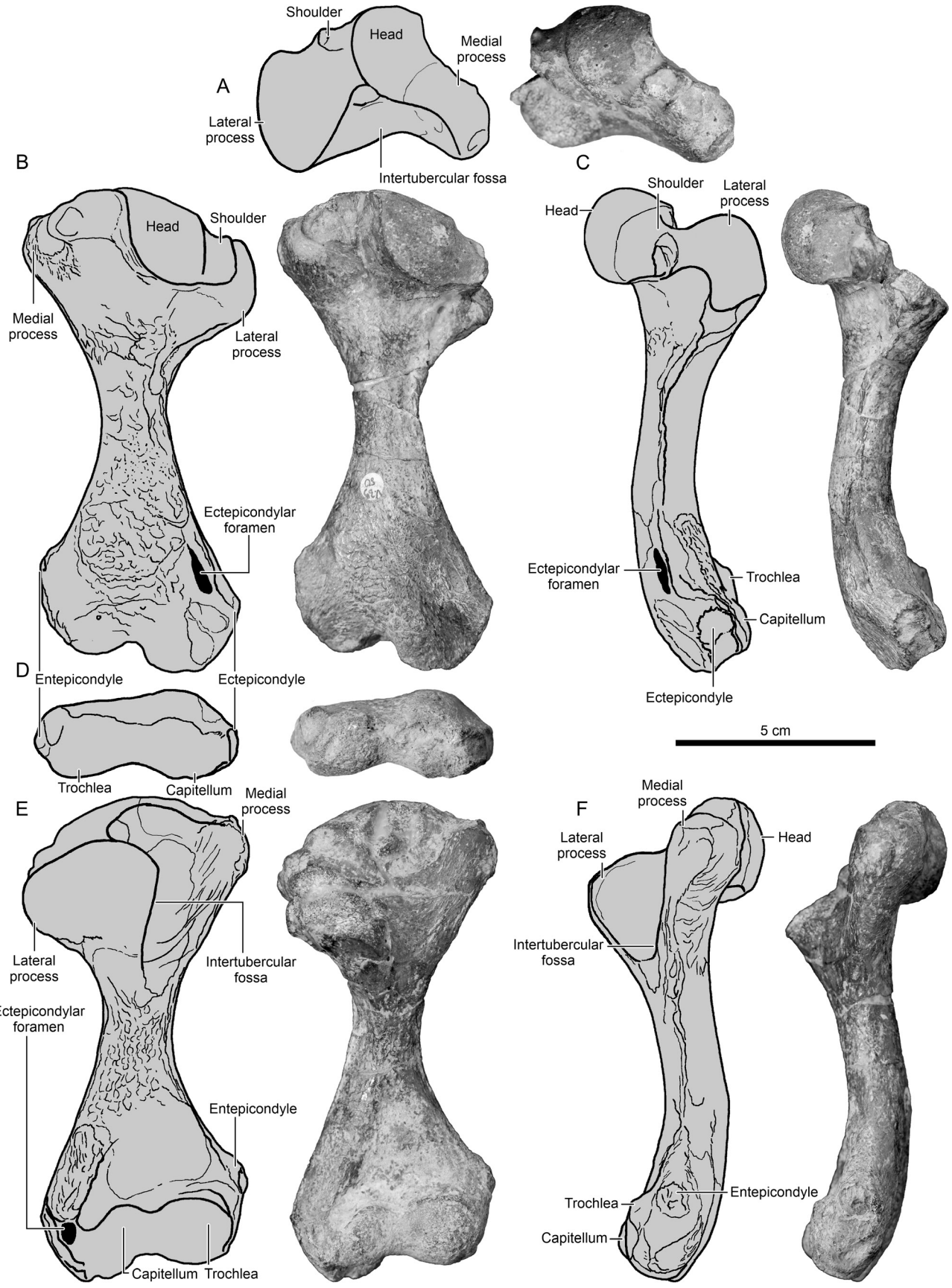

Figure 20. *Proterochersis porebensis*, ZPAL V. 39/50, restoration and photographs of the right humerus in proximal (A), dorsal (B), lateral (C), distal (D), ventral (E) and medial (F) view.

As in the other Triassic pantestudinates (Huene 1926, Gaffney 1990, Sterli *et al.* 2007, Schoch and Sues 2017), the intertubercular fossa is limited anteriorly and posteriorly by the ventral projections of the lateral and medial process, respectively (Fig. 20A, E, F). It is ε-shaped in proximal view, owing to slight ventral expansion of the articular surface of the humeral head, with the anterior portion deeper, owing to the more pronounced ventral expansion of the lateral process. Further distally (away from the articular surface of the head), it gradually becomes C-shaped and shallower, eventually disappearing smoothly just proximal to the base of the proximal expansion of the humerus. Unlike *Palaeochersis talampayensis*, there is no pronounced intertubercular shelf (Sterli *et al.* 2007).

The humeral shaft is sigmoidal in the anteroposterior aspect (Fig. 20C, F). The curvature of the bone is more exaggerated in ZPAL V. 39/50 (Figs 18K'', M'', 19G, I) than in the smaller ZPAL V. 39/156 (Fig. 18U', W', 19C, E) and ZPAL V. 39/446 (Fig. 18Z, B'), but this is mostly caused by the more complete ossification of the distal end and, to a lesser extent, by the increase of the distal reach of the articular surface of the head. As in the remaining Triassic pantestudinates (Huene 1926, Gaffney 1990, Sterli *et al.* 2007, Li *et al.* 2008, 2018, Schoch and Sues 2015, 2017), the shaft is greatly constricted anteroposteriorly relative to the proximal and distal expansions. The most constricted place is located slightly proximal to the midlength of the bone. The shaft is slightly thicker posteriorly than anteriorly, particularly in larger specimens, in which it has a tear-shaped cross-section owing to the development of a low but sharp ridge spanning the length of its anterodorsal surface between the base of the lateral process and the ectepicondyle. An oval to inverted teardrop-shaped fossa along the laterodistal edge of the proximal expansion is visible well, even in the smallest specimens (Figs 18, 19A, C, D, 20B, C). The proximal and distal expansions, as preserved (possibly influenced, to some extent, by post-mortem plastic deformation), are set at an angle of ~30° in ZPAL V. 39/446 (Fig. 18E') and ~15° in ZPAL V. 39/50 (Fig. 18P'') and ZPAL V. 39/156 (Fig. 18Z'). Each of the complete humeri of *Proterochersis porebensis* was broken and subsequently glued together in at least one place along the shaft, possibly altering the original angle slightly. Nonetheless, these values are comparable to the angle between the ends of the humerus in *Palaeochersis talampayensis* (see Sterli *et al.* 2007) and *Proganochelys quenstedtii* (see Gaffney 1990) and are larger than in the crown-group species (Gaffney 1990) but smaller than in *Eunotosaurus africanus* and most less derived tetrapods (Cox 1969, Gaffney 1990).

The distal expansion of the humerus is subtriangular in the dorsoventral aspect and slightly narrower than the proximal expansion (Fig. 20). The anterior (ectepicondylar) expansion is slightly thicker than the shaft and markedly thicker than the posterior (entepicondylar) expansion. The area between them is gently constricted, forming triangular fossae dorsally (narrower) and ventrally (wider anteroposteriorly). In ZPAL V. 39/50 (Figs 18L'', M'', P'', 19H, 20B), the dorsal fossa bears prominent rugosities. In ZPAL V. 39/50 (Figs 18K'', N'', 19J) and ZPAL V. 39/433 (Fig. 18A'', D''), the ventral fossa has an uneven surface with a bump in its posteroproximal part. In ZPAL V. 39/442 (Fig. 18P', S') and ZPAL V. 39/444 (Fig. 18F', I'), in that place the surface is less depressed than in the remaining part of the fossa, but the morphology is less clearly demarked. In the other specimens, this surface is smooth.

The distal articular surface was capped by cartilage; therefore, in all specimens except ZPAL V. 39/50 it is rough and morphologically simplified. In ZPAL V. 39/439, ZPAL V. 39/442 and ZPAL V. 39/446, the distal surfaces are uniform, and the distal end is level. In ZPAL V. 39/156 and ZPAL V. 39/444, the distal ends exhibit subdivision into two condyles, and in ZPAL V. 39/444, the capitellum (the condyle for the radius) and trochlea (the condyle for the ulna) become expressed ventrally. ZPAL V. 39/50 presents the most advanced stage of ossification, with well-differentiated condyles and an almost completely ossified distal surface. In that specimen, only a small, tripartite cavity remains, mostly located within the ectepicondyle. This cavity *in vivo* could be filled by cartilage and gradually be enclosed by the bone or it represents some pathology of the elbow.

The progressive ossification is also well visible in the process of formation of the ectepicondylar foramen for the radial nerve (Walker 1947, 1973). In ZPAL V. 39/439 (Fig. 18K, L, O), ZPAL V. 39/442 (Fig. 18P', Q', T') and ZPAL V. 39/446 (Figs 18Z, A', E', 19A), there is only a short, open groove ending distally. In ZPAL V. 39/156 (Figs 18U', V', Z', 19C, D), the groove continues across the distal surface and ends ventrodistally. In ZPAL V. 39/444 (Fig. 18F', G', I', J'), the groove is roofed dorsodistally by a short sheath of bone only barely separating the dorsal opening from the distal end of the humerus, creating a canal, which is still open ventrodistally. In ZPAL V. 39/50 (Figs 18K'', L'', N'', P'', 19G, H, J, 20B, E), the formation of the ectepicondylar foramen is complete; the dorsal opening is well separated from the distal end of the humerus, and the canal opens completely ventrally, anterior to the capitellum. Topological comparison between the specimens shows that this process is almost entirely caused by ossification of the distal cartilage, and there is little to no ossification of the bony roofing towards the proximal end of the humerus, meaning that the dorsal ectepicondylar foramen is proximodistally elongated (a remnant of the initial groove) while the ventral opening is ovoid. This distalmost, late-ossifying part of the humerus is bent more ventrally relative to the rest of the distal expansion, accentuating the curvature of the bone. As in other turtles and Triassic pantestudinates (Gaffney 1990, Schoch and Sues 2015, 2017), but unlike *Eunotosaurus africanus* (see Cox 1969, Gow 1997, Gow and Klerk 1997), there is no entepicondylar foramen.

In distal view, the capitellum and trochlea (Fig. 20C–F) of ZPAL V. 39/50 (Figs 18P'', 20D) and ZPAL V. 39/444 (Fig. 18J') are equal in size, and the distal end is 8-shaped, but in ventral view the capitellum is smaller and oval (with the long axis directed anterolaterally), while the trochlea is larger and subcircular (Figs 18I', N'', 19J, 20E). This is unlike *Pappochelys rosinae*, *Proganochelys quenstedtii* and most (but not all; Walker 1973) crown-group turtles, in which the capitellum is larger than the trochlea (Huene 1926, Gaffney 1990, Schoch and Sues 2017), but similar to *Palaeochersis talampayensis* (see Sterli *et al.* 2007). These articular surfaces are not developed in the holotype of *O. semitestacea* (*IVPP 15639*), and in the paratype (*IVPP V 13240*) their morphology is obscured by other bones, but they seem to be subequal in size in that specimen (Li *et al.* 2008, Rothschild and Naples 2015; T. Szczygielski, personal observation). The

humeri of *Eorhynchochelys sinensis* are only exposed dorsally (Li *et al.* 2018). The proximal limit of the capitellum and trochlea in *Proterochersis porebensis* takes the form of a continuous, ridge-like edge. The ridge is particularly sharp along the anteroproximal edge of the trochlea in ZPAL V. 39/50 (Fig. 18N'', 19J, 20E). Both surfaces are gently convex.

ZPAL V. 39/50 (Figs 18L''–N'', P'', 19H–J, 20B, D–F) and ZPAL V. 39/444 (Fig. 18G'–J') are the only specimens with clearly developed entepicondyles. The entepicondyle is subtriangular in the dorsoventral aspect, roughened, and nearly symmetrical with regard to the ectepicondyle, but located slightly more proximally. It is more pronounced than in *Palaeochersis talampayensis*, giving the distal end of the humerus more conspicuous anteroposterior flaring (Sterli *et al.* 2007). In less ossified specimens, the entepi- and ectepicondylar processes were either not yet ossified or they coincided with the proximal edge of the distal cartilage.

Ulna

The ulna of *Proterochersis porebensis* (Figs 21, 22) is represented by two complete left bones (ZPAL V. 39/218, Figs 21G–L, 22; and ZPAL V. 39/219, Fig. 21A–F) and a single right proximal end (ZPAL V. 39/463, Fig. 21M–Q). In contrast to some modern species, in the case of Triassic stem turtles the body side from which each ulna comes is relatively easy to establish based on the distinctive dorsomedially located radial notch and bicipital condyle. All three specimens come from small individuals and show minor differences in size, with ZPAL V. 39/219 being the smallest and ZPAL V. 39/218 the largest. Despite its small size, ZPAL V. 39/218 appears relatively well ossified and presents many morphological details.

In proximal view, the sigmoid notch is subtriangular with a distinct dorsal projection, nearly flat ventral edge and rounded medial and lateral corners (Fig. 22A). The latter are subequal in ZPAL V. 39/219 (Fig. 21E) and ZPAL V. 39/463 (Fig. 21Q), but in ZPAL V. 39/218 (Fig. 21K) the medial part of the surface is larger than the lateral. As in *Proganochelys quenstedtii*, the sigmoid notch is subdivided into two parts: a gently concave ventromedial facet and a gently convex dorsolateral facet (Gaffney 1990). The inclination of these facets is slightly divergent (the dorsolateral one is facing slightly more dorsally), but they are both directed predominantly proximomedially.

In dorsoventral aspect, the proximal end is subtriangular and turned slightly proximomedially (Fig. 22C, E). Unlike *Eunotosaurus africanus*, *Proganochelys quenstedtii* and *Palaeochersis talampayensis*, the sigmoid notch is shallow and lacks a prominent coronoid process (Gaffney 1990, Sterli *et al.* 2007, Lyson *et al.* 2016, Scheyer *et al.* 2022). The olecranon processes of ZPAL V. 39/219 (Fig. 21A–E) and ZPAL V. 39/463 (Fig. 21M–Q) are rounded and show signs of a cartilaginous cap all around, but in ZPAL V. 39/218 (Figs 21G–K, 22A–C, E, F) the process appears close to termination, with only a several millimetre unossified field on the tip. In all specimens, it is much lower than in *Eunotosaurus africanus* (see Lyson *et al.* 2016), *Proganochelys quenstedtii* (see Gaffney 1990, Scheyer *et al.* 2022), *Palaeochersis talampayensis* (Sterli *et al.* 2007) and the new taxon from Greenland (Marzola 2019) and only slightly larger than in most crown-group turtles (Gaffney 1990). A very similar-sized olecranon without a prominent coronoid process is, however, present in *Eorhynchochelys sinensis* (see Li *et al.* 2018) and *O. semitestacea*, including the very well-ossified paratype of the latter, *IVPP V 13240* (Li *et al.* 2008). *Pappochelys rosinae* lacks the olecranon altogether (Schoch and Sues 2017). The attachment of the bicipital tendon of the muscle biceps profundus (Walker 1973, Gaffney 1990; Figs 21A–D, G–J, M–P, 22B–E) takes the form of merely a low rugosity in ZPAL V. 39/219 (Figs 21A, B, D), a well-defined ridge in ZPAL V. 39/463 (Fig. 21M, N, P) and a conspicuous tubercle in ZPAL V. 39/218 (Figs 21G, H, J, 22B, C, E). As in *O. semitestacea*, *Proganochelys quenstedtii*, *Palaeochersis talampayensis* and the new taxon from Greenland, in the medial part of the proximal end is a triangular, flat field between the medial corner of the sigmoid notch, its dorsal projection and the bicipital tubercle, outlined by low ridges between these points, which served as an articular facet for the proximal end of the radius (Gaffney 1990, Sterli *et al.* 2007, Li *et al.* 2008; Fig. 22B, C). The dorsal ridge between the bicipital tubercle and the dorsal projection of the sigmoid notch might have served as an attachment site for the radioulnar ligament (Gaffney 1990). In ZPAL V. 39/218 (Figs 21J, 22E), a low but distinct ridge nearly parallel to the lateral edge (and thus oblique to the medial edge of the proximal expansion) runs across the medial part of the ventral surface, starting proximally around the level of the bicipital tubercle and nearly merging with the medial edge of the shaft distally.

The shaft is nearly oval in cross-section, flattened dorsoventrally, with the medial edge slightly thicker than the lateral. As in *Proganochelys quenstedtii*, it reaches its minimal width (slightly more than half of the proximal expansion) at the level of about two-thirds of the bone length and further distally widens again into the distal expansion (Gaffney 1990, Scheyer *et al.* 2022). The ventral surfaces of the proximal and distal ends of ZPAL V. 39/218 (Fig. 21L) and ZPAL V. 39/219 (Fig. 21F) are set at an angle of ~35° to each other, with the distal twisted dorsomedially.

The distal expansion is subtriangular, about the same size as the proximal in ZPAL V. 39/219 (Figs 21B, D, 22C, E) and slightly smaller than the proximal in ZPAL V. 39/218 (Fig 22H, J). It is turned slightly mediodistally. In ZPAL V. 39/219 (Fig. 21F) it is nearly flat, with the medial part being barely thicker than the lateral, but in ZPAL V. 39/218 (Fig. 21L) it bears a low, rounded ridge dorsally, close to the medial edge. The distal articulation surface is composed of two mediodistally directed facets for the intermedium (medially) and ulnare (laterally) and terminates distolaterally in a styloid process. These facets are set at an angle of ~20°.

Radius

The radius of *Proterochersis porebensis* is represented by only a single left distal end (ZPAL V. 39/471; Figs 23, 24) of what appears to be a small individual. Fortunately, the specimen appears to be well ossified, revealing morphological details. It is identified as the left radius based on the inclination of the distal articular surface (sloped proximolaterally), the presence of a distinct ventrolateral ridge, and the flat dorsal surface.

The preserved part of the shaft is rounded dorsolaterally but bears two pronounced ridges: ventrolateral (which disappears

Figure 21. *Proterochersis porebensis*, ulnae in medial (A, G, M), dorsal (B, H, N), lateral (C, I, O), ventral (D, J, P), proximal (E, K, Q) and distal (F, L) view. A–F, ZPAL V. 39/219, left ulna. G–L, ZPAL V. 39/218, left ulna. M–Q, ZPAL V. 39/463, proximal end of the right ulna. Specimens are presented as three-dimensional models in orthographic projection with Radiance Scaling enabled.

as the dorsal part starts to expand laterally) and along the medial edge.

The distal part is flattened and subtriangular, with the medial edge nearly straight and the lateral part expanded into a process (attachment for the superior radio-ulnar ligament; Haines 1946, Gaffney 1990, Sterli *et al.* 2007). The distal articular surface is elongated and subdivided into two facets, proximolateral (for the intermedium and medial centrale) and distomedial (for the first distal carpal), set at an angle of ~30° to each other. Its dorsoventral diameter is nearly two times as large in the lateral part compared with the medial, but the decrease is very gradual. As is typical for turtles (Walker 1973, Gaffney 1990, Sterli *et al.* 2007), it is set at an angle relative to the medial edge, such that the bone terminates distomedially into a styloid process (Fig. 24). In *Proterochersis porebensis*, this angle is ~110° in the medial part and 140° in the lateral part. In *Eorhynchochelys sinensis*, *O. semitestacea* and *Pappochelys rosinae*, the subdivision into two facets is less pronounced, and the distal articular surface as a whole is set at an angle more in line with the medial part of the articular surface of *Proterochersis porebensis*, i.e. ~110° (Li *et al.* 2008, 2018, Schoch and Sues 2017; T. Szczygielski, personal observation). Although this might also be influenced by incomplete ossification of the distal end of the bone, this morphology is also present in the well-ossified paratype (*IVPP V 13240*) of *O. semitestacea*, in which the articulation with the hand leaves virtually no place for an additional cartilaginous cap on the radius (Li *et al.* 2008, Lyson *et al.* 2016).

Sacrum

The sacrum of *Proterochersis porebensis* (Figs 1, 3, 25E, L, 26A–E, K–N, S–D') is represented by six specimens: *ZPAL V. 39/48*

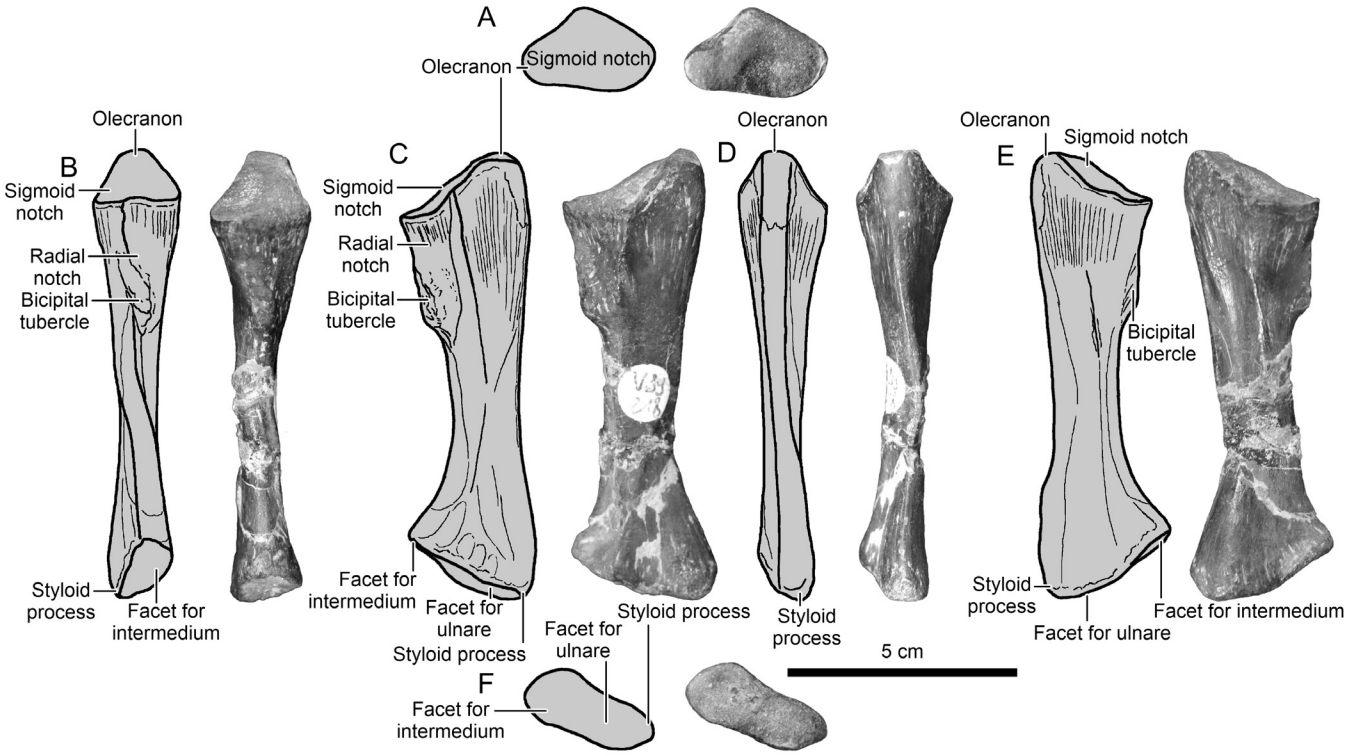

Figure 22. *Proterochersis porebensis*, ZPAL V. 39/218, restoration and photographs of the left ulna in proximal (A), medial (B), dorsal (C), lateral (D), ventral (E) and distal (F) view.

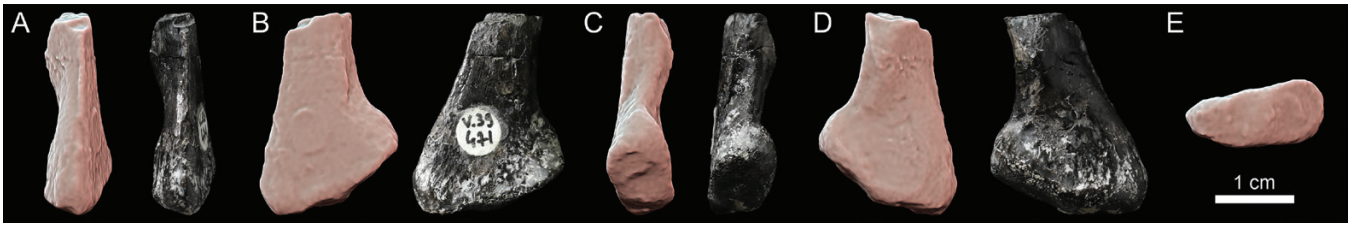

Figure 23. *Proterochersis porebensis*, ZPAL V. 39/471, distal part of left radius in medial (A), dorsal (B), lateral (C), ventral (D) and distal (E) view. Three-dimensional models presented in orthographic projection with Radiance Scaling enabled.

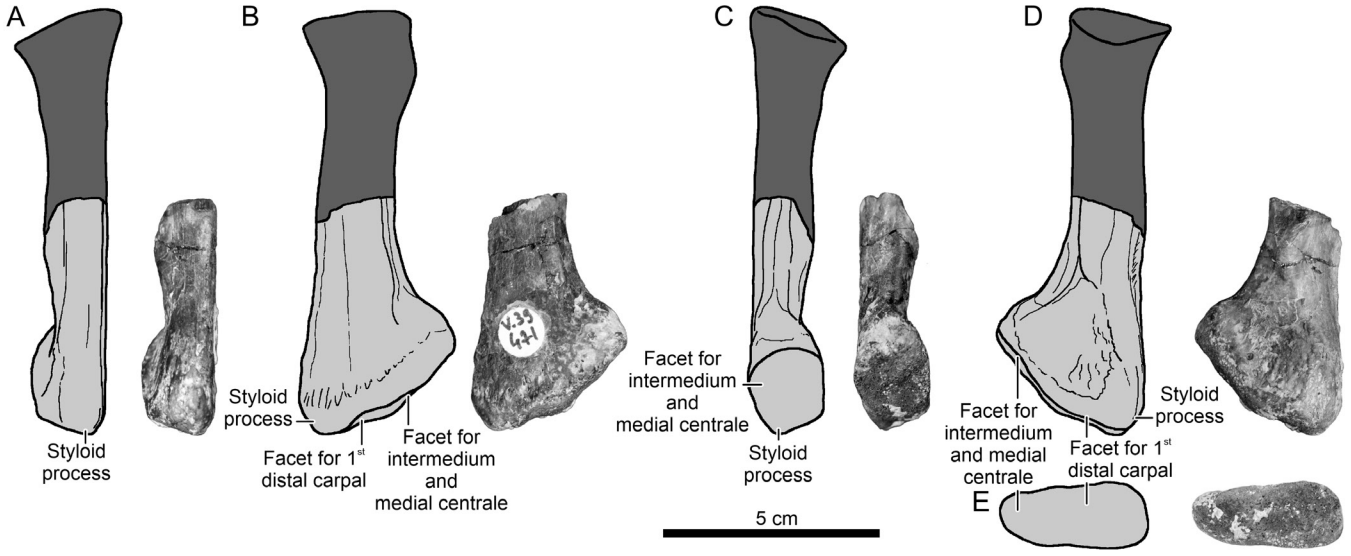

Figure 24. *Proterochersis porebensis*, ZPAL V. 39/471, restoration and photographs of the left radius in medial (A), dorsal (B), lateral (C), ventral (D) and distal (E) view. Missing parts of the bone are marked with dark grey.

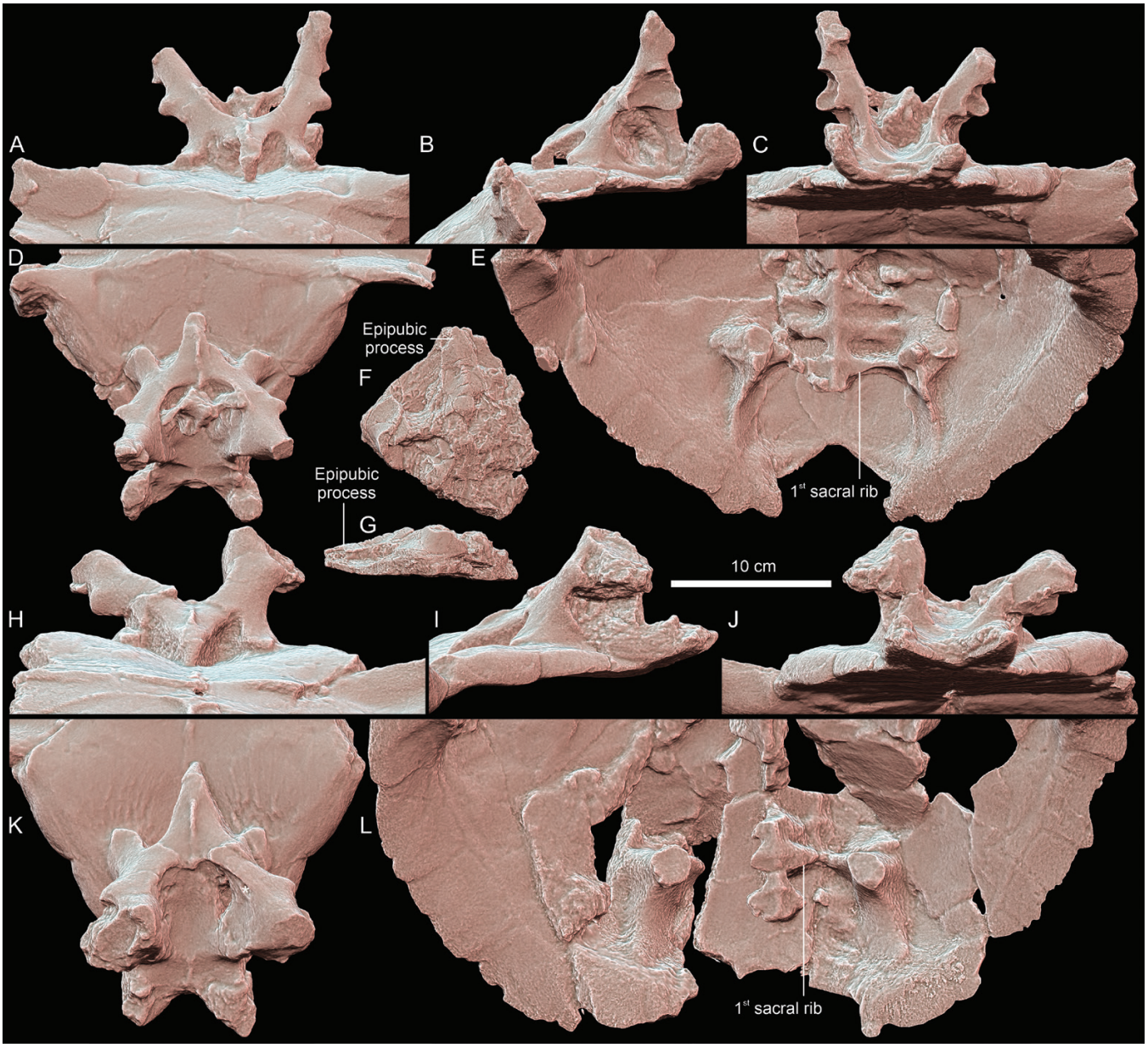

Figure 25. *Proterochersis porebensis*, pelves and sacra. A–E, *ZPAL V. 39/48*, pelvis connected to the plastron in anterior (A), left lateral (B), posterior (C) and dorsal view (D), and sacrum and dorsal parts of ilia connected to carapace in ventral (visceral) view (E). F, G, ZPAL V. 39/498, partial pelvis attached to plastron fragment in dorsal (F) and left lateral (G) view. H–L, *ZPAL V. 39/49*, pelvis connected to the plastron in anterior (H), left lateral (I), posterior (J) and dorsal view (K), and sacrum and dorsal parts of ilia connected to carapace in ventral (visceral) view (L). Specimens are presented as three-dimensional models in orthographic projection with Radiance Scaling enabled. Asterisks indicate thyroid fenestra.

(holotype; Figs 3A, 25E), *ZPAL V. 39/49* (paratype; Figs 3B, 25L), ZPAL V. 39/223 (broken off second sacral vertebra; Fig. 26S–X), ZPAL V. 39/225 (isolated second sacral vertebra; Fig. 26Y–D'), *ZPAL V. 39/370* (paratype; Fig. 26K–N) and ZPAL V. 39/402 (Fig. 26A–E). The sacrum is probably also preserved inside *ZPAL V. 39/34* (paratype), but it is completely covered by the sediment. These specimens were figured and described by Szczygielski and Sulej (2016, 2019) , Szczygielski (2017) and Szczygielski *et al.* (2018). The sacrum of the holotype of *Proterochersis robusta*, *SMNS 122777* (Fig. 27P), is partly exposed from under the matrix and was described by Fraas (1913), who concluded, incorrectly, that it incorporates four (rather than two) vertebrae and their ribs. Partly prepared sacra are also present in the juvenile SMNS 16603 (Fig. 27H) and SMNS 56606 (Fig. 27J). Sacra might also be present inside the shells CSMM uncat. and SMNS 17561, but embedded in matrix. At least a part of the sacrum seems to be present inside SMNS 17755a; a faint outline is visible in the computed tomography scans of that specimen performed for Szczygielski and Sulej (2019), but the contrast obtained is very low.

Unlike other turtles (e.g. Gaffney 1990), the sacrum in *Proterochersis porebensis* is usually attached to the carapace (Szczygielski and Sulej 2016, 2019). It is composed of two vertebrae and their respective ribs connecting to the medial surfaces

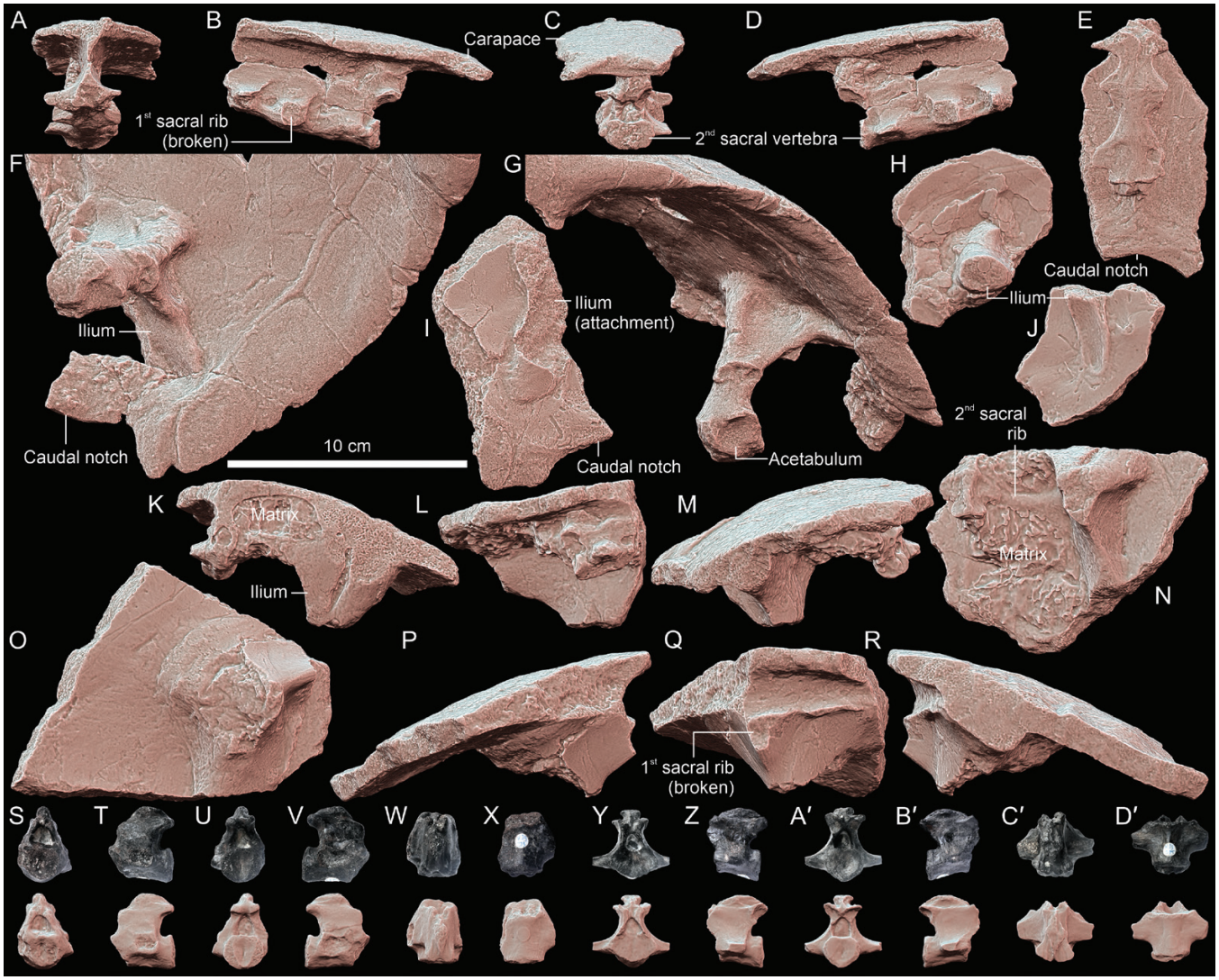

Figure 26. *Proterochersis porebensis*, sacrum and connections between the ilia and carapace. A–E, ZPAL V. 39/402, sacrum with attached carapace fragment in anterior (A), lateral left (B), posterior (C), lateral right (D) and ventral (E) view. F, G, *ZPAL V. 39/72*, left ilium connected to the carapace in ventral (F) and ventrolateral (G) view. H, ZPAL V. 39/481, dorsal part of the right ilium attached to carapace fragment in ventral view. I, ZPAL V. 39/18, carapace fragment with damaged attachment of the right ilium. J, ZPAL V. 39/193, carapace fragment with left posterior iliac process in ventral view. K–N, *ZPAL V. 39/370*, fragmentary sacrum and dorsal part of the left ilium attached to carapace fragment in anterior (K), right lateral (L), posterior (M) and ventral (N) view. O–R, ZPAL V. 39/63, dorsal part of the right ilium attached to carapace fragment in ventral (O), anterior (P), medial (Q) and posterior (R) view. S–X, ZPAL V. 39/223, second sacral vertebra in anterior (S), left lateral (T), posterior (U), right lateral (V), dorsal (W) and ventral (X) view. Y–D', ZPAL V. 39/225, second sacral vertebra in anterior (Y), left lateral (Z), posterior (A'), right lateral (B'), dorsal (C') and ventral (D') view. 3D models are presented in orthographic projection with Radiance Scaling enabled.

of the ilia. The first sacral vertebra is co-ossified with the carapace and the last dorsal vertebra in all specimens in which it is preserved (Figs 1, 3, 25E, L, 26A–E, K–N). The second sacral vertebra was apparently free in juvenile and subadult specimens and fused later. It is missing (disarticulated) in the supposed subadult *ZPAL V. 39/48*, with no evidence of osseous attachment on the visceral surface of the carapace (Figs 3A, 25E; Szczygielski and Sulej 2016). The second isolated sacral vertebra ZPAL V. 39/225 (Fig. 26Y–D') also does not show any clear evidence of broken osseous attachment to the shell and preceding vertebra, but otherwise it is morphologically consistent with the second sacral vertebrae of other specimens. *ZPAL V. 39/370* (Fig. 26K–N) has its second sacral vertebra fused with the first, but the character of the connection between the neural process of its second sacral and its carapace is ambiguous, and it might represent fusion, suture, or tight articulation with a ligamentous link (Fig. 26L; Szczygielski and Sulej 2016). The time of the fusion with the shell and the first sacral vertebra was apparently somewhat varied in the ontogeny, because ZPAL V. 39/225 is slightly larger than the corresponding vertebra of *ZPAL V. 39/370*. The slightly larger second sacral ZPAL V. 39/223 was found in separation from the shell, but bears an attached posterior part of a broken preceding centrum and has a damaged, worn neural process, exposing spongiosa (Fig. 26Y–D'), indicating that it came from a fused individual. The second sacral is completely fused to the carapace in *ZPAL V. 39/49* (Figs 3B, 25L; Szczygielski and

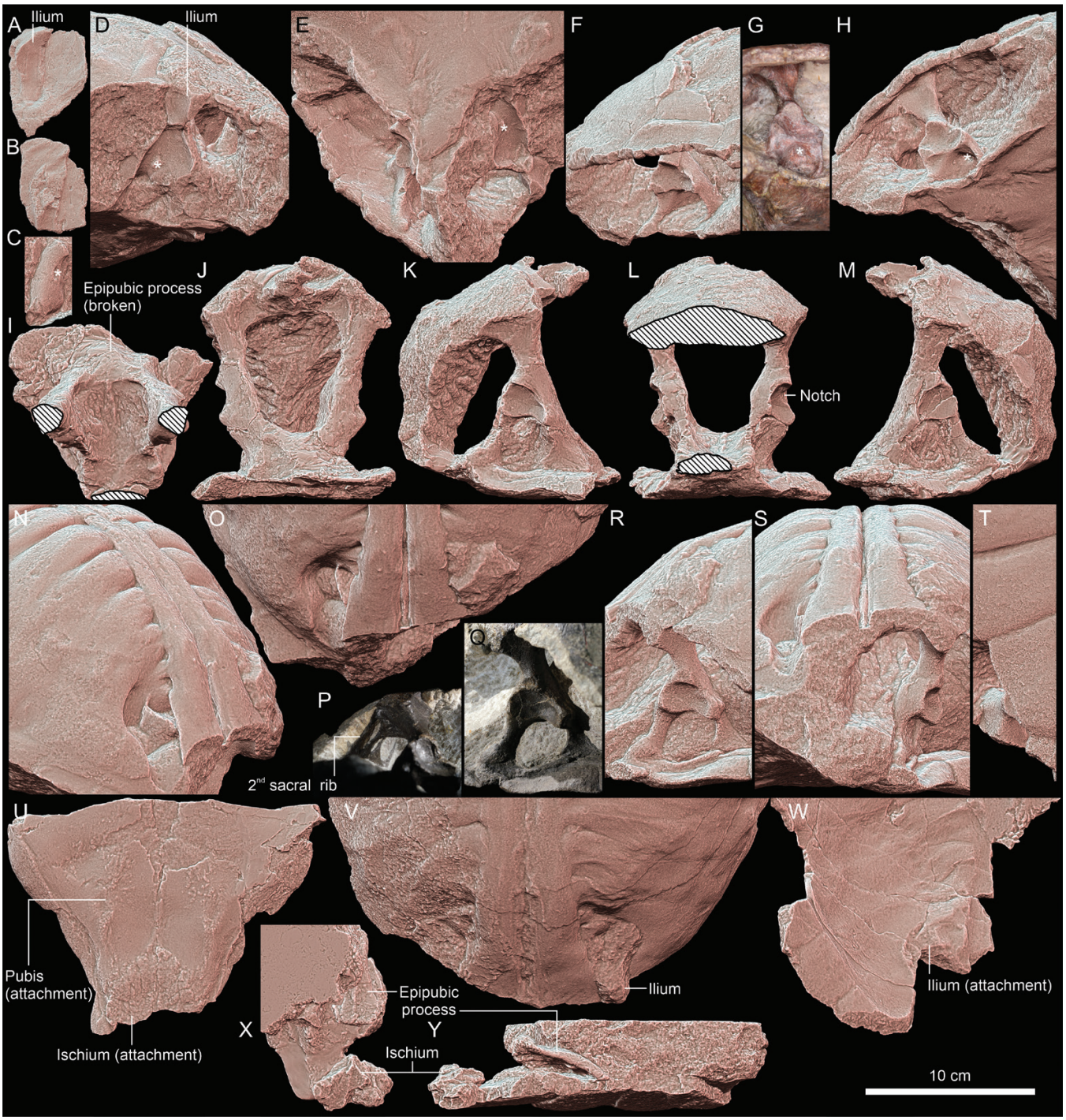

Figure 27. *Proterochersis robusta*, pelves and sacra. A, NHMUK 38650, carapace fragment with attached dorsal part of the right ilium in ventral (visceral) view. B, NHMUK 38653, carapace fragment showing the contact with the right ilium in ventral (visceral) view. C–H, SMNS 16603, partial left pubis showing the thyroid fenestra (C) digitally reconstructed from the natural cast in the steinkern and the posterior portion of the steinkern itself with partly preserved left ilium and preserved right side of the pelvis in left lateral (D), ventral (E), right lateral (F), right posteroventrolateral (G) and right ventrolateral (H) view. I–M, SMNS 56606, nearly complete pelvis with attached weathered parts of carapace and plastron in dorsal (I), anterior (J), right lateral (K), posterior (L) and left lateral (M) view. N–T, *SMNS 12777*, posterior part of the steinkern showing moulds of the dorsal part of the left ilium and sacrum in left posterolaterodorsal (N) and dorsal (O) view, photograph of the sacrum in right posteroventrolateral view (P) and preserved right side of the pelvis in lateral (Q, R), posterior (S) and ventral (T) view. U, SMNS 16442, posterior lobe of the plastron in dorsal (visceral) view showing the attachments for the ischia and pubes. V, W, SMNS 17930, posterior part of the steinkern in dorsal view showing damaged dorsal part of the right ilium (V) and the corresponding posterior part of the preserved carapace in ventral (visceral) view presenting the attachment area for the right ilium (W). X, Y, SMNS 50917, partial plastron with attached bases of the ischia and epipubic process in dorsal (X) and right lateral (Y) view. Specimens in A–F, H–O and R–Y are presented as three-dimensional models in orthographic projection with Radiance Scaling enabled. Dorsal parts of the ilia with overlying carapace in I and chunk of sediment in I and L have been removed digitally to clear the view. Asterisks indicate thyroid fenestrae.

Sulej 2016) and ZPAL V. 39/402 (Fig. 26A–E; Szczygielski *et al.* 2018, Szczygielski and Sulej 2019).

Both sacral vertebrae are gently keeled ventrally. The keel is narrower and more pronounced in *ZPAL V. 39/370* (Fig. 16K, N) than in *ZPAL V. 39/48* (Figs 3A, 25E), ZPAL V. 39/225 (Fig. 26D') and, particularly, in the larger *ZPAL V. 39/49* (Figs 3B, 25L), ZPAL V. 39/223 (Fig. 26X) and ZPAL V. 39/402 (Fig. 26A, E). Their centra are wider than high and kidney-shaped, with some variability concerning their height-to-width ratio (Fig. 26C, S, U, Y, A').

The first sacral vertebra does not show any particular lateral structures on the neural arch; it is modified and simplified, as in the case of the dorsal vertebrae. Its posterior articular surface, exposed in *ZPAL V. 39/48*, bears a small pit.

The second sacral vertebra has pronounced, bilaterally symmetrical pits on its ventral surface at the level of attachment of the ribs. The anterior articular surface of the second sacral, exposed only in ZPAL V. 39/225 (Fig. 26Y), is completely flat. As in the first sacral vertebra and in *Proganochelys quenstedtii*, its posterior articular surface bears a central dorsoventrally elongated concavity (Gaffney 1990), which is best exposed in ZPAL V. 39/223 (Fig. 26U) and ZPAL V. 39/225 (Fig. 26A'). It lacks developed prezygapophyses but has clear postzygapophyses, which are subhorizontal and subcircular to ovoid, but the size and proportions of which vary between specimens. It has a low neural process, which in ZPAL V. 39/225 is semicircular in lateral view (Fig. 26Z, B') and expands dorsally into a diamond-shaped table with rugose surface (Fig. 26C'), whereas in the remaining specimens it is directed very slightly posterodorsally (Fig. 26B, D, L, T, V).

The first pair of sacral ribs is more strongly developed than the second, triangular in cross-section, with a ridge-like apex along the ventral surface and a gently concave posterior surface. It expands ventrally towards the ilium. The second pair is nearly flat, plate-like, with the anterior edge barely thicker than the posterior. Both pairs of sacral ribs appear to contact both their respective and the preceding vertebral centrum, with the intervertebral contact usually more pronounced in the case of the first sacral rib pair (with about the anterior one-third of the rib attachment contacting the last dorsal vertebra) and only slight anterior extension in the case of the second sacral rib pair. The morphology and number of the sacral ribs of *Proterochersis porebensis* is consistent with that of *Proterochersis robusta* (*contra* Fraas 1913; Fig. 27P), *K. limendorsa* (Fig. 28E–H), *Proganochelys quenstedtii* and cryptodires (Gaffney 1990, Joyce *et al.* 2013; T. Szczygielski, personal observation). The co-ossification of the sacrum with the carapace is uncertain in *Proterochersis robusta*, because neither specimen is prepared or preserved sufficiently in that region.

Given that the pelvis in proterochersids is co-ossified with the shell, the biomechanical role of the sacrum as a tight connection between the axial skeleton and pelvic limb (at least in adults) was probably minor.

Pelvis

The pelvis of *Proterochersis porebensis* is represented by numerous specimens. The best-prepared of these are the nearly complete *ZPAL V. 39/48* (the holotype, subadult; Figs 9A, 25A–E, 29) and *ZPAL V. 39/49* (paratype, large, probably adult specimen; Figs 9B, 25H–L), described and figured in detail by Szczygielski and Sulej (2016, 2019), Szczygielski (2017) and Szczygielski *et al.* (2018). ZPAL V. 39/498 (Fig. 25F, G) preserves damaged parts of the pubis (left lateral pubic process, epipubic process) and ischium in articulation with the plastron. *ZPAL V. 39/34* (paratype, juvenile; Fig. 30) preserves its pelvis, which was exposed, in part, from underneath the matrix, but it is badly broken owing to severe crushing. *ZPAL V. 39/72* (paratype, intermediate in size between *ZPAL V. 39/48* and *ZPAL V. 39/49*; Fig. 26F, G) preserves only the dorsal part of the left ilium. Several specimens present the bases of the pubis and/or ischium attached to the plastron, the most notable being ZPAL V. 39/13 (Fig. 31H, I), ZPAL V. 39/69 (Fig. 31A–D) and ZPAL V. 39/157 (Fig. 31E, F) (Szczygielski *et al.* 2018, Szczygielski and Sulej 2019). Besides that, a number of fragmentary specimens are known. These include mostly ilia: 20 specimens (ZPAL V. 39/18, Fig. 26I; ZPAL V. 39/63, Fig. 26O–R; ZPAL V. 39/177, Fig. 32U–X, S', T'; ZPAL V. 39/193, Fig. 26J; ZPAL V. 39/276, Fig. 32Y–B', U'; ZPAL V. 39/279; ZPAL V. 39/280; ZPAL V. 39/447–ZPAL V. 39/456, Fig. 32E–T, G'–J'; ZPAL V. 39/458, Fig. 32C'–F'; ZPAL V. 39/459, Fig. 32A–D; ZPAL V. 39/481, Fig. 26H), of which 11 are identifiable as left and five as right. Much less common pelvic bones found in Poręba are the pubes, represented by three left specimens (virtually complete ZPAL V. 39/58 (Fig. 33A–F) and ZPAL V. 39/437 (Fig. 33M–R), missing only the posterior plate, and fragmentary ZPAL V. 39/438 (Fig. 33G–L), representing the dorsal branch) coming from juveniles. Three middle-sized specimens represent the ischium: ZPAL V. 39/486 (Fig. 34G–L) and ZPAL V. 39/487 (Fig. 34A–F) are left dorsal (acetabular) parts, and ZPAL V. 39/488 (Fig. 34M–R) is a right disarticulated element. Four specimens represent the acetabulum: two from the right side (ZPAL V. 39/460, Fig. 32K'–N'; ZPAL V. 39/461, Fig. 32O'–R', V', W'), one from the left side (ZPAL V. 39/451, Fig. 32I–L) and one too poorly preserved to determine (ZPAL V. 39/457). The pelvis of *Proterochersis robusta* is present in the holotype (*SMNS 12777*, exposed on the right side of the specimen, with the exception of the epipubis and described by Fraas 1913; Figs 11B, 27N–T), SMNS 16603 (partial, right side also exposed; Figs 11A, 27C–H), SMNS 17930 (dorsal part of the right ilium partly embedded in the steinkern and attachment site on the visceral surface of the carapace; Fig. 27V, W) and SMNS 56606 (subcomplete, missing the epipubis, but prepared from all sides; Fig. 27I–M). Additionally, the xiphiplastron of SMNS 16442 (Fig. 27U) preserves the attachment site, SMNS 50917 (Fig. 27X, Y) preserves the base of the ischium, part of the left lateral process of the pubis and the epipubis, NHMUK 38650 (the syntype of '*Chelytherium obscurum*'; Fig. 27A) and one of the fragments numbered NHMUK 38653 (Fig. 27B) show details the attachment site of the ilium to the carapace, and another fragment of NHMUK 38653 includes poorly preserved connection between the plastron and the ischium (Szczygielski 2020). It seems likely that unprepared pelves are also present within CSMM uncat. and SMNS 17561.

The pelvis in *Proterochersis porebensis* is co-ossified with the carapace and plastron, as in the remaining Proterochersidae (Fraas 1913, Joyce *et al.* 2013, Szczygielski and Sulej 2016, 2019, Szczygielski 2020). The pelvis of *Palaeochersis talampayensis* was described as either sutured to the shell (see Rougier *et al.* 1995,

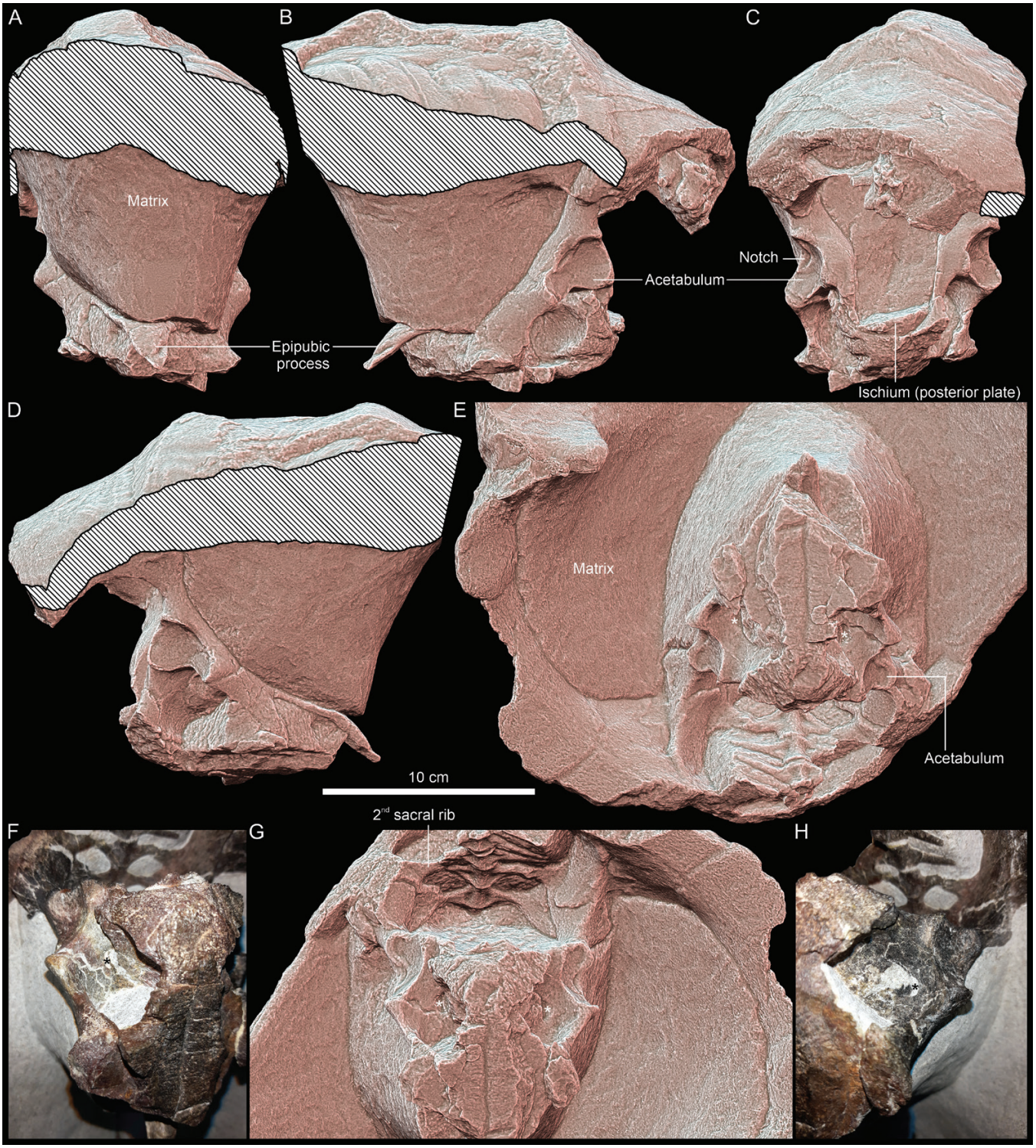

Figure 28. *Keuperotesta limendorsa*, *SMNS 17757*, pelvis and sacrum. A, anterior view. B, left lateral view. C, posterior view. D, right lateral view. E, ventral view. F, photograph in left posterolateroventral view showing the undamaged thyroid fenestra. G, posteroventral view showing sacrum and both thyroid fenestrae. H, photograph in right posterolateroventral view, showing partly damaged right thyroid fenestra. Specimens in A–E and G are presented as a three-dimensional model in orthographic projection with Radiance Scaling enabled. Overhanging parts of the carapace have been removed digitally in A–D to clear the view. Asterisks indicate thyroid fenestrae.

Sterli *et al.* 2007) or free (Gaffney *et al.* 2006, Sterli *et al.* 2021, de la Fuente *et al.* 2021). This discrepancy is understandable, given that in the holotype (*PULR 068*) the morphology is ambiguous; the specimen is severely cracked, and it is difficult to identify unequivocally the sediment-filled discontinuities between the pelvis and the shell as either cracks or natural articulations (T. Szczygielski, personal observation). According to de la Fuente *et al.* (2021), new, yet unpublished specimens present these attachments better. Even if not sutured, the pelvis apparently formed a very secure connection with the shell, because it is preserved

Figure 29. *Proterochersis porebensis*, *ZPAL V. 39/48*, photographs of the pelvis in dorsal (A), anterior (B), lateral left (C) and posterodorsal (D) view.

completely symmetrically despite crushing and is morphologically very similar to that of the Proterochersidae. The possibility of a sutural contact between the pelvis and shell was also suggested by Marzola (2019) for the new taxon from Greenland. The pelvis of *Proterochersis porebensis* (Fig. 35) takes the form of an M-shape in anterior view, with a long epipubis, pronounced lateral processes of the pubis, columnar, subvertical ilia and a deep pelvic fossa in the posteromedial part of the pelvis, as is typical for the Triassic pantestudinates (Fraas 1913, Jaekel 1914, 1918, Gaffney 1990, Rougier *et al.* 1995, Sterli *et al.* 2007, 2021, Li *et al.* 2008, Joyce *et al.* 2013, Schoch and Sues 2015, 2017).

Unsurprisingly, the pelvis of *Proterochersis porebensis* as a whole is virtually identical to that of the other proterochersids: *Proterochersis robusta* and *K. limendorsa* (see Fraas 1913, Joyce *et al.* 2013, Szczygielski and Sulej 2016, Szczygielski 2020). It also bears some strong resemblances to, but is narrower and higher than, the pelves of the australochelyids (Sterli *et al.* 2007, 2021).

Ilium

As in the other Triassic pantestudinates and more derived turtles (Zug 1971, Walker 1973, Gaffney 1990, Rougier *et al.* 1995, Sterli *et al.* 2007, 2021, Li *et al.* 2008, 2018, Joyce *et al.* 2013, Schoch and Sues 2015, 2017, Szczygielski and Sulej 2016, Marzola 2019), the ilium of *Proterochersis porebensis* and *Proterochersis robusta* is δ-shaped in the mediolateral aspect (Fig. 35C), with an expanded ventral part, thinner neck and expanded, posteriorly projecting dorsal part. The anterodorsal expansion is minor relative to the anteroposterior expansion. This differs from the mediolaterally flat ilium of *Eunotosaurus africanus*, which has an anteroposteriorly symmetrical, leaf-shaped dorsal part (Cox 1969).

The ilium must have fused with the carapace very early in development, because even the smallest known specimens (ZPAL V. 39/449, Fig. 32E–H; ZPAL V. 39/450, Fig. 32M–P; ZPAL V. 39/451, Fig. 32I–L) have broken off dorsalmost parts, and all the larger specimens are preserved as: (1) parts of complete pelves still connected to the shell (but still broken along the neck); (2) broken off from the shell (either disarticulated from the remainder of the pelvis or as part of a broken off acetabular region), but missing their dorsal parts; (3) solely the dorsal parts, with attached fragments of the carapace; or (4) necks with both the dorsal and ventral parts broken. Notably, with the exception of the smallest specimens, the ventral edges of the isolated ilia (where the suture with the pubis and ischium would be expected) do not have the characteristics of a suture; instead, they show broken spongiosa and frequently have worn edges. This

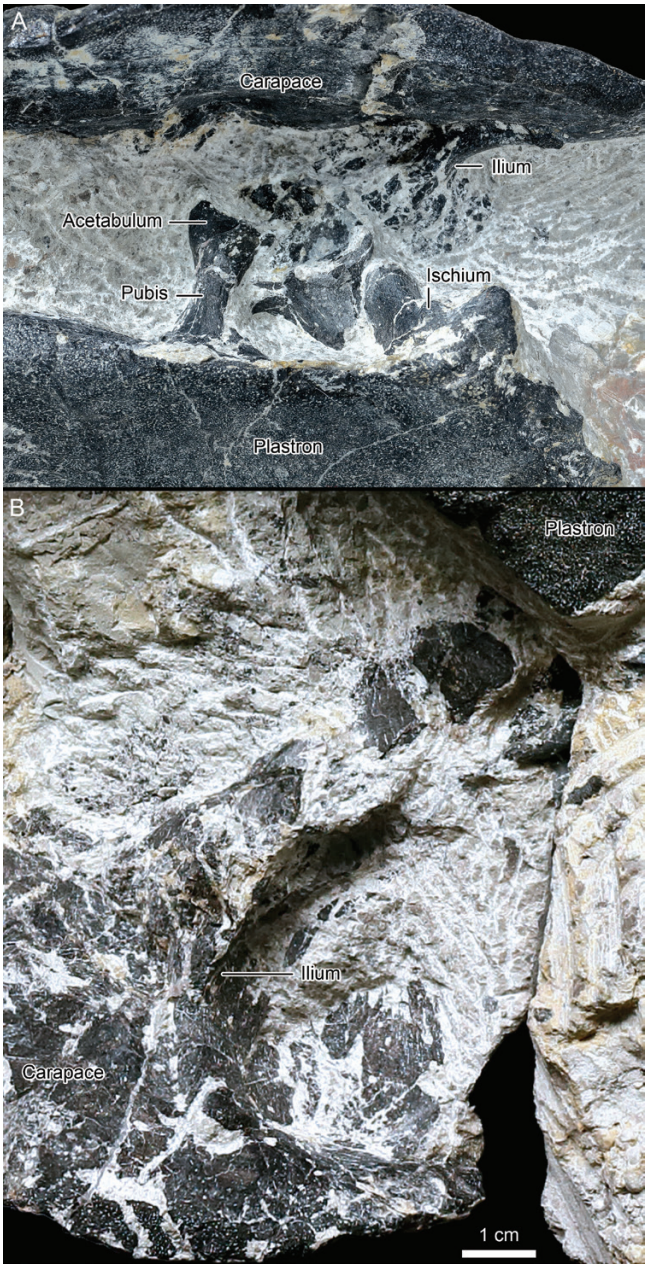

Figure 30. *Proterochersis porebensis*, *ZPAL V. 39/34*, crushed pelvis. A, left side in left ventrolateral view. B, right side in ventral view showing the connection with the carapace.

means that the connections between the pelvic bones in the acetabular region were very strong and the bones fused early, but the acetabulum failed mechanically post mortem, roughly along the lines where the sutures are in small specimens.

The ilium is attached to the carapace across its whole dorsal surface, and in large specimens (e.g. ZPAL V. 39/63, Fig. 26O–R) this attachment becomes massive and swollen, particularly in the anterior part. This differs from *Palaeochersis talampayensis*, in which (aside of the lack of co-ossification; Sterli *et al.* 2021, de la Fuente *et al.* 2021) the tip of the posterior (postacetabular) process of the ilium is free and diverges posteroventrally (Sterli *et al.* 2007). The natural cross-sections of this contact (ZPAL V. 39/63, Fig. 26R; ZPAL V. 39/193, Fig. 26J; ZPAL V. 39/276, Fig. 32Y–B'; *ZPAL V. 39/370*, Fig. 26K, M; *SMNS 12777*, Fig. 27N–S) show that in *Proterochersis* spp., unlike pleurodires, the connection does not retain a sutural character throughout life. The bones lose the intervening layers of compact bone, and the layout of the spongiosa allows them to be distinguished only locally. These rare instances indicate that the posterior process in proterochersids is indeed a part of the ilium (as in the other turtles and pantestudinates) and that the carapace does not form a ventral projection to meet the ilium (*contra* Joyce *et al.* 2013).

The dorsal part of the ilium in *Proterochersis porebensis* and *Proterochersis robusta* becomes L-shaped in cross-section as it approaches the carapace. It projects two main processes: the shorter and more dorsoventrally steep lateral process, and the longer, flatter posterior process (in most specimens directed slightly posterolaterally). This creates a deep posterolateral embayment. The posterior iliac process varies in height between the specimens. It is most pronounced ventrally in *ZPAL V. 39/370* (Fig. 26L–N), but in the remaining specimens it is flatter. It begins as a relatively deep, ridge-like structure, with the dorsal part about the width of the iliac neck in its anterior part, but gradually decreases in depth and width posteriorly, and its ventromedial face quickly dominates, creating a ventromedially facing, elongated facet. In ZPAL V. 39/193 (Fig. 26J), the posterior part of the posterior process becomes depressed relative to its edges. The anterior surface of the dorsalmost part of the ilium is flattened to gently rounded, and it faces predominantly anteriorly or slightly anterolaterally. The medial surface of the dorsal part of the ilium is straight, faces predominantly medially (very slightly posteriorly) and projects a horizontal lamina receiving the sacral ribs, which is separated from the carapace by a longitudinal fossa (Figs 1, 3, 25E, L). The ventral ridge of the first sacral rib continues ventrolaterally towards the iliac neck. The lamina continues anteriorly, towards the attachment of the preceding dorsal rib, and posteriorly, past the posterior edge of the second sacral rib, then gradually disappears into the medial surface of the posterior iliac process. In *Palaeochersis talampayensis* and *W. cavitesta*, the dorsal part of the ilium is flattened anterolatero-posteromedially, has definite concave, posteromedially facing and convex, anterolaterally facing surfaces, and thus shows pronounced curvature in cross-section (Rougier *et al.* 1995, Sterli *et al.* 2007, 2021; T. Szczygielski, personal observation). This morphology of the Triassic australochelyids is not qualitatively novel, but rather an exaggeration of the geometry already detectable in the proterochersids and *Proganochelys quenstedtii*, yet obscured by the more bulky and rounder attachment of the iliac neck in the latter two taxa (Fraas 1913, Gaffney 1990, Joyce *et al.* 2013, Szczygielski and Sulej 2016; T. Szczygielski, personal observation). In *Proterochersis robusta* (Fig. 27A, B, E, G, H, J–T, V, W), the dorsal part of the ilium is identical to that of *Proterochersis porebensis* and presents similar variability concerning the shape and prominence of the lateral and posterior process (Szczygielski 2020; the posterior process is more slender than pictured by Fraas 1913, who considered, incorrectly, the two last dorsal ribs a part of the sacrum). A good view of that region, including the connections between the ilium, carapace and sacral ribs, is presented by NHMUK 38650 and NHMUK 38653 (Fig. 27A, B; Meyer 1865, Szczygielski 2020).

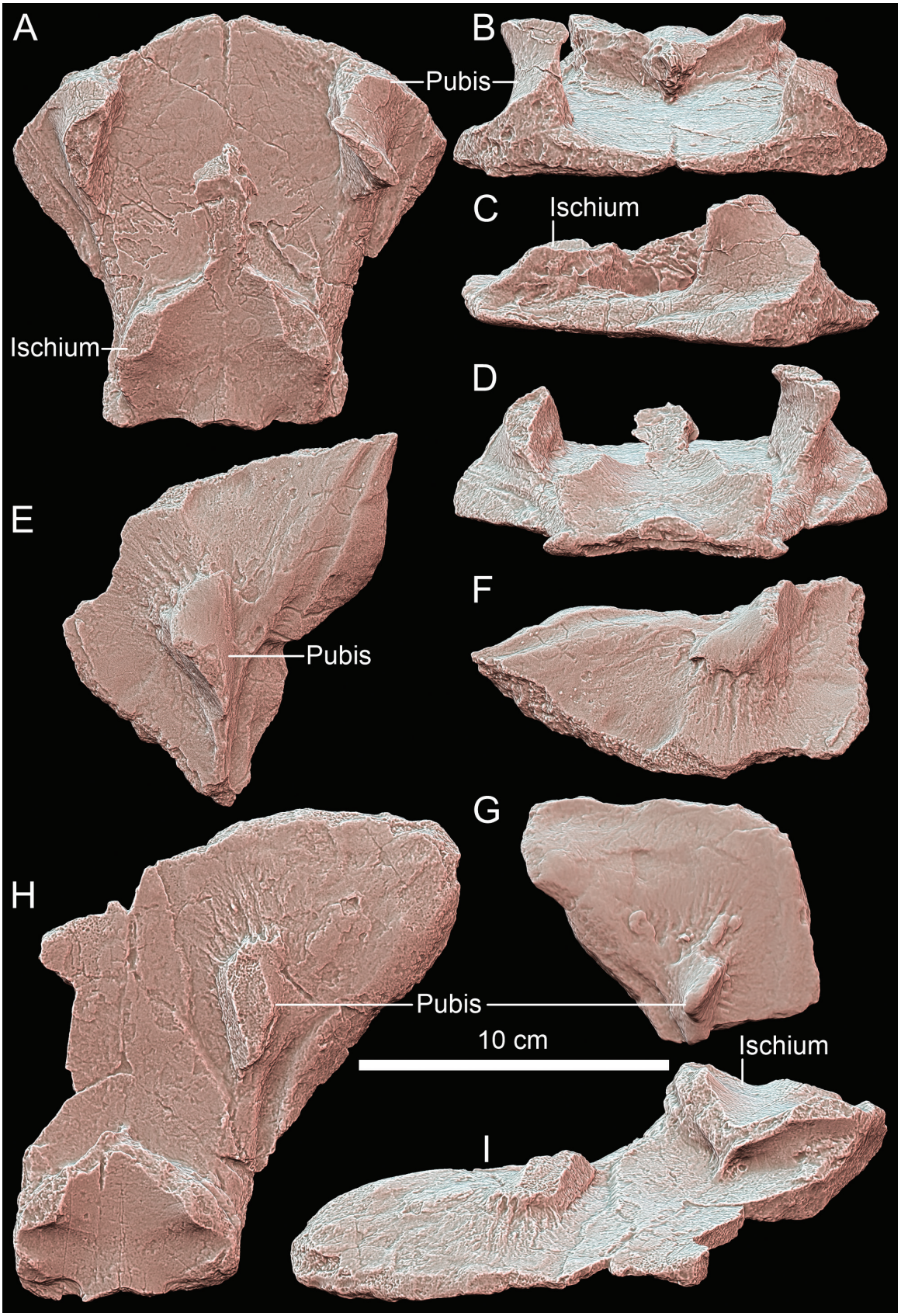

Figure 31. *Proterochersis porebensis*, connections between the pelves and plastron. A–D, ZPAL V. 39/69, posterior plastral lobe with attached bases of ischia and pubes in dorsal (A), anterior (B), right lateral (C) and posterior (D) view. E, F, ZPAL V. 39/157, plastron fragment with attached right lateral process of the pubis in dorsal (E) and anterodorsomedial (F) view. G, ZPAL V. 39/485, plastron fragment with attached left lateral process of the pubis in dorsal view. H, I, ZPAL V. 39/13, partial posterior plastral lobe with attached bases of ischia and right pubis in dorsal (H) and left anterodorsolateral (I) view. Note striations at the bases of the lateral pubic processes. Specimens are presented as three-dimensional models in orthographic projection with Radiance Scaling enabled.

Figure 32. *Proterochersis porebensis*, isolated fragmentary ilia and acetabula in anterior (A, E, I, M, Q, U, Y, C', G', K', O'), medial (B, F, J, N, R, V, Z, D', H', L', P'), posterior (C, G, K, O, S, W, A', E', I', M', Q'), lateral (D, H, L, P, T, X, B', F', J', N', R'), dorsal (S', V') and ventral (T', U', W') view. A–D, ZPAL V. 39/459, (?)right iliac neck. E–H, ZPAL V. 39/449, left ilium. I–L, ZPAL V. 39/451, left ilium. M–P, ZPAL V. 39/450, left ilium. Q–T, ZPAL V. 39/448, left ilium. U–X, S', T', ZPAL V. 39/177, left ilium. Y–B', U', ZPAL V. 39/276, left ilium. C'–F', ZPAL V. 39/458, left ilium. G'–J', ZPAL V. 39/447, left ilium. K'–N', ZPAL V. 39/460, right acetabulum. O'–R', V', W', ZPAL V. 39/461, right acetabulum. Specimens are presented as three-dimensional models in orthographic projection with Radiance Scaling enabled, sorted roughly by size. Asterisks indicate thyroid fenestra.

The iliac neck shows some variability in shape and girth. Generally, it is roughly oval in cross-section, but in some specimens this shape can be distorted by low but wide rounded ridges continuing ventrally from the processes (usually lateral and/or posterior) of the dorsal part or dorsally, above the acetabulum, or by flattening of some surfaces. Investigation of this variability and its potential relationship with the size of the specimen is difficult because, as mentioned above, the ilia are never found in one, unbroken piece, and the breaks usually occur along the neck. Nonetheless, it seems clear that the neck became proportionally thicker as the animal grew. This agrees with its subtle increase in girth with overall size observed in *Proterochersis robusta* (SMNS 16603, Fig. 27D, G, H; *SMNS 12777*, Fig. 27P–S; SMNS 56606, Fig. 27J–M). The anterior surface of the iliac neck faces slightly dorsally, and the posterior surface faces comparatively more ventrally, especially in the dorsal, posteriorly projecting part, such that the ilium as a whole projects posterodorsally and flares anteroposteriorly in the dorsal part. The lateral surface of the neck is gently concave (more dorsally developing into the fossa between the lateral and posterior process). The medial surface is usually flattened, particularly in the ventral part. In some specimens (e.g. ZPAL V. 39/448, Fig. 32R; ZPAL V. 39/449, Fig. 32F; ZPAL V. 39/450, Fig. 32N) there is a distinct ridge along the posteromedial edge of the iliac neck. The neck is proportionally longer and more slender than in *Proganochelys quenstedtii* SMNS 16980 and SMNS 17203 (see Gaffney 1990; the difference is much less distinct in lateral view in MB.R.1910.45.3 and SMF 09-F2, see Jaekel 1918, although Gaffney 1990 attributed the state of MB.R.1910.45.3 to distortion), *Palaeochersis talampayensis* (see Sterli *et al.* 2007) and *W. cavitesta* (see Sterli *et al.* 2021), probably owing to the higher profile of the shell in *Proterochersis porebensis*, and in the carapace-less *Eunotosaurus africanus* (see Cox 1969), *Pappochelys rosinae* (see Schoch and Sues 2015, 2017), *Eorhynchochelys sienensis* (see Li *et al.* 2018) and *O. semitestacea* (see Li *et al.* 2008). It is, nonetheless, substantially shorter than in most crown-group turtles (Ruckes 1929a, Zug 1971, Walker 1973). The shape and proportions of the neck appear to be roughly the same in *Proterochersis porebensis*, *Proterochersis robusta* (see Fraas 1913; Fig. 27D, G, H, J–M, P–S) and *K. limendorsa* (see Joyce *et al.* 2013; Fig. 28).

Acetabulum

The acetabular region of *Proterochersis porebensis* and *Proterochersis robusta* is subtriangular in the lateromedial aspect, concave, and faces posterolateroventrally (Fig. 35C). Each of the three pelvic bones contributes to the acetabulum and creates one of its rounded apices with a lappet of bone that partly embraced the femoral head: the ilium dorsally, pubis anteroventrally and

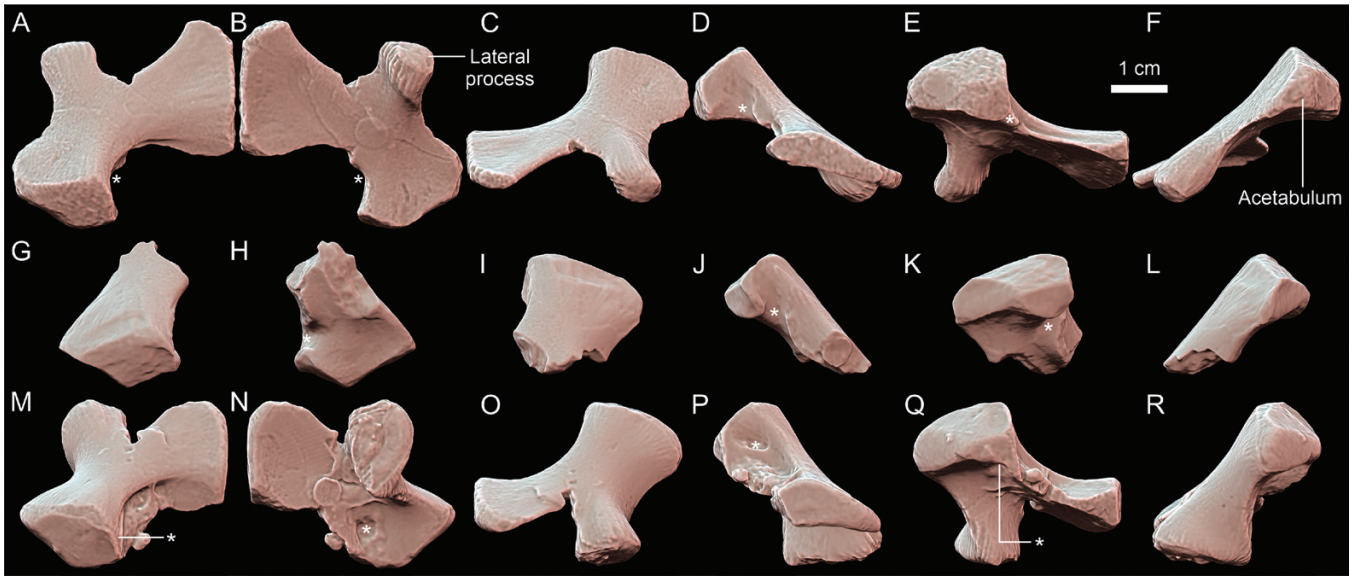

Figure 33. *Proterochersis porebensis*, isolated juvenile left pubes in dorsal (A, G, M), ventral (B, H, N), anterior (C, I, O), medial (D, J, P), posterior (E, K, Q) and lateral (F, L, R) view. A–F, ZPAL V. 39/58. G–L, ZPAL V. 39/438, dorsal branch of the left pubis. M–R, ZPAL V. 39/437. Specimens are presented as three-dimensional models in orthographic projection with Radiance Scaling enabled. Asterisks indicate thyroid fenestra.

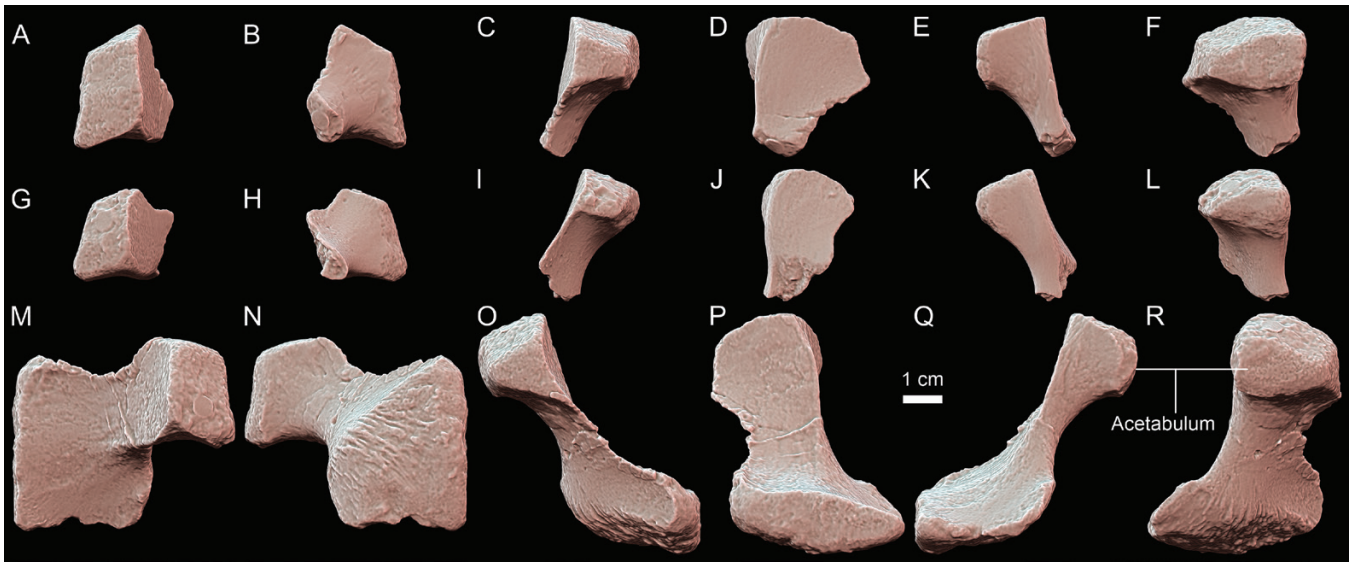

Figure 34. *Proterochersis porebensis*, isolated ischia in dorsal (A, G, M), ventral (B, H, N), anterior (C, I, O), medial (D, J, P), posterior (E, K, Q) and lateral (F, L, R) view. A–F, ZPAL V. 39/487, dorsal part of the left ischium. G–L, ZPAL V. 39/486, dorsal part of the left ischium. M–R, ZPAL V. 39/488, right ischium. Specimens are presented as 3D-models in orthographic projection with Radiance Scaling enabled.

ischium posteroventrally. Of these, the anteroventral apex is the longest and most acute, whereas the posteroventral apex is the shortest, roundest and set at the lowest angle. Aside from those apical parts, the margins along the edges of the acetabulum are much less pronounced [notched *sensu* Zug 1971; the anterodorsal (puboiliac) and ventral (puboischial) more so than the posterodorsal (ischioiliac)], but clear, nonetheless. In articular view, the posterodorsal edge is gently convex, and the ventral and anterodorsal edges are gently concave. In some specimens of *Proterochersis porebensis* (*ZPAL V. 39/48*, Figs 25B, 42B, 44A, C; ZPAL V. 39/448, Fig. 32T; ZPAL V. 39/449, Fig. 32H; ZPAL V. 39/460, Fig. 32N') and all specimens of *Proterochersis robusta* with that part preserved (*SMNS 12777*, Fig. 27Q, R; SMNS 16603, Figs 11A, 27E–H; SMNS 56606, Fig. 27K–M), within the acetabulum, close to its anterodorsal edge, there is a small, semicircular flat or gently notched area (Fig. 35C), in most cases exhibiting striation parallel to the edge. A similar structure is present in that area in *K. limendorsa* (Fig. 28B–H), *Proganochelys quenstedtii*, the new Greenland taxon and, possibly, *Chinlechelys tenertesta* but, apparently, not in *Eunotosaurus africanus*, *Pappochelys rosinae*, *Palaeochersis talampayensis* and *W. cavitesta* (see Jaekel 1918, Cox 1969, Gaffney 1990, Sterli *et al.* 2007, 2021, Joyce *et al.* 2013, Schoch and Sues 2015, 2017, Marzola 2019, Lichtig and Lucas 2021). This area is not exposed

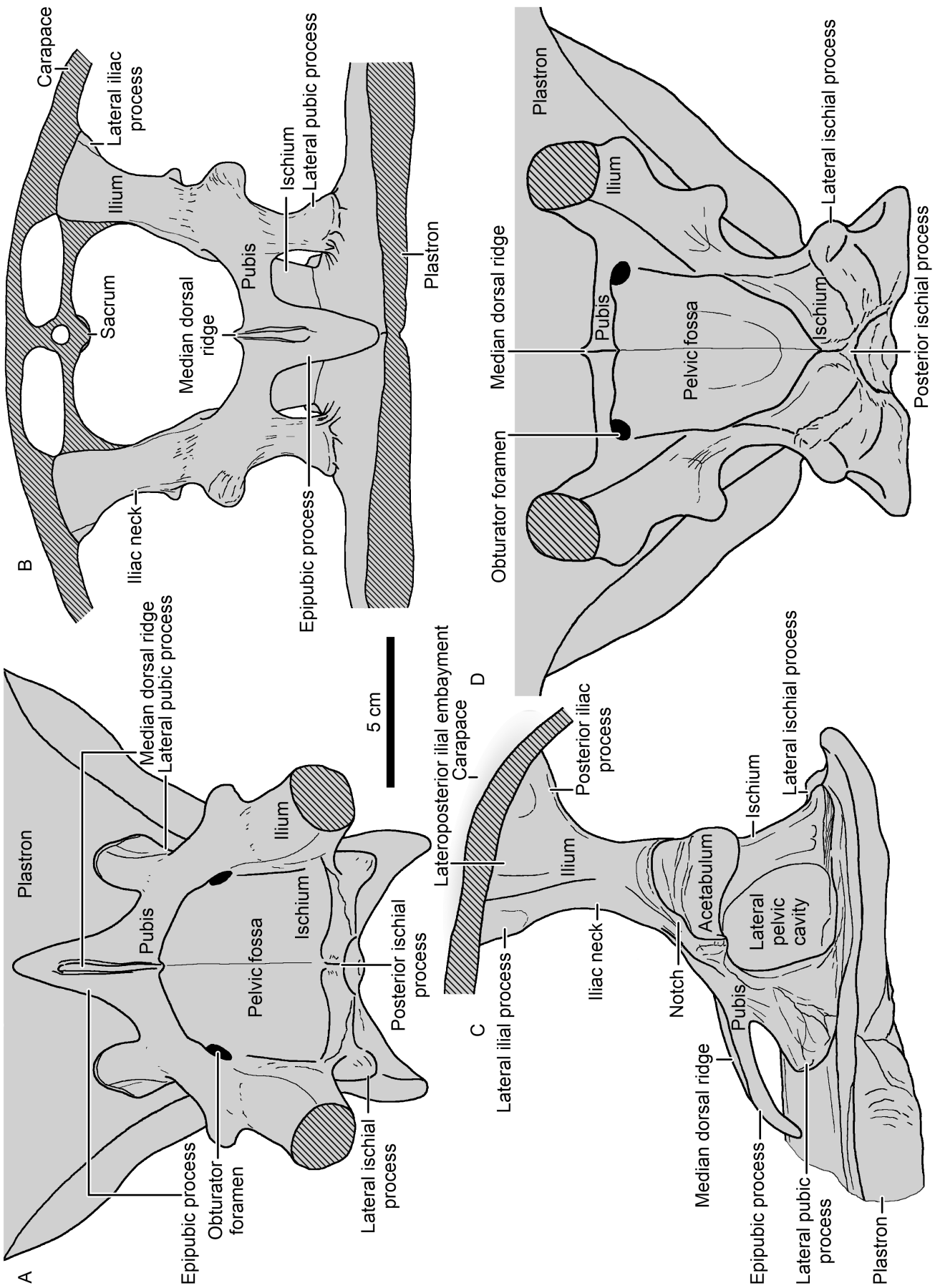

Figure 35. *Proterochersis porebensis*, *ZPAL V. 39/48*, restoration of the pelvis with partial shell in dorsal (A), anterior (B), left lateral (C) and posterodorsal (D) view.

in *Eorhynchochelys sinensis* and *O. semitestacea*. The sutures between the bones are not clearly visible in any of the articulated specimens of *Proterochersis porebensis*, but isolated pubes and ilia suggest that while the acetabular part of each of the bones was expanded, the ilium formed a larger part than the remaining two bones, and the pubic portion of the acetabulum is elongated. In *Proterochersis robusta SMNS 12777*, the articular surface of the acetabulum shows sediment-filled cracks apparently corresponding to sutures (Fraas 1913; Fig. 27Q). Their layout agrees with that deduced from disarticulated pubes and ilia of *Proterochersis porebensis*. Each of the bones had separate facets set at an oblique angle for the contact with the other two, resulting in a typical Y-shaped suture. In modern turtles, the ilium and pubis are connected with fascia most probably representing a reduced iliopubic ligament (Hutchinson 2001). The medial surface of the acetabular region is flattened, but clearly shows that the ilium is set at a different angle (more lateroventrally) than the pubis and ischium, the acetabular parts of which lie in more or less the same plane (Figs 25C, J, 27J, L, S, 29A, B, D, 32A, B, D). In large specimens (e.g. ZPAL V. 39/461, Fig. 32O'–R', V', W'), the acetabulum was proportionally thicker and more massive than in smaller individuals. The material of *Proterochersis robusta* presents a negative allometry; in SMNS 16603 (Fig. 27E–H), the acetabulum is nearly the same size as in *SMNS 12777* (Fig. 27R, S) and SMNS 56606 (Fig. 27J–M), but proportionally larger relative to the rest of the pelvis than in the latter two (see Supporting Information, Table S1). The damage or incompleteness of the material of *Proterochersis porebensis* unfortunately prohibits such comparisons.

Pubis

The pubis is a triradiate element, best presented by the small, isolated *Proterochersis porebensis* specimens ZPAL V. 39/58 (Fig. 33A–F; similar, but with different proportions compared with the juvenile *Proganochelys quenstedtii* SMNS 17203; see Gaffney 1990) and ZPAL V. 39/437 (Fig. 33M–R). It consists of the posterolaterodorsal (towards the ilium and ischium; for simplification called dorsal), anteroventrolateral (the lateral pubic process) and medial (the main plate with the epipubis) branches.

The dorsal branch contributes to the acetabulum and is the most massive part of the pubis. It is subtriangular in cross-section, with a nearly flat or gently convex anterodorsolateral surface and a concave posteroventromedial and (narrower) medial surface. Each of the corners of that branch projects a ridge anteroventrally (Fig. 33). The sharpest, lateral corner (which at the same time forms the anteroventral corner of the acetabulum) continues as a ridge along the lateral edge of the bone onto the lateral pubic process (Fig. 35A–C). The dorsomedial corner continues along the anterolateral edge of the pelvic fossa, anterodorsally to the obturator foramen (Fig. 35A, D). The ventromedial corner continues as the posterior edge of the bone to form the suture with the ischium. The obturator foramen is small (Figs 25K, 27C–E, G, H, 29A, 32O', P', V', W', 35A, D; *contra* Gaffney *et al.* 2006, possibly misled by the damaged walls of the pelvic fossa in SMNS 56606), proportionally smaller than in *Proganochelys quenstedtii* SMNS 16980 and MB.1910.45.3 (Jaekel 1918, Gaffney 1990), but similar in relative size to *O. semitestacea* (see Li *et al.* 2008), *K. limendorsa* (Fig. 28E–H; note that the foramen figured by Joyce *et al.* 2013 is artificially enlarged owing to damage, and *in vivo* their maximum diameter probably reached ~6–7 mm; Szczygielski and Sulej 2016) and *Proganochelys quenstedti* SMNS 17204 and (possibly, partly obscured by matrix) MSF 09-F2 (Gaffney 1990, Scheyer *et al.* 2022). The foramen is located on the medial face of the dorsal branch, immediately below the level of the acetabulum. It opens medially, but the short obturator canal pierces the bone subvertically, at a low angle relative to its surface, and is shielded medially just below the dorsal foramen by a very thin sheet of bone (Fig. 33P), which gives the opening an oval, slightly skewed anteroventrally outline. The dorsal opening is best preserved in *Proterochersis porebensis* ZPAL V. 39/437 (Fig. 33M–R), and the ventral opening, located in a conical pit in the roof of the lateral pelvic cavity below the acetabulum, is best preserved and prepared in *Proterochersis robusta* SMNS 16603 (Fig. 27G, H). ZPAL V. 39/437 (Fig. 33M–R) does not show any sign of a suture with the ischium, and the foramen is well separated from the posterior edge of the bone, and thus completely encased by the pubis. This morphology is shared with *Pappochelys rosinae* (see Schoch and Sues 2015, 2017), but in *Eunotosaurus africanus* and *Eorhynchochelys sinensis* the obturator foramina connect via notches with the posterior edge of the pubis, meaning that the ischium contributes to the formation of its posterior edge (Seeley 1892, Cox 1969, Gow 1997, Lyson *et al.* 2013a, Li *et al.* 2018). The morphology in *O. semitestacea* is ambiguous. The foramina seem to be fully enclosed in the paratype (*IVPP V 13240*), but the pelvis of that specimen is crushed and broken, potentially obscuring the notches (Li *et al.* 2008, 2018). In the specimen IVPP V 15653 there certainly are grooves connecting the obturator foramina with the edge, but given that the specimen is only prepared ventrally, it is unclear whether there are very narrow, nearly closed notches there or whether the foramina are, in fact, enclosed posteriorly but the closure is obscured by a residue of the matrix. In the remaining Triassic turtles, the posterior extent of the pubis is unknown owing to the complete fusion of the sutures or damage, but it is generally assumed that the obturator foramen is located in its entirety in the pubis (Gaffney 1990, Sterli *et al.* 2007). The variable size of the obturator foramina in *Proganochelys quenstedtii* was attributed by Gaffney (1990) to their artificial enlargement owing to damage, but at least in SMSN 16980, the lateral outline of the dorsal opening incised in the medial surfaces of the ilia (and thus not composed solely of thin bony plate prone to damage) appears relatively large, hinting at intraspecific or ontogenetic variability; small foramina in that species are evident only in large individuals (Gaffney 1990, Scheyer *et al.* 2022), hence it seems plausible that their size could decrease during ontogeny. Crown-group turtles have a large opening between the pubis and ischium, the thyroid foramen, which is considered an evolutionarily enlarged obturator foramen (Zug 1971, Walker 1973, Gaffney 1990).

The lateral pubic (pectineal, pectinal) process in ZPAL V. 39/58 (Fig. 33A–F) is ovoid in cross-section (thicker medially than laterally), bears pronounced striations dorsally and ventrally, and has a small bulbous protrusion on its ventral surface, but it is mostly flat; its anterodorsolateral surface lies in roughly in the same plane as that of the dorsal branch, and it is morphologically very reminiscent of the lateral processes of typical cryptodires (Zug 1971, Walker 1973, Gaffney 1990).

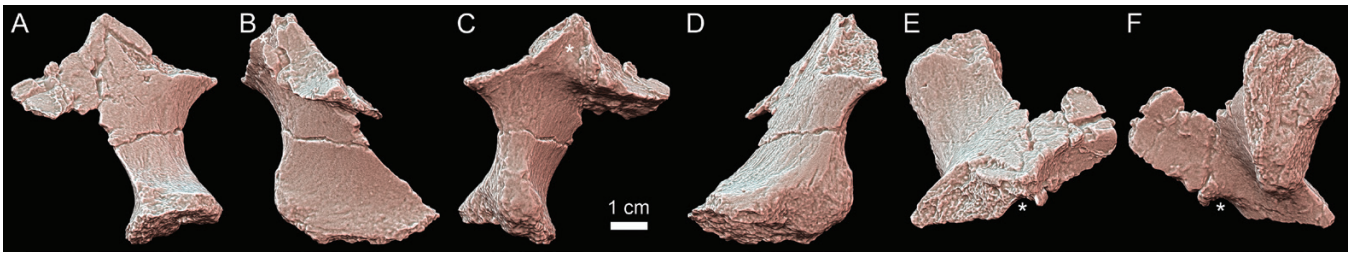

Figure 36. *Proterochersis* cf. *porebensis*, ZPAL V. 66/20, left pubis in anterior (A), medial (B), posterior (C), lateral (D), dorsal (E) and ventral (F) view. The specimen is presented as a three-dimensional model in orthographic projection with Radiance Scaling enabled. Asterisks indicate thyroid fenestra.

In ZPAL V. 39/437 (Fig. 33M–R), this morphology changes a lot: the ventral surface is expanded posteriorly, such that its anteroposterior diameter is nearly two times as large as the mediolateral diameter, and a flat articulation to the plastron is formed. Interestingly, the surface of this articulation is divided nearly in half, with the medial part forming a clear lamellar suture and the lateral part rough but featureless, probably not fully ossified. Some suture-like lamellae are also present along the posterior part of the lateral edge. Despite its more advanced stage of ossification and larger massiveness, ZPAL V. 39/437 is slightly smaller than ZPAL V. 39/58 (3.2 vs. 3.4 cm wide, measured between the lateral extreme of the lateral process and the medial edge of the main plate), exemplifying the variable tempo of development in natural populations. This variation is further accentuated by the juvenile *Proterochersis robusta* SMNS 16603 (Fig. 27F–H), which has its pubis roughly the same size as ZPAL V. 39/437 (note that *Proterochersis robusta* was a smaller species than *Proterochersis porebensis*; see Szczygielski *et al.* 2018) but the shape and size of the lateral process intermediate between ZPAL V. 39/58 and ZPAL V. 39/437 (i.e. with incipient expansion directed posterolaterally rather than posteriorly). In juvenile *Proterochersis porebensis*, the posterior expansion of the lateral pubic process is better developed. Both *ZPAL V. 39/34* (Fig. 30) and SMNS 16603 (Figs 11A, 27D–H) have their pelves firmly co-ossified with the shell; the attachments remain intact in *ZPAL V. 39/34* despite crushing, which led to breakage of the pelvis around the acetabulum (Fig. 30). In larger specimens, the lateral process is also attached to the lateral part of the xiphiplastron and is tear-shaped or crescentic in cross-section, with a rounded anterolateral edge, concave posteromedial edge and pronounced posterior expansion (best visible in ZPAL V. 39/13, Fig. 31H, I; and ZPAL V. 39/69, Fig. 31A–D). The process has a markedly sharp anteromedial edge in *Proterochersis* cf. *porebensis* from Kocury (ZPAL V.66/20; Czepiński *et al.* 2020; Fig. 36), comparatively sharper than in isolated specimens of *Proterochersis porebensis*. This might be a potential taxonomic difference, but it seems more likely that it results from preservation or ontogeny; the specimen is larger than ZPAL V. 39/437, about the size of *ZPAL V. 39/48*. In the latter and larger specimens (and in the specimens of *Proterochersis robusta*), the anteromedial edge is not prepared. The anterodorsal surface and posterior edge of the lateral process are convex, such that in lateral view the process distinctively flares ventrally, posteriorly significantly more than anteriorly. There is also some gentle lateral concavity, such that the attachment to the plastron attains a characteristic shape of a gently flattened foot (Figs 9, 25A–D, F–K, 29A–C, 31A–G, 35A–C). The morphology of the lateral process in large *Proterochersis robusta* specimens is the same (Fig. 27I–K, M, Q, R; Fraas 1913).

The lateral process is absent in *Eunotosaurus africanus* (see Seeley 1892, Watson 1914, Cox 1969, Lyson *et al.* 2013a) and *Eorhynchochelys sinensis* (see Li *et al.* 2018). In the latter, a small tubercule is present on the ventral surface of the pubis, close to the edge (Li *et al.* 2018). A distinct lateral pubic process is present in the more basal *Pappochelys rosinae* and all the remaining Triassic pantestudinates (Fraas 1913, Jaekel 1918, Gaffney 1990, Sterli *et al.* 2007, 2021, Li *et al.* 2008, Joyce *et al.* 2013, Schoch and Sues 2015, 2017, Szczygielski and Sulej 2016). Joyce *et al.* (2013) noted that in *K. limendorsa* (*SMNS 17757*, their '*Proterochersis robusta*'; Fig. 28) the contact between the lateral pubic process and plastron is intermediate between a simple articulation and sutural connection. This is difficult to confirm owing to the damage and preservation of that specimen, but if correct, it could represent a taxonomic difference; *SMNS 17757* is a large, well-ossified specimen, and the connection appears pretty secure even in relatively small specimens of *Proterochersis robusta* (SMNS 16603) and *Proterochersis porebensis* (T. Szczygielski, personal observation). The posterior ischial process of that specimen (hypothetized to represent the hypoischium by Joyce *et al.* 2013) is misaligned (Fig. 28C), but it is uncertain whether this signifies its incomplete co-ossification with the plastron or merely damage.

Proterochersis porebensis ZPAL V. 39/48 has relatively large (nearly as long as the whole pelvis), gentle but noticeable depressions on the plastron, anterior to the lateral processes of the pubis (Fig. 25D), whereas *Proterochersis porebensis* ZPAL V. 38/13 (Fig. 31H, I), *ZPAL V. 39/49* (Figs 9B, 25K), ZPAL V. 39/157 (Fig. 31E, F) and ZPAL V. 39/485 (Fig. 31G) and *Proterochersis robusta* SMNS 16442 (Fig. 27U) and SMNS 16603 (Figs 11A, 27E, H) have large, radially wrinkled surfaces in approximately the same area and medially to at least the anterior half of the attachments of the lateral pubic processes to the plastron (Szczygielski and Sulej 2019). These wrinkles begin right by the anterior and anteromedial edges of the bases of the lateral pubic processes, which are clearly raised and form transverse, rugose grooves, also constituting well-developed surfaces. The observed rugosities stretch nearly to the level of the inguinal notch and are separated by a low midline ridge running between the area of the pericardium attachment and the epipubis (Figs 6, 9, 11A, 25A, D, H, K). Similar bilateral depressions are also present in *Palaeochersis talampayensis* and *Proganochelys quenstedtii* (see Fraas 1899, Jaekel 1914, 1918, Gaffney 1990, Sterli *et al.*

2007). It seems reasonable that these structures were associated with pelvic muscles.

The medial branch of the pubis in ZPAL V. 39/58 (Fig. 33A–F) and ZPAL V. 39/437 (Fig. 33M–R) takes the form of a subtriangular plate in the dorsoventral aspect (extending anteromedially, with an almost straight posterior edge), which gradually increases in thickness posteriorly up to the point of the anterior edge of the pelvic fossa (continuation of the dorsomedial ridge projected by the dorsal branch), then thins out again, more rapidly (this change is relatively gentle in ZPAL V. 39/58, Fig. 33D; more pronounced in ZPAL V. 39/437, Fig. 33P; but very sharp in *ZPAL V. 39/48* and *ZPAL V. 39/49*). Thus, the medial branch has three main surfaces: the anterodorsolateral (almost flat, continuous with the anterodorsolateral surfaces of the lateral and dorsal branch), posterodorsal/posterodorsomedial (concave, continuous with the medial surface of the dorsal branch) and ventral (gently concave). The medial branches in ZPAL V. 39/58 (Fig. 33A, B) and ZPAL V. 39/437 (Fig. 33M, N) extend barely more anteriorly than the lateral processes and have rounded anterior terminations. At this stage, the epipubic process was apparently cartilaginous. In larger individuals, the right and left pelves are fused along the median symphysis, M-shaped in anterior view (Fig. 35B), and the ossified epipubic process is long, reaching at least twice the distance of the lateral processes (Fig. 35A, C). The symphysis bears a median dorsal ridge along the posterior half of its length, which terminates in a small posterior protrusion overhanging the anterior edge of the pelvic fossa (Figs 9, 25D, K, 29A, 35A). This ridge is also present in *Proterochersis robusta* (SMNS 50917, the only specimen with that structure preserved and exposed; Fig. 27X, Y), but absent or unknown in other Triassic pantestudinates (Gaffney 1990, Sterli *et al.* 2007, 2021, Scheyer *et al.* 2022; the dorsally exposed part of the epipubis of *K. limendorsa* is completely smooth, but this is only the anterior end, which might not be representative of the whole structure; Fig. 28A, B, D). The epipubis gradually decreases in width and bends ventrally towards its anterior tip. Apparently depending on the degree of ossification, it could either reach the plastron (*ZPAL V. 39/49*, terminating in a pit on its visceral surface, Figs 9B, 25H, I, K; probably also in *Proterochersis robusta* SMNS 50917, Fig. 27Y) or not (*ZPAL V. 39/48*, Figs 9A, 25A, B, D, 29A–C). Overall, in large individuals, the epipubis is significantly longer, more pronounced and wider posteriorly than in *Proganochelys quenstedtii* (see Jaekel 1918, Gaffney 1990, Scheyer *et al.* 2022), more similar to *Pappochelys rosinae* (see Schoch and Sues 2015, 2017), *O. semitestacea* (see Li *et al.* 2008) and *Palaeochersis talampayensis* (see Sterli *et al.* 2007). Even in small specimens, the notch between the lateral process and the medial branch in *Proterochersis porebensis* and *Proterochersis robusta* is narrower and more subtriangular in anterior and dorsal views than the rounded notch of *Proganochelys quenstedtii* (see Jaekel 1918, Gaffney 1990, Scheyer *et al.* 2022), more similar to that of *Palaeochersis talampayensis* (T. Szczygielski, personal observation; the anterior view presented by Sterli *et al.* 2007 shows this notch rounder than in reality, either as a result of an idealized interpretation based on *Proganochelys quenstedtii* or owing to some excess matrix obscuring the true shape, which has since been removed). Unfortunately, in SMNS 56606, the best-prepared pelvis of *Proterochersis robusta*, the epipubis had been broken off close to its base and subsequently restored very short (Fig. 27I–K, M), probably based on *Proganochelys quenstedtii*. Curiously, in *Eorhynchochelys sinensis* the epipubis is absent, and the anterolateral edge of the pubis is rounded and even (Li *et al.* 2018), as is the case in *Eunotosaurus africanus* (see Seeley 1892, Watson 1914, Cox 1969, Lyson *et al.* 2013a). ZPAL V. 39/69 (Fig. 31A–D) shows that in large specimens of *Proterochersis porebensis* the posteriormost part of the symphysis is supported by the anterior part of the puboischiadic keel, which takes the form of a ridge-like, bilaterally concave buttress fused mesially to the xiphiplastron.

The posterior extent of the pubis is unknown. ZPAL V. 39/437 (Fig. 33M–R) is the only isolated specimen with a preserved part of the pubis posterior to the anterior edge of the pelvic fossa, and its edge is damaged. The bone lining the anterolateral part of the fossa in that specimen is hair-thin, and even in the much larger *ZPAL V. 39/48* its thickness decreases in that region to 1 mm or less (T. Szczygielski, personal observation), which easily explains why, in the remaining specimens, it is broken off at the level of the obturator foramen. In *ZPAL V. 39/48* (Figs 25C, 29A, D) and (to a lesser extent) *ZPAL V. 39/49* (Figs 9B, 25K), the walls of the pelvic fossa are largely preserved, but these specimens are completely fused, rendering observation of the border between the pubis and ischium impossible.

Ischium

The ischium is best represented by ZPAL V. 39/488 (Fig. 34M–R). It contributes to formation of the posteroventral part of the acetabular region and forms a buttress below the acetabulum, and thus the posterior part of the pelvic fossa. The buttress is subvertical, as in *Proterochersis robusta* (see Fraas 1913; Fig. 27F–H, K, M, Q, R) and *K. limendorsa* (see Joyce *et al.* 2013, Szczygielski and Sulej 2016; Fig. 28B, D), but more upright than the anterodorsally slanted buttress in undistorted specimens of *Proganochelys quenstedtii* (see Gaffney 1990) and *Palaeochersis talampayensis* (see Sterli *et al.* 2007). Its dorsal part is subtriangular in cross-section, with well-defined, flat posterior and medial faces, a slightly rounded anterolateral face and a thin, sheet-like anterior extension, which met at some point with the pubis. The exact position of the puboischiadic suture is unknown, meaning that it is, unfortunately, impossible to determine how far anteriorly the ischium extended (see Pubis above). In ZPAL V. 39/488 (Fig. 34M–R), that part of the edge is concave in the mediolateral aspect, but it is extremally thin and probably does not represent the natural anterior border of the bone. The dorsal part of each buttress is expanded laterally and anteriorly. The buttresses gradually decrease in width around the middle of their height, then broaden ventrally again, this time expanding posteriorly and medially, such that their medial faces converge towards the bottom of the pelvic fossa. At the same time, the posterior surface of each buttress turns posteromedially, giving its ventral part a spindle-shaped cross-section (best visible in ZPAL V. 39/69, Fig. 31A). The dorsal part of the buttress is surprisingly thin, even in the middle-sized ZPAL V. 39/460 (Fig. 32K'–N', W'), and the buttress overall appears pretty slender in the remaining specimens.

Ventrally, the ischium attaches to the plastron across a subtriangular area, the posterior part of which is as wide as the plastron below (Fig. 6). This attachment is best visible as a suture in *Proterochersis porebensis* ZPAL V. 39/488 (Fig. 34N) and on the plastron in *Proterochersis porebensis* ZPAL V. 39/13 (Fig. 31H, I) and ZPAL V. 39/69 (Fig. 31A) and *Proterochersis robusta* SMNS 16442 (Fig. 27U). A poorly preserved ischial part of the pelvis is also present in SMNS 50917 (Fig. 27X, Y). The anterior corner of that area in large specimens of *Proterochersis porebensis* (e.g. ZPAL V. 39/69, Fig. 31A–D) projects anteriorly the mesial puboischiadic keel. A mesial ridge projecting anteriorly from the attachment of the ischium is also present in SMNS 16442 (Fig. 27U), although preservation of that specimen makes it ambiguous whether this ridge was expressed as a keel connecting to the pelvis. The left and right ischia meet mesially along approximately their whole length. The ventral plate is relatively thick and aligned ventromedially rather than completely vertical. Its ventral surface is mostly set at an angle of ~40° relative to the medial surface of the buttress, parallel to the floor of the ischial part of the pelvic fossa. This agrees with the medially decreasing thickness of the isolated xiphiplastron ZPAL V. 39/170 (Szczygielski and Sulej 2019) and fits the angles observed in more complete specimens. In *Proganochelys quenstedtii*, despite the lack of co-ossification with the plastron, the ischium forms a substantial, oval ventral tubercle (Gaffney 1990). Curiously, in the juvenile *Proganochelys quenstedtii*, SMNS 17203, the ventral surface of the ischium exhibits a suture-like, lamellar surface very similar to that in *Proterochersis porebensis* ZPAL V. 39/488 (Fig. 34N). The ischium in *Proganochelys quenstedtii* was positioned behind the plastron and free from it; therefore, this cannot be a remnant of a sutural connection between these structures.

Posteriorly to the pelvic fossa, the ischial plate is damaged in ZPAL V. 39/488 (Fig. 34M–R), and it is completely fused to the plastron and the intercaudal and caudal ossifications (possibly homologous to the hypoishium or neomorphic; Szczygielski and Sulej 2019) in the remaining specimens. Thus, it is difficult to distinguish boundaries between those elements. The structures present there, however, correspond well to the posterior ischial structures of the remaining Triassic pantestudinates (Gaffney 1990, Sterli *et al.* 2007, Li *et al.* 2008, 2018, Joyce *et al.* 2013). The posterolateral corner of each ischium projects a short, rounded, slightly raised lateral ischial process (lateral ischial tuberosity *sensu* Gaffney 1990, Fig. 35A, C, D). Those processes are directed predominantly laterally in juveniles (*Proterochersis porebensis ZPAL V. 39/34*. Fig. 30A; and *Proterochersis robusta* SMNS 16603, Fig. 27F, H), and in larger specimens they turn posteriorly (the process in *ZPAL V. 39/48*, Figs 9A, 25D, 29A, C, D, is still directed slightly more laterally than in *ZPAL V. 39/49*, Figs 9B, 25K), brace dorsally the caudal processes (*sensu* Fraas 1913; Fig. 6), and their dorsal, convex surfaces continue as rounded ridges towards the posterolateral edges of the ischial buttresses. In ZPAL V. 39/488 (Fig. 34M, N, Q, R), the preserved posterolateral corner of the ventral plate is relatively thin, raised dorsolaterally, and its ventral surface is suture-like, suggesting that the caudal ossification (Szczygielski and Sulej 2019) supported the lateral ischial process and, possibly, contributed to the lateral surface of the structure. In the remaining specimens of *Proterochersis porebensis* and *Proterochersis robusta*, no boundary is visible, but it seems that much of the structure (including its posterior, rounded part, not preserved in ZPAL V.38/488) was formed by the lateral ischial process proper and that the caudal ossification acted as its elevation. In *Proterochersis porebensis* (and, most probably, *Proterochersis robusta*), this area is beyond the posterior part of the xiphiplastron (Szczygielski and Sulej 2019), and in *Proterochersis robusta SMNS 12777* (Fig. 27Q, R) the lateral ischial process is separated from the underlying bone by an undulating discontinuity, possibly representing a remnant of a suture, and its surface of is distinctly rugose around that part. Mesially, there is a plate-like posterior ischial process composed of both co-ossified ischia (Fig. 35A, D). In general, it is W-shaped in the dorsoventral aspect, with slanted posteromedially, gently concave edges and a rounded mesial notch. Dorsally, it bears a low mesial ridge running along the symphysis and flanked by teardrop-shaped shallow fossae. For the most part, particularly in the anterior portion, the dorsal surface of the posterior process faces more posteriorly than the floor of the posterior part of the pelvic fossa. The posterior extent of that process is varied; in some specimens (*ZPAL V. 39/48*, Figs 9A, 25D, 29A; *ZPAL V. 39/49*, Figs 9B, 25K; ZPAL V. 39/68) it is very short to nearly non-existent and covered ventrally by the intercaudal ossification, whereas in others (*ZPAL V. 39/34*, Fig. 30A; ZPAL V. 39/66; ZPAL V. 39/69, Fig. 31A; ZPAL V. 39/70; ZPAL V. 39/71) it protrudes posteriorly past the intercaudal ossification and is exposed ventrally between the caudal processes (Szczygielski *et al.* 2018). However, it never seems to be longer than the lateral ischial processes, and in all instances it is shorter than the posterior ischial processes of *Eorhynchochelys sinensis* (see Li *et al.* 2018), *O. semitestacea* (see Li *et al.* 2008, 2018) and *Palaeochersis talampayensis* (see Rougier *et al.* 1995, Sterli *et al.* 2007). The ventral surface of the process, if exposed, bears usually weakly expressed longitudinal striations and openings of vascular canals.

Fossae of the pelvis

The pelvic fossa (Fig. 35A, D), created by the pubis anteriorly and ischium posteriorly, is U-shaped in posterior view, slightly wider anteriorly than posteriorly and dorsally than ventrally. Its anterior wall is steep, but gradually becomes subvertical posteriorly and continues into the floor without any sharp turns. The posterior part of the floor faces predominantly dorsally and slightly posteriorly. It is significantly deeper and narrower than in *Proganochelys quenstedtii* (see Jaekel 1918, Gaffney 1990, Scheyer *et al.* 2022), *Palaeochersis talampayensis* (see Sterli *et al.* 2007) and *W. cavitesta* (see Sterli *et al.* 2021), but identical to *Proterochersis robusta* (Fig. 27I, L) and *K. limendorsa* (Fig. 28C; T. Szczygielski, personal observation). Comparison with *Pappochelys rosinae*, *Eorhynchochelys sinensis* and *O. semitestacea* in this regard is difficult because of the crushing, flattening or disarticulation of all the available specimens (Li *et al.* 2008, 2018, Schoch and Sues 2015, 2017). In modern turtles, owing to the development of the large thyroid foramen and associated reduction of the ischial plates, the pelvic fossa loses its continuous character. In *Proterochersis robusta* SMNS 56606, the symphysis bears dorsally a subtle mesial ridge (Fig. 27I, L).

The space under the pelvis, limited anterolaterally by the lateral pubic processes, medially by the attachment of the puboischiadic keel to the xiphiplastron, posteriorly by the attachment of the

ischium and dorsally by the acetabular region of the pelvis and the puboischiadic plate, is additionally enclosed in the Triassic turtles ventrally by the plastron, and thus takes the form of a well-defined, deep bilateral fossa, here termed the lateral pelvic cavity (Fig. 35C). As for most structures of the pelvis, the lateral pelvic cavity in *Proterochersis porebensis* is proportionally significantly higher than in undistorted specimens of *Proganochelys quenstedtii* (see Gaffney 1990), *Palaeochersis talampayensis* (see Sterli *et al.* 2007) and *W. cavitesta* (see Sterli *et al.* 2021), but roughly identical in large specimens of *Proterochersis robusta* (Fig. 27K, M, R; the shape pictured on the drawing by Fraas 1913 is exaggerated anteroposteriorly). Apart from the generally higher profile of the pelvis in proterochersids than in the remaining Triassic turtles, this is accentuated by the posterolateral expansion of the lateral pubic process; in *Proterochersis robusta* SMNS 16603 (Fig. 27D, F), which has this expansion still incipient, the cavity is more equidimensional in lateral view. In crown-group turtles, this space is less defined owing to the presence of large thyroid fenestrae, reduction of the puboischiadic keel and (in the case of cryptodires) partial or complete disarticulation of the pelvis from the plastron, such that the pelvis is 'see-through' below the acetabulum in lateral view. Nonetheless, it is topologically recognizable and occupied by muscles.

Femur

The femur of *Proterochersis porebensis* (Figs 37, 38) is represented by 14 specimens, including 10 right (ZPAL V. 39/26, Fig. 37Y'–C''; *ZPAL V. 39/48*, Fig. 37N'–S'; ZPAL V. 39/52, Fig. 37E'–I'; ZPAL V. 39/53, Fig. 37K–O; ZPAL V. 39/166, Fig. 37T'–X'; ZPAL V. 39/216, Fig. 37Z–D'; ZPAL V. 39/432, Figs 37I''–N'', 38; ZPAL V. 39/435, Fig. 37P–T; ZPAL V. 39/436; ZPAL V. 39/500; Fig. 37D''–H'') and four left (ZPAL V. 39/217, Fig. 37A–E; ZPAL V. 39/434, Fig. 37U–Y; ZPAL V. 39/468, Fig. 37J'–M'; ZPAL V. 39/499, Fig. 37F–J). Of these, two are complete (*ZPAL V. 39/48*, Fig. 37N'–S'; and ZPAL V. 39/432, Figs 37I''–N'', 38; unfortunately, both broken along the shaft, impacting the angle between the ends), six represent the proximal ends (ZPAL V. 39/52, Fig. 37E'–I'; ZPAL V. 39/53, Fig. 37K–O; ZPAL V. 39/166, Fig. 37T'–X'; ZPAL V. 39/435, Fig. 37P–T; ZPAL V. 39/436; ZPAL V. 39/468, Fig. 37J'–M'), and six represent the distal ends (ZPAL V. 39/26, Fig. 37Y'–C''; ZPAL V. 39/216, Fig. 37Z–D'; ZPAL V. 39/217, Fig. 37A–E; ZPAL V. 39/434, Fig. 37U–Y; ZPAL V. 39/499, Fig. 37F–J; ZPAL V. 39/500, Fig. 37D''–H''). Similar to humeri, the femora of Triassic stem turtles are asymmetrical and can easily be identified as left or right based on the position of the trochanters (the trochanter minor, separate from the femoral head, is located anteriorly) and ventral fossae and ridges on the distal end (the narrow posterior fossa and iliofemoralis ridge *sensu* Schoch and Sues 2017 are located posteriorly). As for the other bones with abundant representation, the sample includes specimens coming from very small individuals (ZPAL V. 39/52, Fig. 37E'–I'; ZPAL V. 39/53, Fig. 37K–O; ZPAL V. 39/216, Fig. 37Z–D'; ZPAL V. 39/217, Fig. 37A–E; ZPAL V. 39/434, Fig. 37U–Y; ZPAL V. 39/435, Fig. 37P–T; ZPAL V. 39/468, Fig. 37J'–M'; ZPAL V. 39/499, Fig. 37F–J) and very large individuals (ZPAL V. 39/432, the largest and best-ossified femur, Figs 37I''–N'', 38; ZPAL V. 39/500, Fig. 37D''–H''). *ZPAL V. 39/48* was described and figured by Szczygielski and Sulej (2016).

Typically for turtles and Triassic pantestudinates (Jaekel 1918, Gaffney 1990, Jenkins *et al.* 1994, Sterli *et al.* 2007, Li *et al.* 2008, 2018, Schoch and Sues 2015, 2017, Marzola 2019), the proximal end of the femur bears the femoral head and two trochanters, the trochanter minor (lesser or internal trochanter) and trochanter major (greater trochanter), separated by the intertrochanteric fossa (Fig. 38). In proximal view, this end is roughly T-shaped, with the trochanter minor projecting approximately perpendicular to the plane of the femoral head and trochanter major, roughly midway between their terminal points (Fig. 38C).

As in other Late Triassic pantestudinates and more derived forms (Jaekel 1918, Zug 1971, Walker 1973, Gaffney 1990, Sterli *et al.* 2007, Li *et al.* 2008, 2018, Schoch and Sues 2015, 2017), the femoral head is offset dorsally from the shaft, relatively large, and bears a convex, proximally and dorsally facing articular surface (Fig. 38). This surface runs diagonally (posterodorsodistally) and is broad spindle-shaped, with the posteroventral edge more convex than the anterodorsal edge, terminating into a sharp (*ZPAL V. 39/48*, Fig. 37O'; ZPAL V. 39/166, Fig. 37U') or rounded, but still pronounced (ZPAL V. 39/52, Fig. 37F'; ZPAL V. 39/432, Figs 37K''; ZPAL V. 39/435, Fig. 37Q) point, giving the femoral head a subtriangular outline in dorsal view. Only ZPAL V. 39/53 (Fig. 37K–O), the smallest and least-ossified (and, possibly, slightly worn) specimen preserving the proximal part, lacks the posterodorsodistal projection of the articular surface; the head in this specimen is rounded, finger-like and featureless. The triangular outline differentiates *Proterochersis porebensis* from *Palaeochersis talampayensis* and *Proganochelys quenstedtii*, in which the articular surface also projects anterodorsodistally in a distinctive manner, and thus attains a subrectangular or trapezoid outline in dorsal view (Gaffney 1990, Sterli *et al.* 2007). It is, however, very similar to *O. semitestacea* (see Li *et al.* 2008, 2018), *Chinlechelys tenertesta* (T. Szczygielski, personal observation), the Triassic turtles from Greenland (Marzola 2019; T. Szczygielski, personal observation), swimming recent species such as *Chrysemys* spp., *Malaclemys* spp. or *Trionyx* spp. (Zug 1971), and somewhat similar to *Pappochelys rosinae* (see Schoch and Sues 2017); the morphology in *Eorhynchochelys* is not exposed (Li *et al.* 2018). Given that the same morphology is present in both the small and large, well-ossified *Proterochersis porebensis* specimens, it is clearly not dependent on the ontogenetic age and stage of ossification. As in the case of the humerus, there is some variability regarding the distal extent of the articular surface. In the small ZPAL V. 39/52 (Fig. 37E'–I'), this extent is less than in the larger specimens, and the base of the distal limit of the articular surface is directed dorsoproximally in the anteroposterior aspect, at an angle of ~75° relative to the ventral surface of the proximal end of the femur. In *ZPAL V. 39/48* (Fig. 37N', P') and ZPAL V. 39/432 (Figs 37I'', K'', 38A, D), this surface extends further distally, creating a small overhang. Interestingly, this overhang is larger in the former than in the latter (140° vs. 110°, respectively), although the distal reach of the articular surface relative to the other structures of the proximal end is approximately even. This is because, in the larger specimen (ZPAL V. 39/432), the buttress supporting the distal edge of the head is more massive, meaning that the distal concavity was partly filled by bone. The femoral heads of *Pappochelys rosinae* and *O. semitestacea* are offset at a smaller angle. *Odontochelys semitestacea* also seems to have

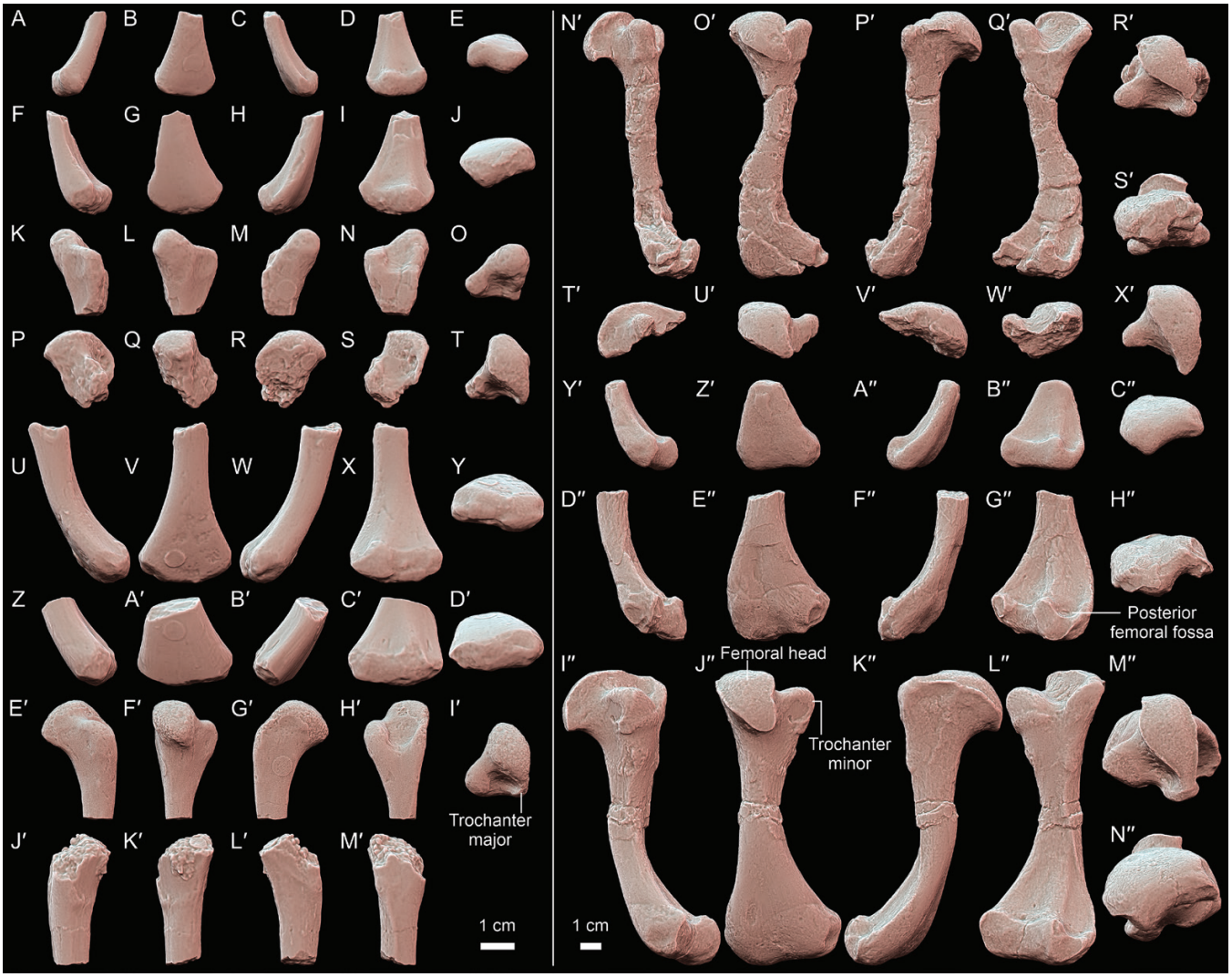

Figure 37. *Proterochersis porebensis*, femora in anterior (A, F, K, P, U, Z, E', J', N', T', Y', D'', I''), dorsal (B, G, L, Q, V, A', F', K', O', U', Z', E'', J''), posterior (C, H, M, R, W, B', G', L', P', V', A'', F'', K''), ventral (D, I, N, S, X, C', H', M', Q', W', B'', G'', L''), proximal (O, T, I', R', X', M'') and distal (E, J, Y, D', S', C'', H'', N'') view. A–E, ZPAL V. 39/217, distal part of the left femur. F–J, ZPAL V. 39/499, distal part of the right femur. K–O, ZPAL V. 39/53, proximal part of the right femur. P–T, ZPAL V. 39/435, proximal part of the right femur. U–Y, ZPAL V. 39/434, distal part of the right femur. Z–D', ZPAL V. 39/216, distal part of the right femur. E'–I', ZPAL V. 39/52, proximal part of the right femur. J'–M', ZPAL V. 39/468, proximal part of the left femur. N'–S', *ZPAL V. 39/48*, right femur. T'–X', ZPAL V. 39/166, proximal part of the right femur. Y'–C'', ZPAL V. 39/26, distal part of the right femur. D''–H'', ZPAL V. 39/500, distal part of the right femur. I''–N'', ZPAL V. 39/432, right femur. Specimens are presented as three-dimensional models in orthographic projection with Radiance Scaling enabled, sorted roughly by size.

the femoral head raised further away dorsally from the shaft, such that in anterior view the articular surface is separated by a relatively long and slender, neck-like constriction (Li *et al.* 2008, 2018, Schoch and Sues 2015, 2016).

The trochanter minor is located anteroventrally to the head (Fig. 38). It is slightly lower than the head and connected to it by a rounded ridge (web) of bone. In ZPAL V. 39/53 (Fig. 37K–O), the trochanter minor is level with that ridge and only slightly thicker; in ZPAL V. 39/52 (Fig. 37E', F', H', I'), it becomes higher (such that there is a rounded notch between it and the head), and in larger specimens it gains prominence. In *ZPAL V. 39/48* (Fig. 37N', O', Q', R'), it is about one-third higher and twice as wide as the ridge, and it is polygonal in cross-section; it has three distinct, nearly flat surfaces (anterodorsodistally, anterodistally and ventromedially) and a convex posterodorsal and posterior edge. In ZPAL V. 39/432 (Figs 37I'', J'', L'', M'', 38A–C, F), it expands dorsally and profoundly posteroventrally around the base, attaining a swollen appearance. The ridge connecting it to the femoral head also increases in robustness, becoming relatively slightly higher (about three-quarters of the height of the trochanter) and losing definition towards the intertrochanteric fossa. In that specimen, the trochanter minor is subtriangular in cross-section, as the anterodistal face is raised into a rounded ridge. The proximal tip of the trochanter minor is rounded. In *ZPAL V. 39/48* (Fig. 37N', O', Q', R'), ZPAL V. 39/52 (Fig. 37E', F', H', I') and ZPAL V. 39/53 (Fig. 37K, L, N, O), the anterior and posterior (towards the trochanteric fossa) walls of the trochanter minor are roughly parallel along most of its length, and only in the proximal third does the posterior surface turn to face posteroproximoventrally, such that the tip of the trochanter

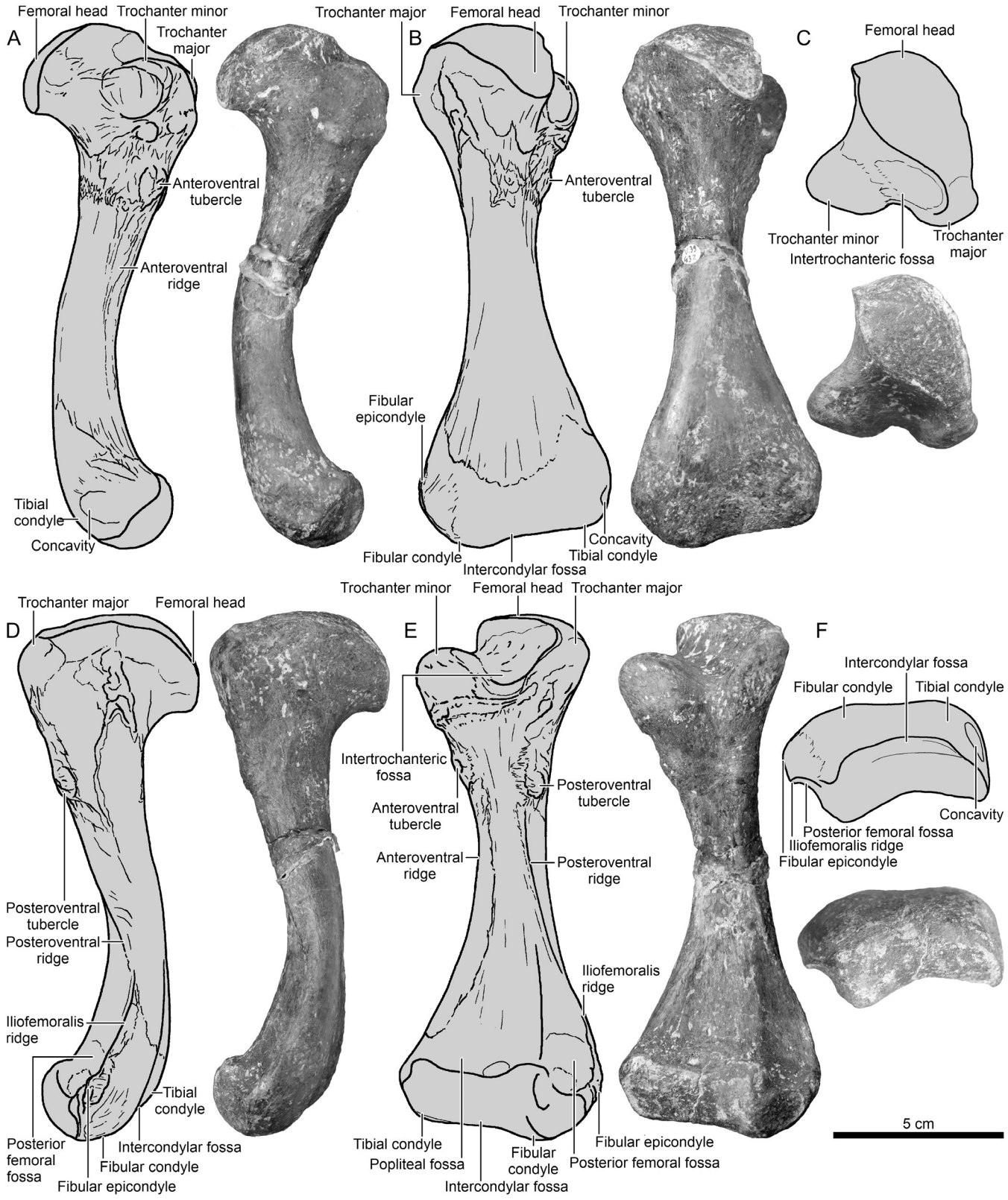

Figure 38. *Proterochersis porebensis*, ZPAL V. 39/432, restoration and photographs of the right femur in anterior (A), dorsal (B), proximal (C), posterior (D), ventral (E) and distal (F) view.

becomes thinner. In ZPAL V. 39/432 (Figs 37I'', J'', L'', M'', 38A–C, E), owing to the swelling of the base of the trochanter, this surface faces mostly proximoposteriorly along the whole length. At the base of the trochanter minor, on its anterior surface, is a small tubercle, which continues posteriorly along its ventral surface. This structure is present even in ZPAL V. 39/52 (Fig. 37E'). In *ZPAL V. 39/48* (Fig. 37N'), the tubercle is subdivided into two parts located on the edges of the anterodistal surface of the

trochanter. A similar structure is present in the paratype of *O. semitestacea* (T. Szczygielski, personal observation).

The trochanter major (Fig. 38B–E) is located posteroventrally to the head and connected to it by a rounded ridge (or web) of bone along its whole height. In general, it is thinner than the trochanter minor. It is practically absent in ZPAL V. 39/53 (Fig. 37M–O), taking the form of a low knob of bone distal to the head and proximal tip of the trochanter minor and barely more proximal than the distal limit of the intertrochanteric fossa. In ZPAL V. 39/52 (Fig. 37H', I') and ZPAL V. 39/435 (Fig. 37Q, R–T), it is more pronounced, but still distal to the head and the trochanter major (at least in ZPAL V. 39/52; ZPAL V. 39/435 has the trochanter major broken). In *ZPAL V. 39/48* (Fig. 37P'–R'), it is subequal in its proximal extent to the trochanter major, and in ZPAL V. 39/432 (Figs 37I'', K''–M'', 38A, C–F) it reaches further proximally, becoming almost level with the proximal limit of the head. Even when its proximal extent is limited (apart from ZPAL V. 39/53, in which the angle between both structures is very steep; Fig. 37M–O), the connection of the trochanter major with the head is very fluid, and both were covered by a single cartilaginous cap, as evidenced by their continuous rough surface. In all specimens, except for ZPAL V. 39/432 and ZPAL V. 39/435, the trochanter major is as thin as or barely thicker than the web of bone connecting it to the femoral head and, with the exception of ZPAL V. 39/435, about half the thickness of the trochanter major. In ZPAL V. 39/435 (Fig. 37S, T) it is even thinner, such that it terminates ventrally in a sharp edge. In ZPAL V. 39/432 (Figs 37L'', M'', 38C, F) it is notably thicker, mostly expanding anteriorly/anteroventrally in its ventral part (but the proportion of its thickness relative to the trochanter minor remains roughly the same owing to the increased robustness of the latter). To a much lesser extent, this expansion is also present in the other specimens (except ZPAL V. 39/53), meaning that the anteroventral face of the trochanter major is concave. A distinct tubercle is present in the larger specimens distal to the trochanter major, on the shaft.

The angle between the trochanters apparently increased with ontogeny. It is (measured along the external edges of the trochanters) ~30° in ZPAL V. 39/53 (Fig. 37N), 40° in ZPAL V. 39/52 (Fig. 37H'), 50° in *ZPAL V. 39/48* (Fig. 37Q') and 60° in ZPAL V. 39/432 (Figs 37L'', 38E). In well-ossified specimens (*ZPAL V. 39/48* and ZPAL V. 39/432) this angle is thus larger than in *Proganochelys quenstedtii* (see Gaffney 1990) and approaches that seen in *Palaeochersis talampayensis* (see Sterli *et al.* 2007).

The intertrochanteric fossa is a rounded V-shape in ventral view (Fig. 38E), except for ZPAL V. 39/53, in which it is nearly open posteriorly (Fig. 37N). It is proportionally deeper (proximodistally) in *ZPAL V. 39/48* (Fig. 37Q') than in ZPAL V. 39/432 (Figs 37L'', 38E) owing to the excessive thickening of the base of the trochanter minor and resulting partial filling of the fossa with bone in the latter. In any case, it is proportionally much shallower than in *Pappochelys rosinae* and more in line with other Late Triassic pantestudinates and more derived forms (Zug 1971, Walker 1973, Gaffney 1990, Sterli *et al.* 2007, Schoch and Sues 2017, Marzola 2019), including *O. semitestacea* (T. Szczygielski, personal observation). It is open proximally and ventrally (with the exception of the very minor anterior projection of the trochanter major) and is limited anteriorly by the trochanter minor, anterodorsally by the ridge between the trochanter minor and the femoral head, dorsally and posterodorsally by the femoral head and posteriorly by the trochanter major and its connection to the femoral head (Fig. 38C, E). Only in ZPAL V. 39/432 is there an incipient, barely detectable ventral closure of the intertrochanteric fossa (Figs 37L'', M'', 38C, E). A more pronounced, albeit still very limited closure is present in *Palaeochersis talampayensis* (see Sterli *et al.* 2007) and *Chinlechelys tenertesta* (see Lichtig and Lucas 2021; T. Szczygielski, personal observation), and complete or subcomplete ventral closure is typical for extant terrestrial and sea turtles (Zug 1971, Walker 1973, Lichtig and Lucas 2017). In *ZPAL V. 39/48* (Fig. 37Q'), a low ridge spans across the ventral surface of the bone, between the bases of the trochanters, along the distal limit of the intertrochanteric fossa, but this ridge is not conspicuous in the remaining specimens, and it does not obstruct the ventral opening of the fossa.

The posterior face of the proximal end of the femur, approximately halfway between the dorsal surface of the head and the ventral surface of the trochanter major, bears a rough surface that projects a low ridge ventrodistally (Fig. 38B, D). Proximal to that is a shallow concavity sharply limited proximally by the edge of the articular surface of the head. This rugosity is also present in the paratype (*IVPP V 13240*) of *O. semitestacea* (T. Szczygielski, personal observation). The state of preservation of the material of *Palaeochersis talampayensis* and *Proganochelys quenstedtii* does not allow unambiguous verification of the presence of this feature.

As is typical for turtles (Zug 1971, Walker 1973, Gaffney 1990, Sterli *et al.* 2007, Marzola 2019), the shaft bends gently ventrodistally and is triangular in cross-section in the proximal part, and more distally it becomes oval and eventually flattened, as it approaches the distal expansion (Fig. 38). Distal to the bases of the trochanters, on the anteroventral and posteroventral edges of the shaft, there are two tubercles (Fig. 38A, B, D, E). A similar morphology is pictured for *Proganochelys quenstedtii* but not described by Jaekel (1918) and Gaffney (1990) and is also present in the new taxon from Greenland (Marzola 2019). At least the anteroventral tubercle seems to be present in *Chinlechelys tenertesta* and *Palaeochersis talampayensis*, but in the latter the preservation makes it difficult to confirm (Lichtig and Lucas 2021; T. Szczygielski, personal observation). The anteroventral tubercle is located a bit more proximally than the posteroventral and projects a low, rugose, gently bowed (concave proximally) ridge dorsally or dorsoproximally across the anteroventral surface of the proximal part of the shaft, all the way to its dorsal edge (Fig. 38A, B, E). These structures are best visible in ZPAL V. 39/432 (Figs 37I'', J'', L'', 38A, B, E) and ZPAL V. 39/468 (Fig. 37J', K', M'). Further distally, along the posteroventral edge of the shaft, is a distinct ridge. This ridge is also present (albeit less pronounced) in *Proterochersis* cf. *porebensis* ZPAL V.66/12 (Fig. 39C, D) and *Proganochelys quenstedtii*, and thus is not autapomorphic for the latter, contrary to Gaffney's (1990) assumption. Another ridge is present along the anteroventral edge of the shaft; this ridge is best visible in *Proterochersis* cf. *porebensis* ZPAL V. 66/12 (Fig. 39A) and less clear, owing to preservation, in other specimens.

The distal end of the femur is expanded anteroposteriorly and subtriangular in the dorsoventral aspect (Fig. 38B, E, F). The surface of the distal end is flat and nearly vertical, while along

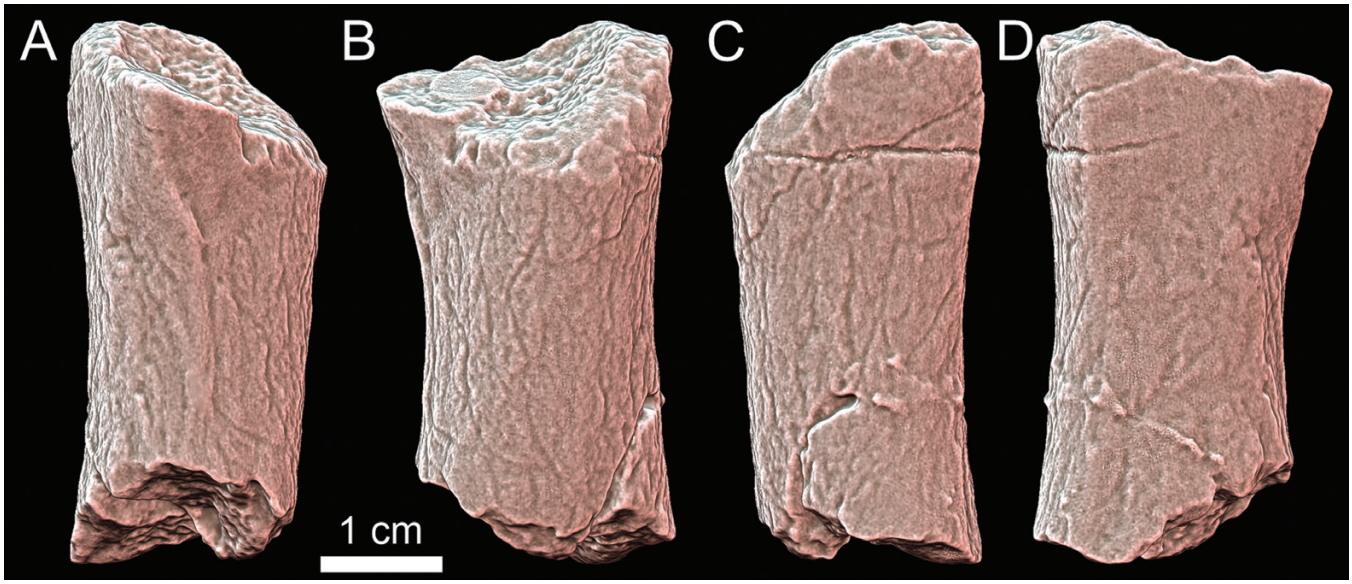

Figure 39. *Proterochersis* cf. *porebensis*, ZPAL V. 66/12, shaft of the left femur in anterior (A), dorsal (B), posterior (C) and ventral (D) view. The specimen is presented as a three-dimensional model in orthographic projection with Radiance Scaling enabled.

the posterior edge is a sharp ridge (the iliofemoralis ridge *sensu* Schoch and Sues 2017; Fig. 38D–F). The distal part of that ridge turns posteroventrally in large specimens (ZPAL V. 39/26, Fig. 37A'', B''; *ZPAL V. 39/48*, Fig. 37P', Q'; ZPAL V. 39/432, Figs 37K'', L'', 38D, E; ZPAL V. 39/500, Fig. 37F'', G'').

The dorsal surface of the distal end is gently convex, a with very light longitudinal fossa (intercondylar fossa *sensu* Gaffney 1990; intercondylar depression *sensu* Schoch and Sues 2017; Fig. 38B, D–F) along the midline visible in the large specimens (ZPAL V. 39/26, Fig. 37Z'–C''; ZPAL V. 39/432, Figs 37J''–L'', N'', 38B, D–F; ZPAL V. 39/500, Fig. 37E''–H'') and mostly featureless. The anterodistal corner bears a shallow, rounded concavity (Fig. 38A, B, F), also present (along with some rugosity) in the paratype (*IVPP V 13240*) of *O. semitestacea*, in *Palaeochersis talampayensis* and in *Proganochelys quenstedtii*, although in the last of these it is subtle, and the preservation makes it somewhat ambiguous (T. Szczygielski, personal observation). Although this feature is clear in all femora of *Proterochersis porebensis* with a well-ossified distal end, it is particularly distinct in the large ZPAL V. 39/500, in which it is surrounded by a well-defined lip (Fig. 37D'', E''). The posterodistal corner is truncated to rounded owing to the presence of a small fibular epicondyle (Fig. 38B, D–F), and in ZPAL V. 39/432 (Figs 37K'', N'', 38N, D, E) and ZPAL V. 39/500 (Fig. 37F'', H'') it bears a small rugosity. This rugosity is not visible in the remaining, smaller specimens.

The ventral surface of the distal end bears up to three longitudinal ridges: the anterior, spanning along the anterior edge to the ventral projection of the tibial (anterior, medial) condyle; the middle, spanning from the shaft to ventral projection of the fibular (posterior, lateral) condyle; and (in medium-sized and large specimens: ZPAL V. 39/26, Fig. 37B'', C''; *ZPAL V. 39/48*, Fig. 37Q', S'; ZPAL V. 39/432, Figs 37L'', N'', 38D, E; ZPAL V. 39/500; Fig. 37G'', H'') the posterior, running towards and slightly past the fibular epicondyle along the posterior edge of the bone (Fig. 38D, E). Between these ridges are located two longitudinal, subtriangular fossae (anterior and posterior; popliteal and posterior femoral fossae *sensu* Schoch and Sues 2017, the latter termed the 'groove for fibula' by Haines 1942; Fig. 38D–F). The posterior fossa is narrower than the anterior and faces posteroventrally. In the case of smaller specimens, it is located simply between the middle ridge and the posterior edge of the bone, and thus less concave. In ZPAL V. 39/26 (Fig. 37B''), *ZPAL V. 39/48* (Fig. 37Q'), ZPAL V. 39/432 (Figs 37L'', 38D, E) and ZPAL V. 39/500 (Fig. 37G''), it is limited distally by a bowed (concave proximally) ridge stretching between the fibular condyle and epicondyle.

The fibular condyle is slightly larger than the tibial condyle; it projects further both distally and ventrally (Fig. 38B, D–F). The condyles are separated by a gentle intercondylar fossa, more prominent ventrally than distally. In large specimens, the tips of the condyles project distally low ridges (Fig. 38E, F). The ridge of the tibial condyle forms the anterodistal edge of the bone. The ridge of the fibular condyle is, in its proximal part, directed distally and very gradually turns dorsally, giving the condyle a rounder, fuller outline, further contributing to its prominence. The ridges are bowed and converge dorsally, such that in distal articular view, together with the ventral edge of the condyles, they form a crescentic surface for the tibia (Fig. 38F). The articular surface for the fibula takes the form of a boomerang-shaped area delineated by three ridges: the distally projecting ridge of the fibular condyle; the ridge between the tip of the condyle and the epicondyle; and a third ridge spanning from the epicondyle along the posterodistal corner of the bone (Fig. 38D–F). It faces predominantly posteriorly and slightly ventrally. In the dorsoventral aspect, the posterior part of the tibial articulation and the fibular articulation are, in ZPAL V. 39/432 (Figs 37J'', L'', 38B, E), set at an angle of ~60°. The articular surfaces for the tibia and fibula do not seem to extend beyond the distal edge of the femur (i.e. they do not enter the dorsal surface). *ZPAL V. 39/48* presents some additional pits and grooves on its distal surface (Fig. 37S'), but these seem to be an effect of damage and/or incomplete ossification.

Among the gathered *Proterochersis porebensis* specimens, only ZPAL V. 39/432 (Figs 37I”–N”, 38) is comparable in its robustness to the femora of *Proganochelys quenstedtii* (see Gaffney 1990) and *Palaeochersis talampayensis* (see Sterli *et al.* 2007), whereas *ZPAL V. 39/48* (Fig. 37N’–S’), ZPAL V. 39/500 (Fig. 37D”–H”) and other specimens are significantly more slender, more in line with the femora of *Pappochelys rosinae* (see Schoch and Sues 2015, 2017), *Eorhynchochelys sinensis* (see Li *et al.* 2018) or *O. semitestacea* (see Li *et al.* 2008). ZPAL V. 39/432 probably belongs to an old, large individual and, despite a small difference in length (~13.5 vs. 12.5 cm for *ZPAL V. 39/48*; even less compared with ZPAL V. 39/500), its increase in robustness is massive. Therefore, although *Proterochersis porebensis* could eventually attain the limb robustness characteristic of later Triassic turtles, it appears that this happened comparatively later in ontogeny.

Tibia

The tibia of *Proterochersis porebensis* is represented by two left proximal ends of apparently small individuals: the slightly smaller ZPAL V. 39/464 (Fig. 40A–E) and slightly larger ZPAL V. 39/467 (Figs 40F–J, 41). ZPAL V. 39/467 shows a more advanced stage of ossification. Nonetheless, both specimens have rather rounded edges, indicative of their still progressing development. The most useful characters for side determination are the ventral ridge (establishing the ventral surface), inclination of the proximal articular surface (slanted medially) and the presence of a rugose surface in the dorsomedial region of the proximal expansion.

The proximal articular surface is oval in articular view, slightly wider mediolaterally than dorsoventrally, and projects ventrally into a small but distinct process (Figs 40E, J, 41E). The dorsolateral part of the articular surface is convex, meaning that it reaches further proximally than the ventromedial part, which is gently concave. As in other testudinates (Gaffney 1990, Sterli *et al.* 2007), these surfaces articulated with the intercondylar trough and medial (tibial) condyle of the femur, respectively. The proximal end is significantly wider than the shaft, apparently even more so than in *Palaeochersis talampayensis* (see Sterli *et al.* 2007), *Proganochelys quenstedtii* (see Gaffney 1990, Scheyer *et al.* 2022) and the new taxon from Greenland (Marzola 2019), definitely more than in most crown-group turtles (Walker 1973, Gaffney 1990), but comparable to at least some specimens of *Pappochelys rosinae* (see Schoch and Sues 2015, 2017). In *Eunotosaurus africanus*, the degree of the proximal expansion appears to vary from very minor (Cox 1969, Gow 1997) to very substantial (Gow and Klerk 1997). As in *Pappochelys rosinae* (see Schoch and Sues 2017), *O. semitestacea* (at least the holotype; T. Szczygielski, personal observation), *Proganochelys quenstedtii* (see Gaffney 1990, Scheyer *et al.* 2022), *Palaeochersis talampayensis* (see Sterli *et al.* 2007), the new taxon from Greenland (Marzola 2019), more derived turtles (Zug 1971, Walker 1973, Gaffney 1990) and, apparently, *Eunotosaurus africanus* (see Cox 1969), the cnemial crest (Fig. 41A–C, E) is very low (the dorsal surface of the tibiae of *Eorhynchochelys sinensis* are embedded in sediment, obscuring the morphology; Li *et al.* 2018). As in *Palaeochersis talampayensis*, *Proganochelys quenstedtii* and more derived turtles (Gaffney 1990, Sterli *et al.* 2007, Scheyer *et al.* 2022), the area of attachment for the patellar tendon, located on the proximomedial part of the dorsal surface of the proximal expansion, is nearly flat but rugose (Fig. 41A, B). Along its mediodistal edge is an elongated, swollen field, which is much more pronounced in ZPAL V. 39/467 (Figs 40F, G, I, 41A, B, D) than in the smaller ZPAL V. 39/464 (Fig. 40A, B, D) and projects slightly beyond the medial edge of the proximal end of the bone. A similar, even more pronounced eminence is present in the paratype (*IVPP V 13240*) of *O. semitestacea* (see Li *et al.* 2008; T. Szczygielski, personal observation) and the new taxon from Greenland (Marzola 2019), and a similar-sized structure was figured, but not mentioned, in *Palaeochersis talampayensis* by Sterli *et al.* (2007). A smaller eminence is also visible in the holotype of *Pappochelys rosinae*, *SMNS*

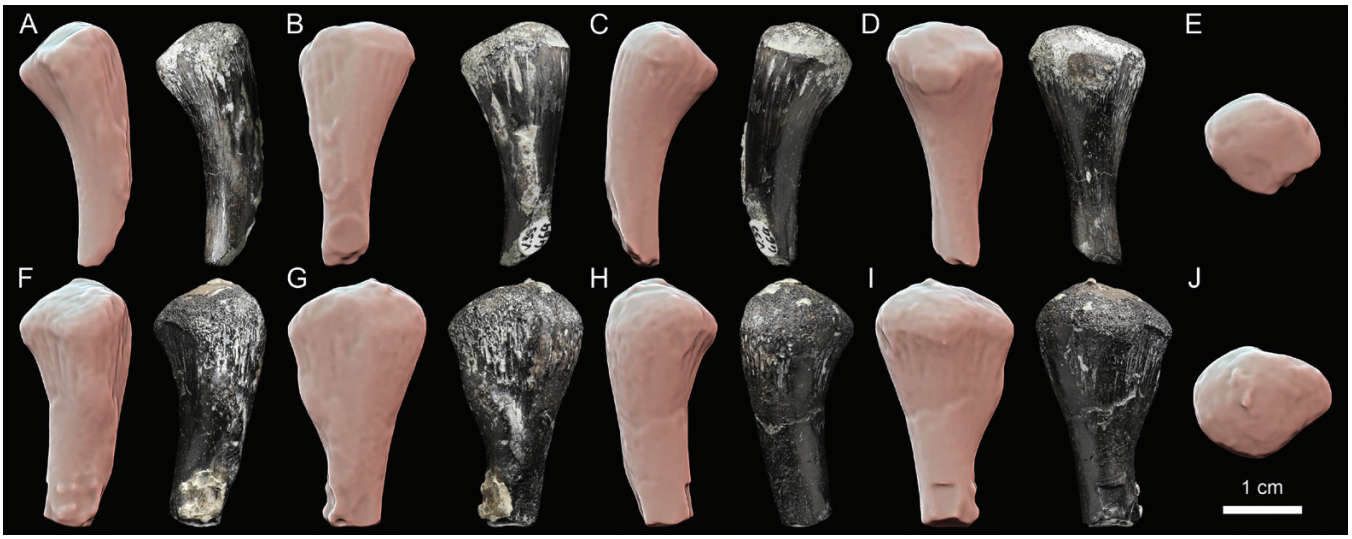

Figure 40. *Proterochersis porebensis*, proximal parts of left tibiae in medial (A, F), dorsal (B, G), lateral (C, H), ventral (D, I) and proximal (E, J) view. A–E, ZPAL V. 39/464. F–J, ZPAL V. 39/467. Three-dimensional models presented in orthographic projection with Radiance Scaling enabled.

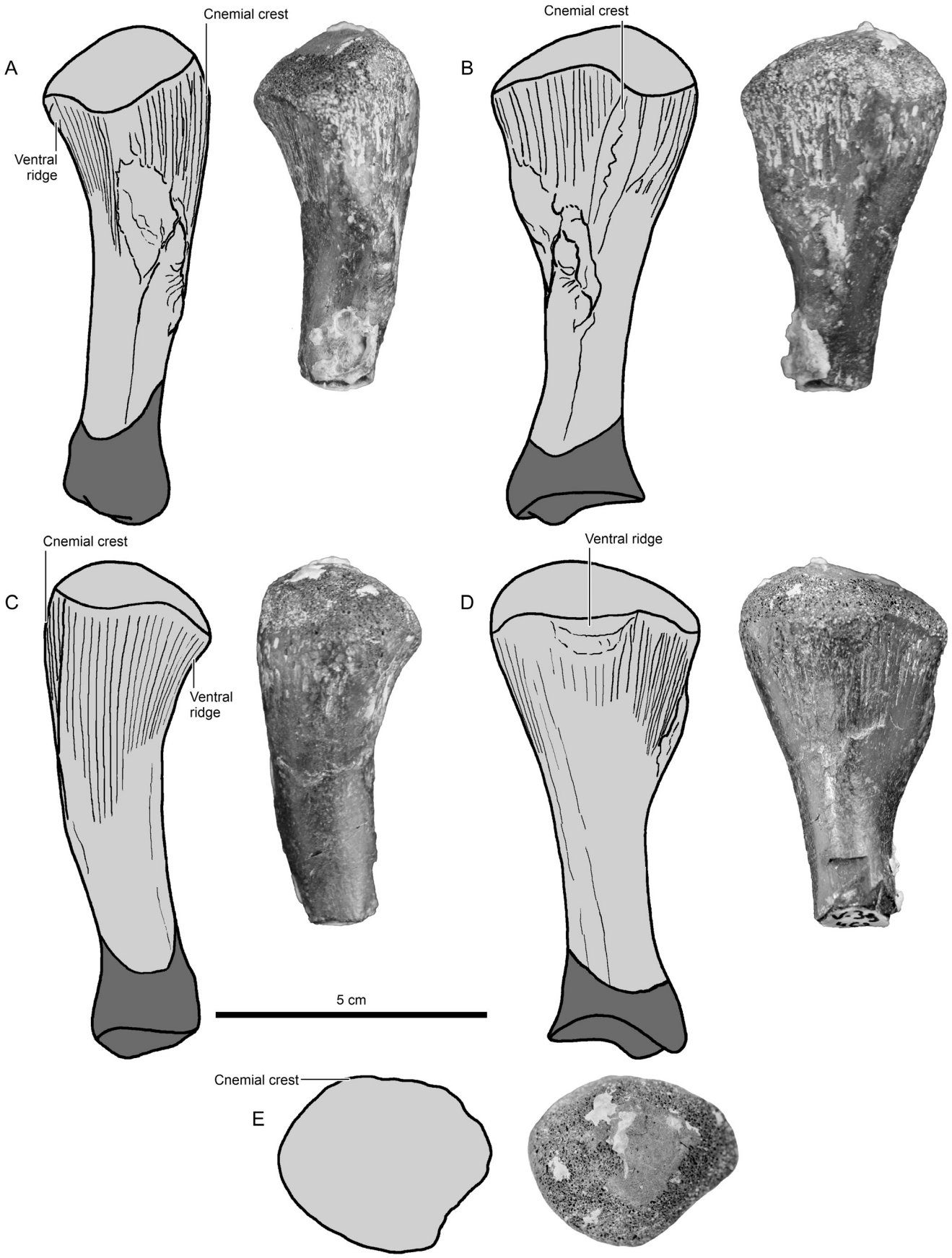

Figure 41. *Proterochersis porebensis*, ZPAL V. 39/467, restoration and photographs of the left tibia in medial (A), dorsal (B), lateral (C), ventral (D) and proximal (E) view. Missing parts of the bone are marked with dark grey.

91360 (Schoch and Sues 2015). In most tibiae of *Proganochelys quenstedtii* it is not conspicuous (Gaffney 1990), although it is visible in SMNS 17204 (T. Szczygielski, personal observation) and SMF 09-F2 (Scheyer *et al.* 2022). As in other Triassic pantestudinates and more derived turtles (Gaffney 1990, Sterli *et al.* 2007, Li *et al.* 2008), ventrally, starting from the ventral projection of the articular surface and continuing towards the shaft, is a low, rounded ridge, which subdivides the ventral surface of the proximal expansion of the tibia into two fields (Fig. 41A, C, D). In the relatively simple tibia of *Eunotosaurus africanus*, this ridge appears to be missing (Cox 1969).

The shaft is subcircular in cross-section and very slender compared with *Eorhynchochelys sinensis* (see Li *et al.* 2018), *Palaeochersis talampayensis* (see Sterli *et al.* 2007), *Proganochelys quenstedtii* (see Gaffney 1990, Scheyer *et al.* 2022) and the new taxon from Greenland (Marzola 2019), more in line with uncrushed tibiae of *Pappochelys rosinae* (see Schoch and Sues 2015, 2017). In the mediolateral aspect, the preserved part is gently curved ventrally (Figs 40A, C, F, H, 41A, C).

Fibula

The fibula of *Proterochersis porebensis* is represented by a single left well-ossified distal end of a seemingly large individual (ZPAL V. 39/220, Figs 42, 43). The side determination is easy, based on the lappet-like crest projecting medially from the flat dorsal surface of the distal expansion and the medial inclination of the distal articular surface.

Very little of the shaft is preserved. It is ovoid in cross-section, wider medially than laterally.

The distal end of the fibula is expanded lateromedially and subtriangular in the dorsoventral aspect. The expansion relative to the shaft is comparable to *Eunotosaurus africanus* (see Gow 1997, Gow and Klerk 1997) and *Proganochelys quenstedtii* (see Gaffney 1990, Scheyer *et al.* 2022), but larger than in *Palaeochersis talampayensis* (see Sterli *et al.* 2007). As in *Proganochelys quenstedtii*, the lateral edge is gently sinuous, while the medial edge bears a conspicuous crest (Figs 42A, B, D, 43A, B, D), which distorts the triangular outline of that part (Gaffney 1990, Scheyer *et al.* 2022). This crest is level with the

Figure 42. *Proterochersis porebensis*, ZPAL V. 39/220, distal part of left fibula in medial (A), dorsal (B), lateral (C), ventral (D) and distal (E) view. Three-dimensional model presented in orthographic projection with Radiance Scaling enabled.

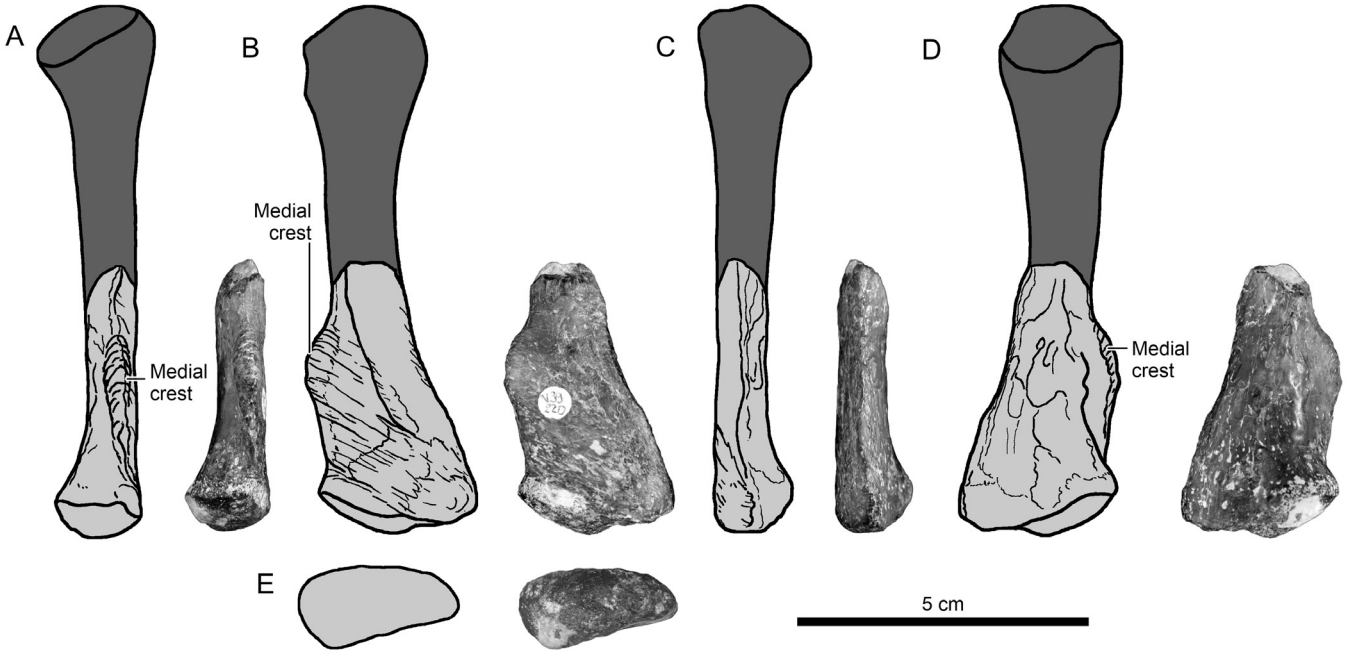

Figure 43. *Proterochersis porebensis*, ZPAL V. 39/220, restoration and photographs of the left fibula in medial (A), dorsal (B), lateral (C), ventral (D) and distal (E) view. Missing parts of the bone are marked with dark grey.

nearly flat dorsal surface of the bone, rugose, and directed more proximally than in case of *Proganochelys quenstedtii* figured by Gaffney (1990) and Scheyer *et al.* (2022), but this might be attributable to the advanced ossification stage of ZPAL V. 39/220. The preserved material of *Palaeochersis talampayensis* lacks this crest (Sterli *et al.* 2007), and a very minor medial flange seems to be present in *Pappochelys rosinae* (see Schoch and Sues 2017) and, more distally, in *Eorhynchochelys sinensis* (see Li *et al.* 2018).

The dorsal surface is nearly flat, with a subtle diagonal, laterodistal ridge. The ventral surface is convex. As in *Proganochelys quenstedtii* but not *Palaeochersis talampayensis*, the medial part of the distalmost end distinctly flares medially and ventrally, towards the expanded articular facet (Gaffney 1990).

The distal articular surface forms two gently convex facets separated by a shallow groove. The lateral facet is nearly perpendicular to the long axis of the bone, and the medial facet is directed mediodistally and set at an angle of ~60° relative to the medial (Figs 42, 43). In articular view, the distal surface is elongated tear-shaped, wider medially than laterally, with a gently convex dorsolateral edge and concave ventrolateral edge (Fig. 42E, 43E).

Ungual

A single ungual of *Proterochersis porebensis* is known, ZPAL V. 39/491 (Fig. 44), probably belonging to a small specimen. The ungual is almost three times as long as it is wide, gently curved ventrally, subcircular in proximal view, but compressed dorsoventrally towards the distal end. The proximodorsal process is slightly larger than the proximoventral; both are moderate in size. The flexor tubercle is located around the proximal third of the length of the ungual and is small. The distal taper is very minor in the dorsoventral aspect. The apex is rounded in the dorsoventral aspect and sharpened in the mediolateral aspect. Overall, the specimen is most similar to the unguals of *Proganochelys quenstedtii* (see Gaffney 1990, Scheyer *et al.* 2022), *Palaeochersis talampayensis* (see Sterli *et al.* 2007) and (less so) *O. semitestacea* (see Li *et al.* 2008, Lyson *et al.* 2016). It differs from the bulbous unguals of *Eunotosaurus africanus* (see Lyson *et al.* 2016) or the narrow unguals of *Pappochelys rosinae* (see Schoch and Sues 2015, 2017) and *Eorhynchochelys sinensis* (see Li *et al.* 2018).

DISCUSSION

Comparison of *Proterochersis* spp. with basal forms

The girdles and limbs of proterochersids exhibit morphology typical for Late Triassic stem turtles and transitional between non-turtle pantestudinates and more derived turtles (Supporting Information, Table S2). This includes, most notably, the shape and length of the dorsal scapular process, acromion, coracoid and puboischiadic plate. The scapula becomes L-shaped, with elongate dorsal and acromial processes; the dorsal process is already rounded and rod-like rather than lateromedially flattened, but the acromion has a triangular cross-section owing to the presence of lamellae connecting it to other structures of the scapulocoracoid. The coracoid is posteriorly elongated but has a rounded posteromedial edge, hence its shape is intermediate between the mostly round, plate-like coracoids of less derived taxa (e.g. Cox 1969, Gaffney 1990, Gow 1997, Lyson *et al.* 2016, Schoch and Sues 2017) and the more rectangular and eventually long and only distally expanded coracoids of modern turtles (e.g. Jaekel 1914, 1918, Walker 1973, Gaffney 1990, Sterli *et al.* 2007, 2021). The coracoid foramen is completely enclosed between the scapula and the coracoid and is relatively small, although larger than in less derived taxa (e.g. Cox 1969, Gaffney 1990, Gow 1997, Lyson *et al.* 2016). Finally, with the development of distinct lateral processes of the pubis, the epipubic process and pelvic fossa, the pelvis attained a more three-dimensionally complex shape compared with the simpler, plate-like configuration of less derived amniotes (e.g. Cox 1969, Gaffney 1990, Li *et al.* 2018).

The humeri of *Pappochelys rosinae* are, in most morphological aspects, similar to small, poorly ossified humeri of *Proterochersis porebensis* (e.g. ZPAL V. 39/165, ZPAL V. 39/446; Schoch and Sues 2015, 2017; T. Szczygielski, personal observation). The main differences include a smaller thickness of the proximal and distal expansions and lesser proximal and mediolateral extent of the medial and lateral processes of the former (Schoch and Sues 2017), which, in the small specimens of the latter, were covered by cartilage.

No specimen of *Pappochelys rosinae* has a visible ectepicondylar foramen or groove (Schoch and Sues 2017), which might also indicate a comparatively lesser extent of ossification in that animal; in the least-ossified specimens of *Proterochersis porebensis*, ZPAL

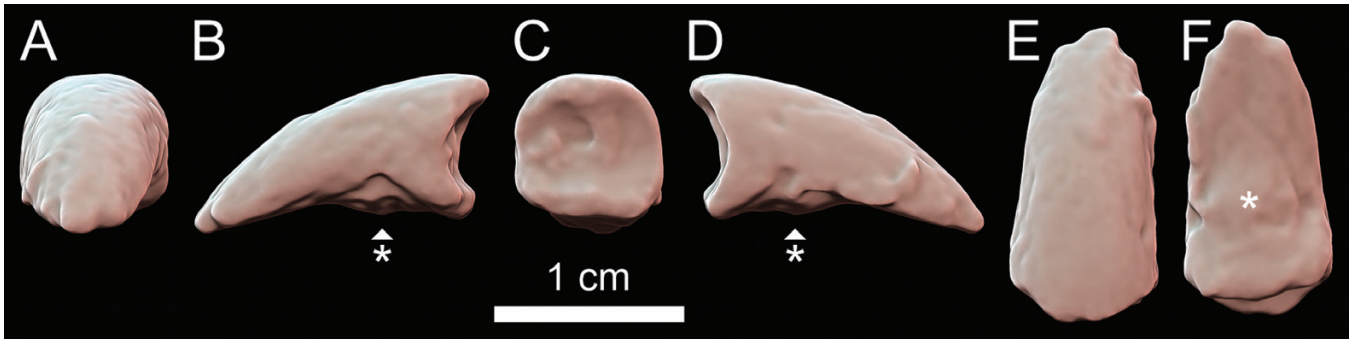

Figure 44. *Proterochersis porebensis*, ZPAL V. 39/491, ungual in apical (A), lateral (B, D), basal (C), dorsal (E) and ventral (F) view. The flexor tubercle is indicated with an asterisk. The specimen is presented as a three-dimensional model in orthographic projection with Radiance Scaling enabled.

V. 39/442 and ZPAL V. 39/446, the ectepicondylar groove is merely several millimetres long and barely registers on the bony distal part of the humeri. The differences might be, to some degree, ontogenetic or taphonomic in nature, but are likely to be related to the miniscule size and aquatic mode of life of *Pappochelys rosinae*. Likewise, the humeri of the holotype of *Eorhynchochelys sinensis* (*SMMP 000016*; rounded humeral head, no pronounced notch between the head and lateral process, large but unroofed ectepicondylar groove), despite their large size, appear to correspond well to the middle-sized and moderately ossified specimen ZPAL V. 39/156 (Li *et al.* 2018). In contrast, the morphology of the humeri in the specimens *IVPP V 15639* (holotype) and IVPP V 15653 of *O. semitestacea* correspond well to the younger, less ossified specimens of *Proterochersis porebensis* (poorly developed articular surfaces and processes, undeveloped ectepicondylar foramen), whereas the morphology of the paratype (*IVPP V 13240*; well-developed articular surfaces, processes and ectepicondylar foramen) is very similar to the large, well-ossified specimens of the latter (Li *et al.* 2008, Rothschild and Naples 2015; T. Szczygielski, personal observation), despite the small size and aquatic ecology of that species. This suggests that forelimb morphology in the Triassic pantestudinates was influenced not merely by the body size and mode of life, but by a more complex interplay of factors, and all those species developed along a very similar developmental pathway. These similarities are also, to an extent, true for the hindlimbs. SMNS 92085, a femur of *Pappochelys rosinae*, is, in many respects, similar to poorly ossified small specimens of *Proterochersis porebensis*, such as ZPAL V. 39/52, but differs in its proportions (more elongated shaft compared with the ends), the lower offset angle of the femoral head and much deeper (proximodistally) intertrochanteric fossa (Schoch and Sues 2017). *Odontochelys semitestacea*, with the exception of the more proximally inclined femoral head and more pronounced constriction below it (Li *et al.* 2008, 2018), shows a morphology very similar to that of *Proterochersis porebensis*. The inclination of the articular surfaces of the humerus and femur in adult *Proterochersis porebensis* is intermediate between the Triassic non-testudinate pantestudinates (Li *et al.* 2008, 2018, Schoch and Sues 2015, 2017) and more derived Triassic turtles (Jaekel 1918, Huene 1926, Gaffney 1990, Jenkins *et al.* 1994, Sterli *et al.* 2007, Marzola 2019).

Functional anatomy

Although the exact proportions of limb bones cannot be established owing to the isolated nature of most specimens, their relative degree of ossification and comparisons with *ZPAL V. 39/48* and other turtles allow some insights (Figs 45, 46). The largest known humerus, ZPAL V. 39/50, is shorter than the femur of *ZPAL V. 39/48*, although the former appears to represent a more advanced stage of ossification than the latter. ZPAL V. 39/432, the largest femur showing an ossification stage seemingly more comparable to ZPAL V. 39/50, is slightly larger. The size of the scapulocoracoid of *ZPAL V. 39/48* suggests that the humerus could not be much smaller (or larger) than ZPAL V. 39/50. This agrees with the relatively constant acetabulum size in *Proterochersis robusta* specimens of varied size and the small difference in length between *ZPAL V. 39/48* and ZPAL V. 39/432 (~1 cm), indicating that, in adults, the bones mainly gained girth and massiveness, and their anatomical features became more prominent. This is confirmed by ZPAL V. 39/17, the partial scapulocoracoid, which, despite its significantly greater massiveness, has its glenoid only slightly larger than the scapulocoracoid of *ZPAL V. 39/48*. Based on that evidence, it seems reasonable that *Proterochersis porebensis* had the humerus (Fig. 45) slightly shorter than the femur (Fig. 46), similar to *Pappochelys rosinae* and *Proganochelys quenstedtii* (*contra* Lyson *et al.* 2016) and in contrast to *O. semitestacea* and *Palaeochersis talampayensis*, which have these bones roughly the same length (Gaffney 1990, Sterli *et al.* 2007, Li *et al.* 2008, Schoch and Sues 2017).

The more or less vertically oriented dorsal scapular process of modern turtles allows rotation of their triradiate scapulocoracoid during walking, which increases the stride length (Walker 1971, Mayerl *et al.* 2019). It was suggested (Joyce *et al.* 2013) that this adaptation appeared in the evolution of Testudinata very early and was already present in the family Proterochersidae, or even in non-testudinate pantestudinates, such as *O. semitestacea*. In the Proterochersidae and *Proganochelys quenstedtii*, the dorsal processes of the scapulae (or their cartilaginous, episcapular extensions) articulated with distinct pits in the visceral surface of the carapace, located in front of the rib pair of the ninth vertebra (Fig. 45) and, in *Proganochelys quenstedtii*, behind the articulation sites of the dorsal processes of the epiplastra (Fraas 1913, Jaekel 1918, Gaffney 1990, Joyce *et al.* 2013, Szczygielski and Sulej 2016). In *Palaeochersis talampayensis* and *W. cavitesta*, this region is not preserved sufficiently (Rougier *et al.* 1995, Sterli *et al.* 2007, 2021), but it seems likely that the articulation was similar. In modern turtles, the distinctiveness of those pits varies (T. Szczygielski, personal observation), but the articulation pattern is the same.

Proterochersidae share an osseous attachment of the pelvis to the shell (Fig. 46) with Pleurodira (Walker 1973). In fact, the original description of *Proterochersis robusta* concluded that this species is a pleurodire (Fraas 1913), and this was widely accepted for nearly a century (Gaffney 1975, 1988, 1990, Gaffney *et al.* 1991, 2006, 2007, Lapparent de Broin 1996, 2000, Sterli *et al.* 2007), until the position of that taxon on the stem was revealed (e.g. Rougier *et al.* 1995, Joyce 2007, Sterli 2010, Anquetin 2012, Joyce *et al.* 2013, Szczygielski and Sulej 2016). Currently, the independent acquisition of the bony connections between these elements in the Proterochersidae and Pleurodira is widely accepted, but aside from its evolutionary origin, the structural (and, accordingly, functional) differences are noteworthy. Apart from the co-ossification, the proterochersids show a generally plesiomorphic structure of their pelves, with the well-developed ischium and pubis in many aspects reminiscent of *Pappochelys rosinae*, *O. semitestacea* and the Australochelyids (Sterli *et al.* 2007, 2021, Li *et al.* 2008, Schoch and Sues 2015, 2017) and less similar to *Proganochelys quenstedtii*, with its reduced epipubis and larger thyroid fenestrae (Jaekel 1918, Gaffney 1990). Most notably, however, they lack many of the modifications typical for the pleurodires. The pleurodires are characterized by the reduced width of the pelvis, reduction of the puboischiadic plate associated with the enlargement and subsequent fusion of the thyroid fenestrae and reduction of the symphyseal surfaces, reduction of the sacral ribs and, in some cases, sacralization of the posterior dorsal vertebrae (Ruckes 1929a, b, Walker 1973, Gaffney 1990, Lapparent de Broin 1996).

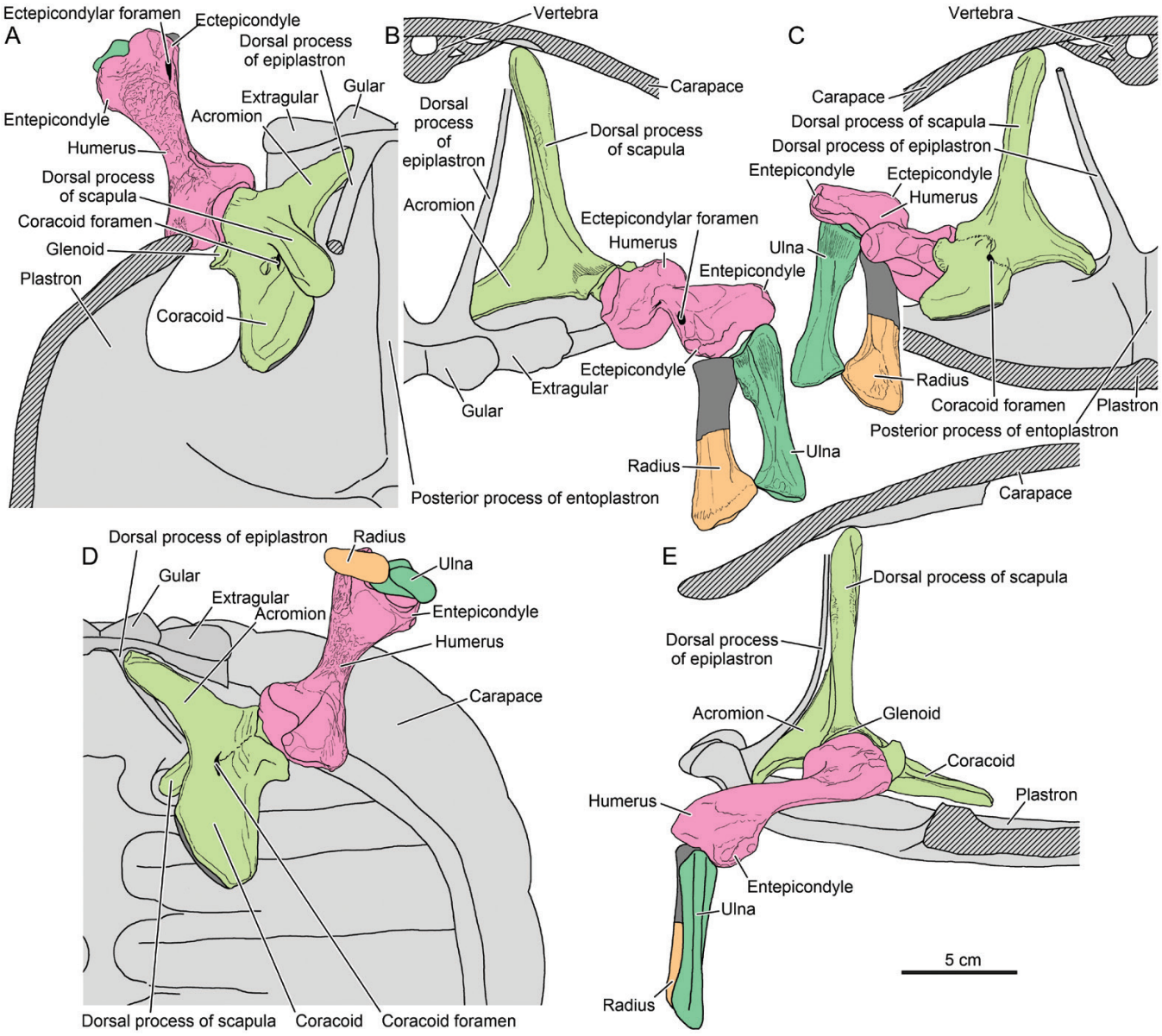

Figure 45. *Proterochersis porebensis*, restoration of the left forelimb skeleton with partial shell in dorsal (A), anterior (B), posterior (C), ventral (D) and lateral (E) view. Missing parts of bones are marked with dark grey.

Mode of life

The life environment of the earliest representatives of the turtle lineage is contentious. Lyson *et al.* (2016) proposed a fossorial origin for turtles, based on the adaptations for fossoriality apparent in *Eunotosaurus africanus* and the earliest members of Pantestudinata. A primarily terrestrial ecology, but associated with water, was found for this taxon based on forelimb measurements by Dudgeon *et al.* (2021). Schoch and Sues (2015, 2017) initially considered *Pappochelys rosinae* an aquatic animal, but Schoch *et al.* (2019) noted that the bone microstructure suggests a semiaquatic or terrestrial habitus. Aquatic or semiaquatic ecology was also proposed for *Eorhynchochelys sinensis* (see Li *et al.* 2018) and is supported by forelimb proportions (Li *et al.* 2008, Benson *et al.* 2011, Dudgeon *et al.* 2021) and diving-related pathology (Rothschild and Naples 2015) for *O. semitestacea*. Joyce (2015) argued for a more terrestrial mode of life for *O. semitestacea*, suggesting that it lacks the phalangeal elongation typical of aquatic and semiaquatic species and has a higher number of wide and short phalanges instead, but this difference might not necessarily preclude formation of a functional paddle (Lichtig and Lucas 2017). In fact, although different from true aquatic turtles (e.g. Hirayama 1998, Evers *et al.* 2019, Joyce *et al.* 2021), limbs with numerous short phalanges (hyperphalangeal or not) are an extremally common adaptation appearing within numerous clades of aquatic tetrapods, including stem tetrapods (e.g. Coates and Clack 1990), cetaceans (e.g. Cooper *et al.* 2007), ichthyosaurs (e.g. Caldwell 2002), *Eusaurosphargis dalsassoi* Nosotti and Rieppel 2003 (Scheyer *et al.* 2017), eosauropterygians (e.g. Rieppel and Lin 1995, Caldwell 2002), placodonts (e.g. Diedrich 2013, Wang *et al.* 2020) and sauroshphargids (e.g. Li *et al.* 2011). Motani and Vermeij (2021) classified both *Eorhynchochelys sinensis*

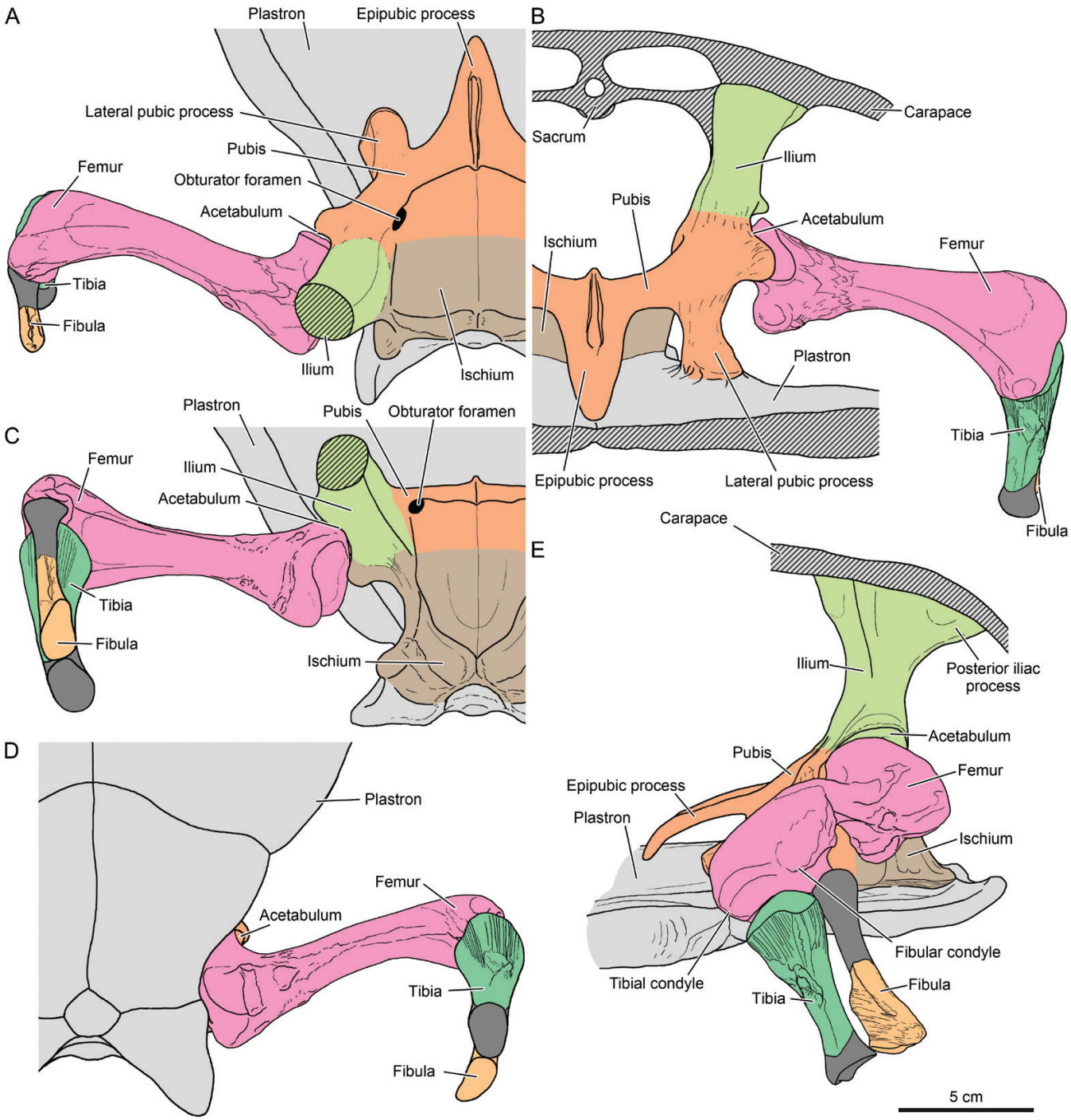

Figure 46. *Proterochersis porebensis*, restoration of the left hindlimb skeleton with partial shell in dorsal (A), anterior (B), posterior (C), ventral (D) and lateral (E) view. Missing parts of bones are marked with dark grey.

and *O. semitestacea* as likely to be secondarily marine and noted that in the latter species the humerus is longer than the femur, suggesting a more advanced adaptation to aquatic lifestyle. However, personal examination (T. Szczygielski) of the material reveals that the femora and humeri are virtually the same length in *IVPP V 13240* (humerus-to-femur length ratio approaching 1.0), and the femur is very slightly longer than the humerus in *IVPP V 15639* (humerus-to-femur length ratio ~0.9).

The situation is even less clear for the first Testudinata. The shell curvature of *Proterochersis robusta* was taken by Fraas (1913) as an indicator of its terrestrial ecology. *Proganochelys quenstedtii* was considered either terrestrial or semiaquatic by Fraas (1899), terrestrial by Jaekel (1918) and a semiaquatic bottom walker by Gaffney (1990). Joyce and Gauthier (2004) noted that there is a correspondence between the length ratio of the whole forelimb and its distal part and the mode of life of modern turtles, and based on that, they proposed a terrestrial lifestyle for *Proganochelys quenstedtii* and *Palaeochersis talampayensis*. This conclusion was subsequently corroborated, with additional inclusion of *Proterochersis robusta*, based on shell

histology of these taxa (Scheyer and Sander 2007). Subsequently, however, based on the analysis of shell geometry performed by Benson *et al.* (2011), *Proterochersis robusta* was classified as semiaquatic. Benson *et al.* (2011) also repeated the analysis of Joyce and Gauthier (2004) and noted that with the extant *Kinixys* spp. classified as semiaquatic, the result suggests a semiaquatic ecology for *Palaeochersis talampayensis* and either semiaquatic or terrestrial for *Proganochelys quenstedtii*. On the contrary, Lichtig and Lucas (2017), using a different set of shell measurements, categorized *Proganochelys quenstedtii* as probably semiaquatic or aquatic and *Proterochersis robusta* (tentatively) as terrestrial; note, however, that their measurements were based on published photographs of those species (Gaffney 1990, Szczygielski and Sulej 2016) and thus might be imprecise, because they have no way of accounting for foreshortening, lens distortion or potential lack of precision regarding scale or reproduction. According to their table 1, the measurements of *Proganochelys quenstedtii* were based on Gaffney's (1990) fig. 63, which is a dorsolateral (not lateral, as written incorrectly by Gaffney 1990) view of SMNS 10012 (incomplete and partly restored carapace embedded in plaster and missing plastron), and either Gaffney's (1990) fig. 87, which is a ventral view of SMSN 17204, or Gaffney's (1990) fig. 69G, which is a drawn reconstruction of SMSN 16980 in lateral view without a scale (not SMSN 17204 in ventral view, as written incorrectly by Lichtig and Lucas 2017). Lautenschlager *et al.* (2018) characterized *Proganochelys quenstedtii* as highly terrestrial but most probably not fossorial based on skull endocasts. Bajdek *et al.* (2019) described probable turtle coprolites with fish remains from the type locality of *Proterochersis porebensis*, suggesting at least a semiaquatic ecology for that turtle. Dziomber *et al.* (2020) concluded that the ecomorphological signal from the shells of *Proterochersis robusta* and *Proganochelys quenstedtii* is ambiguous, with the linear discriminant analyses suggesting them as either intermediate or 'fully webbed' (aquatic or semiaquatic), but with the depositional data and other factors suggesting a dry continental ecology. Dudgeon *et al.* (2021) modified and expanded upon Joyce and Gauthier's (2004) methodology and recovered *Proganochelys quenstedtii* and *Palaeochersis talampayensis* as terrestrial, with a weak semiaquatic signal for the latter. Szczygielski and Słowiak (2022) noted that the shell histology in *Proterochersis porebensis* reveals changes during ontogeny, possibly supporting a more aquatic lifestyle for smaller (younger) individuals and a more terrestrial ecology for large, supposedly older individuals. It is noteworthy that although distorted by crushing, the shells of *Proterochersis porebensis* seem to be flatter than those of *Proterochersis robusta* (see Szczygielski and Sulej 2016, Szczygielski *et al.* 2018), possibly hinting at somewhat differing ecologies of those two species. Finally, Evers *et al.* (2022) found the proportionally small, elongated and narrow labyrinth of *Proganochelys quenstedtii* to resemble morphology observed in terrestrial turtles.

Young *et al.* (2017) noticed that, at least in cryptodires, the forelimb function seems to adapt more dynamically to a change in habitus (from aquatic towards terrestrial) than the hindlimb. The length of the coracoid generally exhibits a positive correlation with swimming ability of derived turtles (e.g. Szalai 1931, Walker 1973, Evers *et al.* 2019, Joyce *et al.* 2021), but the form of that bone is very different in the Triassic pantestudinates, and it is generally short, with rather minor variability in length (Jaekel 1914, 1918, Gaffney 1990, Sterli *et al.* 2007, 2021, Li *et al.* 2008, Joyce *et al.* 2013, Schoch and Sues 2017). Walker (1973) noted enlargement of the medial process of the humerus as typical for aquatic turtles. In *Proterochersis porebensis* and *Proganochelys quenstedtii* the medial process is prominent, but much less so than in *Palaeochersis talampayensis* and extant aquatic turtles (Walker 1973, Gaffney 1990, Sterli *et al.* 2007). The humerus being shorter than the femur (as was most probably the case in *Proterochersis porebensis*; see above) or subequal in length is also correlated with semiaquatic or aquatic (freshwater) ecology; marine turtles and heavily terrestrial forms tend to have their femora shorter than the humeri (e.g. Zangerl 1953, Walker 1973, Evers *et al.* 2019, Joyce *et al.* 2021, Motani and Vermeij 2021). Shortening of the autopodium and reduction of the phalangeal formula is also typical for terrestrial turtles (e.g. Walker 1973, Gaffney 1990, Crumly and Sánchez-Villagra 2004), but unfortunately, this part is not preserved in *Proterochersis porebensis*.

Ruckes (1929a) observed in turtles a connection between the mode of life and depth of the pelvis, with shallow, plate-like pelves and wide arches formed by the pubis and ischium below the acetabulum being more characteristic for swimming species and more upright pelves with pronounced pelvic fossa and higher subacetabular arches (such as in *Proterochersis* spp.) being typical for terrestrial forms, but Zug (1971) was unable to confirm this correlation (with the exception of the elongation of the puboischiadic plate in aquatic turtles) based on his sample of recent cryptodires. Zug (1971) also stated that terrestrial species have a pronounced puboiliac notch in the acetabulum to facilitate the dorsal abduction of the femur (making a space for the dorsal head of the muscle puboischiofemoralis internus) and the trochanter minor wider than the trochanter major, which is also true for *Proterochersis* spp. On the contrary, the shape of the femoral head is elongated in *Proterochersis* spp., and the trochanters are conspicuously flared, as in swimming turtles, in contrast to more spherical femoral heads of terrestrial or even bottom-walking species, and the intertrochanteric fossa is completely open ventrally, unlike the situation in the terrestrial forms (Zug 1971). According to Zug (1971), the lateral pubic process is perpendicular (directed laterally) to the pubic symphysis in terrestrial forms and more parallel (directed anteriorly or anterolaterally) in aquatic species. Replication of that measurement is difficult for *Proterochersis* spp. owing to the complex shape of the process. The angle between the pubic symphysis and the posterior edge of the process (as explained by Zug 1971) measured in dorsal view is ~30–40°, but the long axis of the attachment to the plastron is nearly parallel to the symphysis and not to the long axis of the lateral process (as in, e.g. *Testudo* spp.). This character, however, might be not entirely representative, because it might be impacted by the co-ossification of the pelvis with the shell, and Zug (1971) studied only the pelves of recent cryptodires. Mayerl *et al.* (2016), however, consider the co-ossification of the pelvis itself as a character constraining the pleurodires to a mainly aquatic setting because of its restricting impact on terrestrial locomotion. In cryptodires, the twisting and rocking motions of the pelvis during walking serve to increase the stride length in a similar manner to the rotation of the scapulocoracoid, albeit to a lesser degree (Zug 1971, Blob *et al.* 2016, Mayerl *et al.* 2016, 2019). However, these motions become restrained during swimming (Blob *et al.* 2016, Mayerl *et*

al. 2016, 2019), and the fixed pelvic girdle of pleurodires might even be beneficial in the aquatic setting by increasing their stability (Blob *et al.* 2016, Mayerl *et al.* 2016). As in the case of the carpus and manus, the morphology of the tarsus and pes (correlated with mode of life; e.g. Zug 1971, Walker 1973, Gaffney 1990) of *Proterochersis porebensis* is unknown.

In summary, the Triassic turtles in general, and proterochersids in particular, show a mosaic of characteristics suggesting either terrestrial or aquatic ecology. This might have three possible causes: (1) the ecological adaptations shifted dynamically in the Triassic turtles, and the observed characters represent a mosaic of features adaptive for the current ecology of each taxon and inherited from its ancestors having a different ecology; (2) some characters were constrained owing to complex developmental and functional interplay between the still evolving shell and locomotory apparatus, and these constraints were not resolved until the latest Triassic or Early Jurassic, when further optimization became possible; and (3) the Triassic taxa were indeed semiaquatic, and some of the observed differences result from varied relative adaptations to each of the environments. These possibilities are not mutually exclusive, and given that development of the shell required an overall modification to nearly all anatomical systems, the evolutionary pathways could indeed be complex.

SUPPLEMENTARY DATA

Supplementary data is available at *Zoological Journal of the Linnean Society* online.

Extended material descriptions. Anatomical, preservational, and size characteristics of all the specimens described, including references to previous publications.

Table S1. Measurements of the pelves of Proterochersis robusta in centimeters.

Supplementary references. Bibliography cited in the supplementary file.

ACKNOWLEDGEMENTS

We thank Gabriela Cisterna (PULR), Laura Cotton (NHMD), Zheng Fang (IVPP), Eudald Mujal Grané (SMNS), Chun Li (IVPP), Ning Li (IVPP), Bent Erik Kramer Lindow (NHMD), Andrea Oettl (SMF), Rainer Schoch (SMNS), Daniela Schwarz (MB), Rolf Schweizer (CSMM) and Heike Straebelow (MB) for the access to the specimens housed at their respective institutions, Torsten Scheyer (Paläontologisches Institut und Museum, Universität Zürich) for access to the remainder of the *Proganochelys quenstedtii* material from SMF studied by him, and Nils Natorp (Geocenter Møns Klint) and Volker Neipp (Museum Auberlehaus in Trossingen) for access to 'cf. *Proganochelys*' NHMD 190349 and *Proganochelys quenstedtii* SMNS 17204 on their expositions. We also thank Dawid Dróżdż (ZPAL) and Tomasz Sulej (ZPAL) for the additional photographs of *Chinlechelys tenertesta* and *Waluchelys cavitesta*. Dawid Dróżdż and Marco Marzola are also thanked for their help in photogrammetry of proterochersid shells housed in SMNS and ZPAL. Tomasz Sulej (ZPAL) and all participants of the excavations in Poręba are thanked for their contribution to recovery of *Proterochersis porebensis* material. Finally, we thank Serjoscha Evers and the anonymous reviewer, the Editor, and the Production Office for their time and work needed to process this manuscript.

FUNDING

This study was funded by the National Science Centre, Poland grants no. 2016/23/N/NZ8/01823 (excavations and comparative studies in 2017–2021) and no. 2020/39/B/NZ8/01074 (comparative studies and specimen digitization in 2021–2023) awarded to T.S.

CONFLICT OF INTEREST

The authors declare no conflict of interest.

DATA AVAILABILITY

Relevant data are published alongside the paper as supplementary files. Further requests and enquires are welcome to be directed to the corresponding author.

REFERENCES

Anquetin J. The anatomy of the basal turtle *Eileanchelys waldmani* from the Middle Jurassic of the Isle of Skye, Scotland. *Earth and Environmental Science Transactions of the Royal Society of Edinburgh* 2010;**101**:67–96.

Anquetin J. Reassessment of the phylogenetic interrelationships of basal turtles (Testudinata). *Journal of Systematic Palaeontology* 2012;**10**:3–45.

Bajdek P, Szczygielski T, Kapuścińska A *et al.* Bromalites from a turtle-dominated fossil assemblage from the Triassic of Poland. *Palaeogeogr Palaeoclimatol Palaeoecol* 2019;**520**:214–28.

Baur G. Ueber den Ursprung der Extremitäten der Ichthyopterygia. *Berichte über Versammlungen des Oberrheinischen Vereines* 1887;**20**:17–20.

Benson RBJ, Domokos G, Várkonyi PL *et al.* Shell geometry and habitat determination in extinct and extant turtles (Reptilia: Testudinata). *Paleobiology* 2011;**37**:547–62.

Bever GS, Lyson TR, Field DJ *et al.* Evolutionary origin of the turtle skull. *Nature* 2015;**525**:239–42.

Blob RW, Mayerl CJ, Rivera ARV *et al.* 'On the fence' versus 'all in': insights from turtles for the evolution of aquatic locomotor specializations and habitat transitions in tetrapod vertebrates. *Integrative and Comparative Biology* 2016;**56**:1310–22.

Bojanus LH. *Anatome Testudinis Europaeae*. Vilnius: Joseph Zawadzki, 1819.

de Broin F. *Proganochelys ruchae* n.sp., chélonien du Trias supérieur de Thaïlande. *Studia Palaeocheloniologica* 1984;**1**:87–97.

Caldwell MW. From fins to limbs to fins: Limb evolution in fossil marine reptiles. *American Journal of Medical Genetics* 2002;**112**:236–49.

Cherepanov GO. New morphogenetic data on the turtle shell: discussion on the origin of the horny and bony parts. *Studia Geologica Salmanticensia* 1989;**3**:9–24.

Cherepanov GO. Ontogenetic development of the shell in *Trionyx sinensis* (Trionychidae, Testudinata) and some questions on the nomenclature of bony plates. *Russian Journal of Herpetology* 1995;**2**:129–33.

Cignoni P, Callieri M, Corsini M *et al.* MeshLab: an open-source mesh processing tool. In: Scarano V, De Chiara R, Erra U (ed.), Sixth Eurographics Italian Chapter Conference, Salerno, Italy, July 2nd-4th. Aire-la-Ville: Eurographics Association, 2008, 129–136.

Coates MI, Clack JA. Polydactyly in the earliest known tetrapod limbs. *Nature* 1990;**347**:66–9.

Cooper LN, Berta A, Dawson SD *et al.* Evolution of hyperphalangy and digit reduction in the cetacean manus. *The Anatomical Record* 2007;**290**:654–72.

Cox CB. The problematic Permian reptile *Eunotosaurus*. *Bulletin of the British Museum (Natural History) Geology* 1969;**18**:167–96.

Crumly CR, Sánchez-Villagra MR. Patterns of variation in the phalangeal formulae of land tortoises (Testudinidae): developmental constraint, size, and phylogenetic history. *Journal of Experimental Zoology* 2004;**302**:B134–46.

Czepiński L, Dróżdż D, Szczygielski T *et al*. An Upper Triassic terrestrial vertebrate assemblage from the forgotten Kocury locality in southern Poland with a new aetosaur taxon. *Journal of Vertebrate Paleontology* 2020;**41**:e1898977.

Diedrich CG. Review of the Middle Triassic 'sea cow' *Placodus gigas* (Reptilia) in Pangea's shallow marine macroalgae meadows of Europe. *New Mexico Museum of Natural History and Science, Bulletin* 2013;**61**:104–31.

Dudgeon TW, Livius MCH, Alfonso N *et al*. A new model of forelimb ecomorphology for predicting the ancient habitats of fossil turtles. *Ecology and Evolution* 2021;**11**:17071–9.

Dziomber L, Joyce WG, Foth C. The ecomorphology of the shell of extant turtles and its applications for fossil turtles. *PeerJ* 2020;**8**:e10490.

Evers SW, Barrett PM, Benson RBJ. Anatomy of *Rhinochelys pulchriceps* (Protostegidae) and marine adaptation during the early evolution of chelonioids. *PeerJ* 2019;**7**:e6811.

Evers SW, Joyce WG, Chiniere JN *et al*. Independent origin of large labyrinth size in turtles. *Nature Communications* 2022;**13**:5807.

Fraas E. *Proganochelys quenstedtii* Baur (Psammochelys keuperina Qu.). Einer neuer Fund der Keuperschildkröte aus dem Stubensandstein. *Jahreshefte des Vereins für Vaterlandische Naturkunde in Württemberg* 1899;**55**:401–23.

Fraas E. *Proterochersis*, eine pleurodire Schildkröte aus dem Keuper. *Jahreshefte des Vereins für Vaterlandische Naturkunde in Württemberg* 1913;**69**:13–30.

de la Fuente MS, Sterli J, Krapovickas V. Triassic turtles from Pangea: the legacy from South America. *Journal of South American Earth Sciences* 2021;**105**:102910.

Gaffney ES. A phylogeny and classification of the higher categories of turtles. *Bulletin of the American Museum of Natural History* 1975;**155**:387–436.

Gaffney ES. The shell morphology of the Triassic turtle *Proganochelys*. *Neues Jahrbuch für Geologie und Paläontologie – Abhandlungen* 1985;**170**:1–26.

Gaffney ES. A cladogram of the pleurodiran turtles. *Acta Zoologica Cracoviensia* 1988;**31**:487–92.

Gaffney ES. The comparative osteology of the Triassic turtle *Proganochelys*. *Bulletin of the American Museum of Natural History* 1990;**194**:1–263.

Gaffney ES. The postcranial morphology of *Meiolania platyceps* and a review of the Meiolaniidae. *Bulletin of the American Museum of Natural History* 1996;**229**:1–166.

Gaffney ES, Meylan PA, Wyss AR. A computer assisted analysis of the relationships of the higher categories of turtles. *Cladistics* 1991;**7**:313–35.

Gaffney ES, Rich TH, Vickers-Rich P *et al*. *Chubutemys*, a new eucryptodiran turtle from the Early Cretaceous of Argentina, and the relationships of the Meiolaniidae. *American Museum Novitates* 2007;**3599**:1–35.

Gaffney ES, Tong H, Meylan PA. Evolution of the side-necked turtles: the families Bothremydidae, Euraxemydidae, and Araripemydidae. *Bulletin of the American Museum of Natural History* 2006;**300**:1–698.

Gilbert SF, Bender G, Betters E *et al*. The contribution of neural crest cells to the nuchal bone and plastron of the turtle shell. *Integrative and Comparative Biology* 2007;**47**:401–8.

Gow CE. A reassessment of *Eunotosaurus africanus* Seeley (Amniota: Parareptilia). *Palaeontologia Africana* 1997;**34**:33–42.

Gow C, de Klerk B. First record of *Eunotosaurus* (Amniota: Parareptilia) from the Eastern Cape. *Palaeontologia Africana* 1997;**34**:27–31.

Haines RW. The tetrapod knee joint. *Journal of Anatomy* 1942;**76**:270–301.

Haines RW. A revision of the movements of the forearm in tetrapods. *Journal of Anatomy* 1946;**80**:1–11.

Hirayama R. Oldest known sea turtle. *Nature* 1998;**392**:705–8.

Huene F. Einige Schildkrötenreste aus der obersten Trias Württembergs. *Centralblatt für Mineralogie, Geologie und Paläontologie. Abteilung B: Geologie und Paläontologie* 1926;**1926**:509–14.

Hutchinson JR. *The evolution of hindlimb anatomy and function in theropod dinosaurs*. Unpublished PhD thesis, Department of Integrative Biology, University of California, 2001.

Jaekel O. Über die Wirbeltierfunde aus der oberen Trias von Halberstadt. *Palaeontologische Zeitschrift* 1914;**1**:155–215.

Jaekel O. Die Wirbeltierfunde aus dem Keuper von Halberstadt. Serie II. Testudinata. *Palaeontol Z* 1918;**2**:88–214.

Jenkins FA, Shubin NH, Amaral WW *et al*. Late Triassic continental vertebrates and depositional environments of the Fleming Fjord Formation, Jameson Land, East Greenland. *Medd Grønl Geosci* 1994;**32**:1–25.

Joyce WG. Phylogenetic relationships of Mesozoic turtles. *Bulletin of the Peabody Museum of Natural History* 2007;**48**:3–102.

Joyce WG. The origin of turtles: a paleontological perspective. *Journal of Experimental Zoology Part B: Molecular and Developmental Evolution* 2015;**324**:181–93.

Joyce WG. A review of the fossil record of basal Mesozoic turtles. *Bulletin of the Peabody Museum of Natural History* 2017;**58**:65–113.

Joyce WG, Gauthier JA. Palaeoecology of Triassic stem turtles sheds new light on turtle origins. *Proceedings of the Royal Society of London B: Biological Sciences* 2004;**271**:1–5.

Joyce WG, Jenkins FA, Rowe T. The presence of cleithra in the basal turtle *Kayentachelys aprix*. *Fossil Turtle Research* 2006;**1**:93–103.

Joyce WG, Lucas SG, Scheyer TM *et al*. A thin-shelled reptile from the Late Triassic of North America and the origin of the turtle shell. *Proceedings of the Royal Society of London B: Biological Sciences* 2009;**276**:507–13.

Joyce WG, Mäuser M, Evers SW. Two turtles with soft tissue preservation from the platy limestones of Germany provide evidence for marine flipper adaptations in Late Jurassic thalassochelydians. *PLoS One* 2021;**16**:e0252355.

Joyce WG, Schoch RR, Lyson TR. The girdles of the oldest fossil turtle, *Proterochersis robusta*, and the age of the turtle crown. *BMC Evolutionary Biology* 2013;**13**:266.

Karl HV, Tichy G. *Murrhardtia staeschei*n. gen. n. sp. – eine neue Schildkröte aus der Oberen Trias von Süddeutschland. *Joannea Geologie und Paläontologie* 2000;**2**:57–72.

Keyser AW, Price B. First complete skull of the Permian reptile *Eunotosaurus aricanus* Seeley. *South African Journal of Science* 1981;**77**:417–20.

Lapparent de Broin F. The analysis of the character 'fused pelvis'. *Journal of Vertebrate Paleontology* 1996;**16**:47A.

Lapparent de Broin F. The oldest pre-Podocnemidid turtle (Chelonii, Pleurodira), from the Early Cretaceous, Ceará state, Brasil, and its environment. *Treballs del Museu de Geologia de Barcelona* 2000;**9**:43–95.

Lautenschlager S, Ferreira GS, Werneburg I. Sensory evolution and ecology of early turtles revealed by digital endocranial reconstructions. *Frontiers in Ecology and Evolution* 2018;**6**:7.

Li C, Fraser NC, Rieppel OC *et al*. A Triassic stem turtle with an edentulous beak. *Nature* 2018;**560**:476–9.

Li C, Rieppel OC, Xiao-Chun W *et al*. A new Triassic marine reptile from southwestern China. *Journal of Vertebrate Paleontology* 2011;**31**:303–12.

Li C, Wu XC, Rieppel OC *et al*. An ancestral turtle from the Late Triassic of southwestern China. *Nature* 2008;**456**:497–501.

Lichtig AJ, Lucas SG. A simple method for inferring habitats of extinct turtles. *Palaeoworld* 2017;**26**:581–8.

Lichtig AJ, Lucas SG. *Chinlechelys* from the Upper Triassic of New Mexico, USA, and the origin of turtles. *Palaeontol Electron* 2021;**24**:a13.

Lucas SG, Heckert AB, Hunt AP. Probable turtle from the Upper Triassic of east-central New Mexico. *Neues Jahrbuch für Geologie und Paläontologie – Monatshefte* 2000;**5**:287–300.

Lydekker R. *Catalogue of Fossil Reptilia and Amphibia. Part III. Containing the Order Chelonia*. London: Order of the Trustees, 1889.

Lyson TR, Bever GS, Bhullar BAS *et al*. Transitional fossils and the origin of turtles. *Biology Letters* 2010;**6**:830–3.

Lyson TR, Bever GS, Scheyer TM *et al*. Evolutionary origin of the turtle shell. *Current Biology* 2013a;**23**:1113–9.

Lyson TR, Bhullar BAS, Bever GS *et al*. Homology of the enigmatic nuchal bone reveals novel reorganization of the shoulder girdle in the evolution of the turtle shell. *Evolution & Development* 2013b;**15**:317–25.

Lyson TR, Schachner ER, Botha-Brink J *et al*. Origin of the unique ventilatory apparatus of turtles. *Nature Communications* 2014;**5**:5211.

Lyson TR, Rubidge BS, Scheyer TM *et al*. Fossorial origin of the turtle shell. *Current Biology* 2016;**26**:1887–94.
Martínez RN, Apaldetti C, Correa GA *et al*. A new Late Triassic vertebrate assemblage from northwestern Argentina. *Ameghiniana* 2015;**52**:379–90.
Marzola M. *The Late Triassic vertebrate fauna of the Jameson Land Basin, East Greenland: description, phylogeny, and paleoenvironmental implications*. Unpublished PhD thesis, Faculdade de Ciências e Tecnologia, Universidade Nova de Lisboa, 2019.
Marzola M, Mateus O, Milàn J *et al*. A review of Palaeozoic and Mesozoic tetrapods from Greenland. *Bull Geol Soc Den* 2018;**66**:21–46.
Mayerl CJ, Brainerd EL, Blob RW. Pelvic girdle mobility of cryptodire and pleurodire turtles during walking and swimming. *Bulletin of the Geological Society of Denmark* 2016;**2019**:2650–8.
Mayerl CJ, Capano JG, Moreno AA *et al*. Pectoral and pelvic girdle rotations during walking and swimming in a semi-aquatic turtle: testing functional role and constraint. *Journal of Experimental Biology* 2019;**222**:jeb212688.
Meyer H. Mittheilung an Professor H. B. Geinitz. *Neues Jahrbuch für Mineralogie, Geologie und Palaeontologie* 1863;**1863**:444–50.
Meyer H. Reptilien aus dem Stubensandstein des oberen Keupers. *Palaeontographica* 1865;**14**:99–124.
Motani R, Vermeij GJ. Ecophysiological steps of marine adaptation in extant and extinct non-avian tetrapods. *Biological Reviews* 2021;**96**:1769–98.
Nagashima H, Hirasawa T, Sugahara F *et al*. Origin of the unique morphology of the shoulder girdle in turtles. *Journal of Anatomy* 2013;**223**:547–56.
Niedźwiedzki G, Brusatte SL, Sulej T *et al*. Basal dinosauriform and theropod dinosaurs from the mid-late Norian (Late Triassic) of Poland: implications for Triassic dinosaur evolution and distribution. *Palaeontology* 2014;**57**:1121–42.
Nosotti S, Rieppel OC. *Eusaurosphargis dalsassoi*n. gen. n. sp., a new, unusual diapsid reptile from the Middle Triassic of Besano (Lombardy, N Italy). *Memorie della Societa Italiana di Scienze Naturali e del Museo Civico di Storia Naturale di Milano Ile* 2003;**31**:1–33.
Oken L. Litterarischer Anzeiger. *Isis von Oken* 1823;**12–13**:442–69.
Parker WK. *A Monograph on the Structure and Development of the Shoulder-Girdle and Sternum in the Vertebrata*. London: Robert Hardwicke, 1868.
Pritchard PCH. Evolution and structure of the turtle shell. In: Wyneken J, Godfrey MH, Bels V (eds.), *Biology of Turtles*. Boca Raton, London and New York: CRC Press, 2008:46–83.
Rieppel OC, Lin K. Pachypleurosaurs (Reptilia: Sauropterygia) from the lower Muschelkalk, and a review of the Pachypleurosauroidea. *Fieldiana Geology* 1995;**32**:1–44.
Rothschild BM, Naples V. Decompression syndrome and diving behavior in *Odontochelys*, the first turtle. *Acta Palaeontologica Polonica* 2015;**60**:163–7.
Rougier GW, de La Fuente MS, Arcucci AB. Late Triassic turtles from South America. *Science* 1995;**268**:855–8.
Ruckes H. Studies in chelonian osteology. Part I. Truss and arch analogies in chelonian pelves. *Annals of the New York Academy of Sciences* 1929a;**31**:31–80.
Ruckes H. Studies in chelonian osteology. Part II. The morphological relationships between the girdles, ribs and carapace. *Annals of the New York Academy of Sciences* 1929b;**31**:81–120.
Sánchez-Villagra MR, Müller H, Sheil CA *et al*. Skeletal development in the chinese soft-shelled turtle *Pelodiscus sinensis* (Testudines: Trionychidae). *Journal of Morphology* 2009;**270**:1381–99.
Scheyer TM, Klein N, Evers SW *et al*. First evidence of *Proganochelys quenstedtii* (Testudinata) from the *Plateosaurus* bonebeds (Norian, Late Triassic) of Frick, Canton Aargau, Switzerland. *Swiss J Palaeontol* 2022;**141**:17.
Scheyer TM, Neenan JM, Bodogan T *et al*. A new, exceptionally preserved juvenile specimen of *Eusaurosphargis dalsassoi* (Diapsida) and implications for Mesozoic marine diapsid phylogeny. *Scientific Reports* 2017;**7**:4406.
Scheyer TM, Sander PM. Shell bone histology indicates terrestrial palaeoecology of basal turtles. *Proceedings of the Royal Society of London B: Biological Sciences* 2007;**247**:1885–93.
Schoch RR, Klein N, Scheyer TM *et al*. Microanatomy of the stem-turtle *Pappochelys rosinae* indicates a predominantly fossorial mode of life and clarifies early steps in the evolution of the shell. *Scientific Reports* 2019;**9**:10430.
Schoch RR, Sues HD. A Middle Triassic stem-turtle and the evolution of the turtle body plan. *Nature* 2015;**523**:584–7.
Schoch RR, Sues HD. The diapsid origin of turtles. *Zoology* 2016;**119**:159–61.
Schoch RR, Sues HD. Osteology of the Middle Triassic stem-turtle *Pappochelys rosinae* and the early evolution of the turtle skeleton. *Journal of Systematic Palaeontology* 2017:**16**:1–39.
Seeley HG. On a new reptile from Welte Vreden (Beaufort West), *Eunotosaurus africanus* (Seeley). *Quarterly Journal of the Geological Society* 1892:**48**:583–5.
Sterli J. Phylogenetic relationships among extinct and extant turtles: the position of Pleurodira and the effects of the fossils on rooting crown-group turtles. *Contributions to Zoology* 2010;**79**:93–106.
Sterli J, de la Fuente MS, Rougier GW. Anatomy and relationships of *Palaeochersis talampayensis*, a Late Triassic turtle from Argentina. *Palaeontographica Abt A* 2007;**281**:1–61.
Sterli J, Martínez RN, Cerda IA *et al*. Appearances can be deceptive: bizarre shell microanatomy and histology in a new Triassic turtle (Testudinata) from Argentina at the dawn of turtles. *Papers in Palaeontology* 2021:**7**:1097–136.
Sukhanov VB. An archaic turtle, *Heckerochelys romani* gen. et sp. nov., from the Middle Jurassic of Moscow Region, Russia. *Fossil Turtle Research* 2006;**1**:112–8.
Sulej T, Niedźwiedzki G, Bronowicz R. A new Late Triassic vertebrate fauna from Poland with turtles, aetosaurs, and coelophysoid dinosaurs. *Journal of Vertebrate Paleontology* 2012;**32**:1033–41.
Szalai T. Schildkrötenstudien. *Annalen des Naturhist Museums in Wien* 1931;**46**:155–63.
Szczygielski T. Homeotic shift at the dawn of the turtle evolution. *Royal Society Open Science* 2017;**4**:160933.
Szczygielski T. Obscure by name: solving the enigma of *Chelytherium obscurum*, the first described Triassic turtle. *Zoological Journal of the Linnean Society* 2020;**192**:1111–22.
Szczygielski T, Słowiak J, Dróżdż D. Shell variability in the stem turtles *Proterochersis* spp. *PeerJ* 2018;**6**:e6134.
Szczygielski T, Sulej T. Revision of the Triassic European turtles *Proterochersis* and *Murrhardtia* (Reptilia, Testudinata, Proterochersidae), with the description of new taxa from Poland and Germany. *Zoological Journal of the Linnean Society* 2016;**177**:395–427.
Szczygielski T, Sulej T. The early composition and evolution of the turtle shell (Reptilia, Testudinata). *Palaeontology* 2019;**62**:375–415.
Szczygielski T, Słowiak J. Shell histology of the Triassic turtle, *Proterochersis porebensis*, provides novel insights about shell ankylosis. *Comptes Rendus Palevol* 2022;**21**:619–79.
Szulc J, Racki G. Grabowa Formation – the basic lithostratigraphic unit of the Upper Silesian Keuper. *Przeglad Geologiczny* 2015;**63**:103–13.
Szulc J, Racki G, Jewuła K *et al*. How many Upper Triassic bone-bearing levels are there in Upper Silesia (Southern Poland)? A critical overview of stratigraphy and facies. *Annales Societatis Geologorum Poloniae* 2015;**85**:587–626.
Vallén E. Beiträge zur Kenntnis der Ontogenie und der vergleichenden Anatomie des Schildkrötenpanzers. *Acta Zoologica* 1942;**23**:1–127.
Vergne R, Pacanowski R, Barla P, Granier X, Schlick C. Radiance scaling for versatile surface enhancement. In: Spencer SN (ed.), Proceedings of the 2010 ACM SIGGRAPH symposium on Interactive 3D Graphics and Games, 19–21 February 2010, Washington, DC. New York: Association for Computing Machinery, 2010, 143–50.
Walker WF. The development of the shoulder region of the turtle, *Chrysemys picta marginata*, with special reference to the primary musculature. *Journal of Morphology* 1947;**80**:195–249.
Walker WF. A structural and functional analysis of walking in the turtle, *Chrysemys picta marginata*. *Journal of Morphology* 1971;**134**:195–214.
Walker WF. The locomotor apparatus of Testudines. In: Gans C, Parsons TS (eds.), *Biology of the Reptilia*. London & New York: Academic Press, 1973:1–100.

Wang W, Ma F, Li C. First subadult specimen of *Psephochelys polyosteoderma* (Sauropterygia, Placodontia) implies turtle-like fusion pattern of the carapace. *Papers in Palaeontology* 2020;**6**:251–64.

Watson DMS. *Eunotosaurus africanus* Seeley, and the ancestry of the Chelonia. *Proceedings of the Zoological Society of London* 1914;**84**:1011–20.

Young VKH, Wienands CE, Wilburn BP, Blob RW. Humeral loads during swimming and walking in turtles: Implications for morphological change during aquatic reinvasions. *Journal of Experimental Biology* 2017:**220**(21):3873–7. https://doi.org/10.1242/jeb.156836

Zangerl R. The vertebrate fauna of the Selma Formation of Alabama. Part IV. The turtles of the family Toxochelyidae. *Fieldiana: Geology Memoirs* 1953;**3**:185–277.

Zatoń M, Niedźwiedzki G, Marynowski L *et al*. Coprolites of Late Triassic carnivorous vertebrates from Poland: an integrative approach. *Palaeogeogr Palaeoclimatol Palaeoecol* 2015;**430**:21–46.

Zug GR. Buoyancy, locomotion, morphology and the pelvic girdle and hindlimb, and systematics of cryptodiran turtles. *Miscellaneous Publications, Museum of Zoology, University of Michigan* 1971;**142**:1–98.